





DIPARTIMENTO DI INGEGNERIA CIVILE

Dottorato di Ricerca in Rischio e sostenibilità nei sistemi dell'ingegneria civile, edile ed ambientale

XXXVI Ciclo (2020-2023)

LARGE MASS RATIO TUNED MASS DAMPERS FOR EXISTING BUILDINGS: SSI-INFORMED ASSESSMENT AND OPTIMIZED DESIGN

Pasquale Roberto Marrazzo

I Tutor
Prof. Ing. Elide Nastri
Prof. Ing. Davide Noè Gorini

Il Coordinatore
Prof. Ing. Fernando Fraternali

Co-Tutor
Prof. Ing. Rosario Montuori

TABLE OF CONTENTS

1 CHAPTER 1 INTRODUCTION 4
1.1 Context 4
1.2 State of the art 4
1.3 Motivation of the work and metodology 11
1.4 Organization of the work 12
2 CHAPTER 2 A DESIGN APPROACH FOR SEISMIC RETROFITTING THROUGH LARGE MASS-RATIO TMD 15
2.1 Introduction and metodology 15
2.2 Parametric analysis 18
2.3 Application to Fixed Base structures 30
3 CHAPTER 3 BENCHMARK SOIL-STRUCTURE-TMD SYSTEM: FROM HIGH-FIDELITY NUMERICAL MODELLING TO PERFORMANCE 41
3.1 Introduction 41
3.2 Soil response and record selection 42
3.3 Modeling in the Finite Element analysis framework OpenSees 48
3.4 Results 57
4 CHAPTER 4 AN INTEGRATED DESIGN CRITERION FOR TMDs ACCOUNTING FOR SSI 75
4.1 Introduction 75
4.2 Parametric analysis 79
4.3 Design correlations 83
5 CHAPTER 5 VALIDATION 109

5.1 Validation on the similSDOF 109
5.2 Validation on high-fidelity benchmark soil-structure-TMD models....121
6 CONCLUSIONS 129
7 REFERENCES 133

1 CHAPTER 1 INTRODUCTION

1.1 Context

In the field of modern structural engineering, the ability to control and reduce vibrations induced by dynamic events is a primary challenge. Civil structures such as skyscrapers, bridges, and towers are exposed to various dynamic forces, including wind, earthquakes, and vehicular traffic, which can cause undesirable oscillatory movements, jeopardizing their structural integrity and the comfort of their occupants. In this context, Tuned Mass Dampers (TMD) emerge as crucial engineering solutions for vibration mitigation, offering an effective method to enhance the safety and resilience of structures.
The idea of using tuned masses to control vibrations dates back to the early 20th century, but it was not until the 1970s and 1980s that TMDs gained significant recognition thanks to pioneering works like that of Den Hartog [1]. The basic concept involves using an additional mass attached to the main structure via a system of springs and dampers, tuned to oscillate at the same frequency as the structure but in opposition to its phase, thereby absorbing and dissipating vibrational energy.
TMDs operate on the principle of resonance. When the main structure is excited at a certain frequency, the TMD, tuned to that same frequency, enters into resonance. The mass of the TMD oscillates out of phase with the structure, generating inertial forces that counteract the dynamic forces applied to the structure. This interaction reduces the amplitude of vibrations, thereby improving the stability and comfort of the structure. A notable example is the Taipei 101 skyscraper, where a 660-ton TMD was installed to mitigate oscillations caused by wind and earthquakes [2].

1.2 State of the art

Over the years, various formulations have been proposed and developed through increasingly complex study models. The first formulation proposed

by Den Hartog, which is widely considered a reference for classical TMDs, considered an undamped single-degree-of-freedom (SDOF) system with an installed TMD, all subjected to harmonic forcing. Den Hartog's expressions allow for the calculation of the period and damping to be attributed to the TMD to minimize structural vibrations.

Subsequent numerical studies have considered additional aspects beyond Den Hartog's formulation, such as fully damped systems [3], generic forcing functions [4], contributing to a richer understanding of this solution.

Rana and Soong [5] demonstrated how to apply and tune a TMD in a multi-degree-of-freedom (MDOF) system with three stories, also showing the effect of multiple TMDs. The results indicated mode contamination, making the use of multiple TMDs (MTMD) less effective in controlling the response.

There have been significant phenomenological insights into the functioning and limitations of TMDs, such as the role of structural irregularities and their impact on the performance of these devices. Gutierrez Soto and Adeli [6] studied the response of bidirectional TMDs (BTMDs) designed according to formulations from the literature on 5, 15, and 20-story structures with plan irregularities, in terms of reducing displacements and base shear. The authors found greater effectiveness of this system in flexible structures compared to rigid ones.

Babaei and Moniri [7] studied the response of TMDs in steel structures with vertical mass irregularities, considering seismic events from near or distant faults.

Jangid and Datta [8] considered the use of multiple TMDs (MTMDs) in a torsionally coupled system through a parametric analysis that included the eccentricity of the main system, the frequency ratio, and the damping of the TMDs. They found that the advantage of MTMDs over a single TMD decreases as the eccentricity ratio increases.

The phenomenon of detuning, or the loss of tuning of a TMD, represents one of the most critical challenges in structural vibration mitigation. This issue is particularly relevant when considering structural nonlinearities, which can significantly affect the resonant frequencies of a structure and, consequently, the effectiveness of the TMD. Detuning caused by structural nonlinearities can greatly reduce the effectiveness of a TMD. A TMD tuned to a specific frequency is optimized to reduce vibrations at that frequency. However, if the

resonant frequency of the structure changes due to nonlinearities, the TMD may no longer be correctly tuned, leading to a reduction in effectiveness or, in some cases, a worsening of vibrations.

Soto-Brito and Ruiz [9] studied the effect of structural nonlinearities on the performance of TMDs using a 22-story reinforced concrete structure subjected to motions of varying intensity. The results showed better effectiveness of the TMD with small nonlinearities associated with moderate seismic intensities, recording reductions in the top story displacements by up to 30%. As the intensity of the forcing increases, structural nonlinearities also increase, and the TMD loses effectiveness. The authors therefore suggest the use of multiple TMDs (MTMDs) to address the problem through more robust solutions.

Indeed, variants of the classic TMDs have been studied, such as multiple TMDs (MTMDs), to address uncertainties due to phenomena such as inelastic behavior. Yamaguchi and Harnpornchai [10] investigated the effectiveness of MTMDs in the single-mode response of structures, examining parameters such as frequency range, damping ratio, and the total number of TMDs. The effectiveness derived from using multiple TMDs is greater than that of a single TMD and increases with the number of TMDs. Specifically, the optimal solution with multiple TMDs proved more robust in the case of estimation errors of the structural natural frequency compared to a single TMD, although this condition does not hold for changes in both the damping ratio and the natural frequency of the structure.

Hoang and Warnitchai [4] used a numerical optimizer in the design of MTMDs for a single-degree-of-freedom system subjected to wide-band excitation. They presented the optimal solutions for these TMDs for practical design purposes.

Domizio et al. [11] studied the use of single and multiple TMDs on structures with different ductility demands subjected to near-fault and far-fault records. They found the maximum effectiveness of TMDs arranged in series tuned to half the fundamental period in cases of high ductility demand. Effectiveness was significantly reduced in structures with low periods subjected to near-fault events.

Design formulas can be found in the works of Igusa and Xu [12], Zuo [13], and Abé and Fujino [14].

To overcome uncertainties and variability in boundary conditions, parallel research has emerged on Active TMD (ATMD) and Semi-active TMD (STMD) systems. Active TMDs use electronically controlled actuators to apply supplementary forces to the structure. Unlike passive TMDs, which rely entirely on inertial forces generated by a tuned mass, active TMDs can dynamically react to changes in loading conditions and structural properties. A real-time control system monitors the structure's vibrations and adjusts the actuators to optimize the TMD's response. The main components of an ATMD are thus a tuned mass (usually of reduced size), actuators capable of applying forces and displacing the mass, sensors that can monitor the structure's motion properties in real time, and a control unit that processes data from the sensors and operates the TMDs through the actuators.
In STMD systems, devices are present that can modify their properties in response to loading conditions, without the use of external forces. This allows them to adapt to the structural response with lower energy consumption [15]. Further information can be explored in the works of Setareh [16], Abé [17], Wang et al. [18], Sun and Nagarajaiah [19], Rasouli [20], and Yahyai [20].
An important parameter that characterizes a TMD is the mass ratio, defined as the ratio between the mass of the TMD and the structural mass. In the case of TMDs tuned to multi-degree-of-freedom (MDOF) structures, this ratio is usually defined concerning the modal mass. Typical values considered for this parameter have generally been small percentages (1-5%), especially because the initial applications were related to very tall structures. It has been widely recognized that high mass ratio TMDs (LM-TMD) are characterized by greater robustness against detuning. De Angelis et al. [21] investigated the efficiency of LM-TMDs through numerical analyses and experimental tests, providing a design law related to High-Damping Rubber Bearings (HDRB) devices.
The authors found that high mass ratios simultaneously lead to significant reductions in structural response and greater robustness at off-optimal points, compared to ordinary TMDs. Similar considerations are also evident from the work of Marrazzo et al. [22], where a parametric analysis was conducted on a 2-DOF model. The results of this work will be extensively discussed in the following chapter.

Despite numerous developments in the study and understanding of TMDs, all advanced and modern formulations do not consider soil-structure interaction (SSI). It has been recognized that SSI can significantly alter the dynamic response of structures, causing the detuning of any TMDs from the modal response on which they are tuned. If not considered during the design phase, SSI effects can negatively influence the response of classical TMDs or even lead to adverse effects in terms of deformation and base shear of the structure. Wu Chen and Lou [23] used a frequency-independent model to represent a soil-structure system capable of encompassing many soil and structural characteristics. The model was subjected to stationary random forcing, and the results showed that the effectiveness of the TMD decreases as the shear wave velocity in the soil increases.

To understand the effects of classical TMD design on soil-structure systems, Ghosh and Basu [24] considered a structure modeled as a linear SDOF with a TMD designed under fixed-base assumptions. They obtained an expression for the transfer function of the flexible-base structure-TMD system and then conducted a numerical frequency domain study to investigate the different effects of SSI on TMD performance.

In the study by Salvi et al. [25], the effectiveness of an optimized TMD in the seismic context, considering soil-structure interaction (SSI), was investigated. The authors focused on shear frame structures, both low- and high-rise, subjected to strong earthquakes. The TMD was tuned through a two-variable optimization procedure specific to each case study, considering the characteristics of the structure, soil type, and the specific earthquake considered.

The main objectives of the study were to evaluate the effectiveness of the optimized TMD in reducing the linear response of structures during seismic events and to provide practical guidelines for the design and optimization of TMDs in the presence of SSI. The authors aimed to optimize the average response indices of the structures, also monitoring the maximum responses to ensure overall safety.

The conclusions provided by the authors offer useful guidelines for tuning TMDs in mechanical systems and real structures, highlighting the importance of considering soil interaction to avoid detuning phenomena that could compromise TMD effectiveness.

In the work of Bekdas and Nigdeli [26], an optimization methodology for the optimal design of TMDs using two metaheuristic algorithms was developed. The approach adopted evaluates the time-domain analyses of structures and considers the responses under different seismic records. The optimal design variables, defined as the mass, period, and damping ratio of the TMD, were sought with the objective of minimizing the maximum displacement of the structure and meeting the design constraint related to the limitation of the scaled stroke of the TMD.

The results of the study show that optimized TMDs are effective in reducing critical displacement by up to 25% for a 40-story structure. The proposed methodologies proved to be effective. Among the two algorithms used, the bat algorithm showed advantages in minimizing the optimization objective and finding a precise optimal value. This suggests that the bat algorithm could be preferred in practical applications for the optimal design of TMDs.

Shutong et al. [27] analyzed the seismic control performance of linear TMDs and nonlinear particle TMDs (PTMD), including the effects of SSI. Using shaking table test results, the authors compared the mitigation effects of TMDs and PTMDs on floor acceleration and displacement responses, in terms of average decreasing amplitude ratios and root-mean-square decreased ratios. To better understand the mitigation mechanism of TMDs and PTMDs with SSI, the recorded signals were decomposed and energy response analysis was conducted using wavelet packet transform.

The results of the study indicate that when considering SSI effects, the performance of linear TMDs and nonlinear PTMDs on acceleration response is similar. However, linear TMDs show superiority over PTMDs in reducing displacement response and energy response. The wavelet packet transform analysis allowed for a better understanding of the energy distribution and mitigation mechanisms of TMDs and PTMDs, demonstrating that linear TMDs are more effective in terms of displacement and energy responses.

In the study by Gao et al. [28], the design and performance evaluation of TMDs for seismic control of structures, taking into account SSI, were examined. The work includes SSI modeling, identification of structural dynamic characteristics, and TMD parameter design. The authors constructed a seismic SSI model where the soil is simulated using accurate lumped parameter models (LPMs). Subsequently, a simple and practical method was

used to identify the dynamic characteristics of the structure with SSI. The identified structural frequency was then used to calculate the TMD parameters.
To evaluate the performance of the TMDs, the authors applied the model to two types of structures, three types of soils, and 100 ground motions. The results indicate that TMDs designed with the proposed method show superior performance and greater robustness compared to TMDs designed for fixed-base structures and those designed with optimization algorithms. Specifically, TMDs optimized to account for SSI effectively reduce the seismic response of structures without amplifying vibrations.
An important contribution to understanding the effects of soil-structure interaction on classically designed TMDs comes from the work of Gorini and Chisari [29]. The authors propose an interpretative model of the soil-structure-TMD system expressed in a rigorous non-dimensional form and conduct a global sensitivity analysis of the system's performance under harmonic loading. The authors aim to develop a detailed understanding of the factors that influence TMD performance in different structural configurations and soil conditions and critically evaluate two design methodologies proposed in the literature in light of the proposed interpretative model.
The proposed non-dimensional model replaces the more common single-degree-of-freedom (SDOF) system assumed for fixed-base conditions and is validated against the results of a more refined numerical model. It is then employed for an extensive analysis of TMD performance.
The sensitivity analysis indicates that TMD effectiveness is primarily controlled by a limited number of non-dimensional parameters. In addition to the parameters provided by Den Hartog's solution (mass, frequency, and damping ratios of the TMD) and structural damping, other determining factors are directly related to soil-structure interaction: the structure-to-soil relative stiffness, the foundation aspect ratio, the slenderness, and the normalized radius of gyration of the structure.
Three performance regions were identified. The first is where soil-structure interaction has a positive effect on TMD performance. This occurs in configurations with limited rocking response, such as squat or medium-slender structures, and moderate dynamic coupling between the structure and the soil. In these cases, Den Hartog's solution still represents an optimized

design criterion. In the second region, referred to as neutral, both the TMD and the soil contribute to mitigating internal forces in the structure, but the TMD partially loses its effectiveness, with structural oscillations greater than those in the fixed-base case. In this region, the choice between the two design solutions must be evaluated on a case-by-case basis. The third performance region represents cases where soil-structure interaction has a negative effect on TMD performance, especially when soil stiffness is much lower than structural stiffness. In these cases, the dynamic behavior of the structure is essentially controlled by the foundation soil, with combined sliding and rotation causing a complete detuning of the translational TMD.

1.3 Motivation of the work and metodology

The growing need to retrofit existing buildings, which were not originally designed to withstand seismic events, motivates this work into the application of Tuned Mass Dampers as a dual-purpose intervention. Existing retrofitting techniques often focus on structural strengthening, base isolation, or energy dissipation devices; however, these methods can be invasive, costly, or limited in their adaptability to different building typologies. In this context, the TMD approach investigated in this work offers an innovative alternative that not only improves seismic performance but also provides additional functional space, as the TMD is realized as a superstructure addition suitable for residential use.

A key aspect of this work is the critical evaluation of existing TMD formulations through a twofold modeling strategy. Initially, TMD performance is examined using a case study of existing reinforced concrete structure with fixed-base conditions. This preliminary analysis highlights the strengths and limitations of conventional (fixed base formulations) approaches when applied to non-seismically designed structures. Building on these insights, the research advances to a more comprehensive investigation by incorporating accurate geotechnical models. In this phase, a fully coupled soil-structure-TMD system is developed, which represents a significant innovation in the field. This integrated model captures the complex dynamics of the entire soil-structure-TMD system, thereby providing a more realistic assessment of the TMD's effectiveness in mitigating seismic forces.

The main novelty of the work results in an integrated formulation for TMD design, which bridges the gap between structural retrofitting and soil-structure interaction. By addressing multiple aspects, the proposed formulation lays the groundwork for a versatile retrofitting solution. This methodology not only enhances the seismic resilience of existing buildings but also opens new avenues for multi-functional interventions that are less disruptive and more adaptable to a variety of urban environments.

1.4 Organization of the work

In Chapter 2, a novel formulation for Tuned Mass Dampers (TMDs) is developed, starting from the equations of motion for a two-degree-of-freedom system subjected to generic forcing functions. A distinguishing feature of this formulation is the use of mass ratios, specifically, the ratio between the TMD mass and the structural mass, that are significantly higher than those adopted in conventional approaches. After processing the results, design charts are produced, enabling the identification of optimal TMD configurations that minimize the structural response in terms of displacements and absolute accelerations. This formulation is then applied to a case study involving a four-story existing framed building, where the TMD's efficiency is demonstrated through reductions in interstory drifts and overall structural damage.

Building on the previous work, Chapter 3 tests the same TMD formulation within a high-fidelity, 3D coupled soil-structure model. The objective here is to assess the impact of soil-structure interaction on the performance of a TMD designed under fixed-base assumptions. The case study in this chapter considers an eight-story existing building, sharing the same geometry as the earlier case, which is subjected to natural seismic events. The building's response is examined in detail, highlighting the modifications in TMD efficiency due to the dynamic interplay between the structure and the supporting soil.

Chapter 4 introduces an innovative analytical formulation for the design of TMDs in integrated soil-structure systems. This approach stands out from existing literature by incorporating a wide range of structural and geotechnical factors, thereby offering a more comprehensive and realistic design tool. The chapter details the methodological procedure used to develop the formulation and presents key synthetic results.

Chapter 5 provides a validation of the proposed method. To validate the proposed procedure, simplified models as well as advanced models have been adopted for comparisons with regards to standard design procedures.
Together, these chapters not only advance the theoretical understanding of TMD applications in non-seismically designed existing buildings but also offer practical design solutions that effectively enhance seismic resilience through both traditional fixed-base and advanced soil-structure integrated models.

2 CHAPTER 2
A DESIGN APPROACH FOR SEISMIC RETROFITTING THROUGH LARGE MASS-RATIO TMD

2.1 Introduction and metodology

The study and application of TMDs in structures, as discussed in the previous chapter, can vary widely depending on the different types and technologies available. The quickest way to address the problem is to consider the structure + TMD system as a two-degree-of-freedom dynamic system.
For existing structures, this system can be structured as follows: the first mass, with its associated stiffness and damping, represents the existing structure, while the second mass represents the TMD. In this way, the dynamic properties of the existing structure, which are known, are simplified through a single-degree-of-freedom system (representing, for example, the first mode response), and the TMD, whose properties are the subject of design, is represented by the second mass.
This approach is certainly convenient where the model assumptions hold true: the structure under analysis must exhibit a translational first mode response, which is typical of regular structures in both plan and elevation. Additionally, for the results presented later to be practically applicable, it is necessary that a high percentage of participating mass is involved in the first mode response, which generally occurs in medium-low-rise structures.
It is worth noting that, in the context of employing a TMD on an existing building, it is sufficient to consider an elevation of one or more floors that dynamically act as a passive vibration control system. The connection between the existing structure and the TMD will be designed to reproduce the same properties (stiffness and damping) derived from the analysis phase. Figure 2.1 illustrates a schematic of this seismic risk reduction system, which can replace or complement a traditional structural reinforcement system.

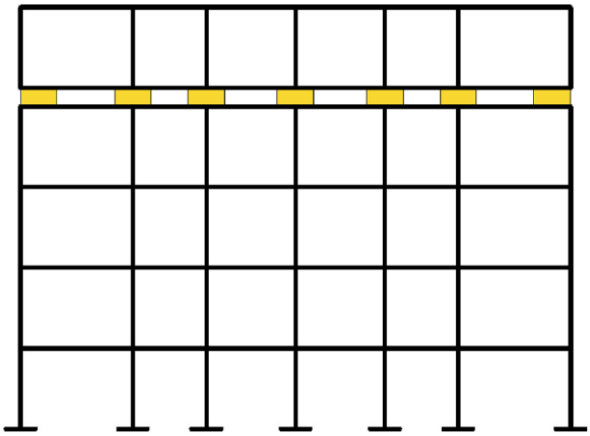


Figure 2.1 – Vertical section of the reference building and seismic-resistant superelevation

The study of a two-degree-of-freedom system subjected to a generic forcing function is carried out through the formulation of the equations of motion:

$$m_b(\ddot{u}_g + \ddot{x}_b) + c_b\dot{x}_b + k_b x_b - c_{tmd}\dot{x}_{tmd} - k_{tmd}x_{tmd} = 0 \tag{2.1}$$

$$m_{tmd}(\ddot{u}_g + \ddot{x}_b + \ddot{x}_{tmd}) + c_{tmd}\dot{x}_{tmd} + k_{tmd}x_{tmd} = 0 \tag{2.2}$$

The Eq. (2.1) refers to the lower mass (the primary system) and Eq. (2.2) to the upper mass (the TMD). The quantities $x_b(t), \dot{x}_b(t), \ddot{x}_b(t)$ represent the relative displacement, velocity, and acceleration of the lower mass with respect to the ground; $x_{tmd}(t), \dot{x}_{tmd}(t), \ddot{x}_{tmd}(t)$ represent the relative displacement, velocity, and acceleration of the TMD with respect to the primary system; $\ddot{u}_g(t)$ is the ground motion; m_b, c_b, k_b are the mass, damping coefficient, and stiffness of the base mass, and $m_{tmd}, c_{tmd}, k_{tmd}$ are those of the upper mass, i.e., the TMD.
Eqs. (2.1) and (2.2) can be rewritten by normalizing all terms with respect to the mass, resulting in units of acceleration:

$$(1 + \bar{m})\ddot{x}_b + \bar{m}\ddot{x}_{tmd} + 2\xi_b\omega_b\dot{x}_b + \omega_b^2 x_b = -(1 + \bar{m})\ddot{u}_g \tag{2.3}$$

$$(1+\bar{m})\ddot{x}_b + \bar{m}\ddot{x}_{tmd} + 2\xi_b\omega_b\dot{x}_b + \omega_b^2 x_b = -(1+\bar{m})\ddot{u}_g$$

(2. 2)

$$\ddot{x}_{tmd} + \ddot{x}_b + 2\xi_{tmd}\omega_{tmd}\dot{x}_{tmd} + \omega_{tmd}^2 x_{tmd} = -\ddot{u}_g \quad (2.4)$$

With $\bar{m}$ mass ratio, defined as ratio between the TMD and main structure's masses ($\bar{m} = m_{tmd}/m_b$); ξ_b and ξ_{tmd} are the damping ratios of base structure and TMD, respectively. ω_b and ω_{tmd} are the angular frequencies defined as:

$$\omega_b = \sqrt{\frac{k_b}{m_b}} \quad (2.5)$$

$$\omega_{tmd} = \sqrt{\frac{k_{tmd}}{m_{tmd}}} \quad (2.6)$$

The solution of the system of equations (2.3) and (2.4), in the case of a generic forcing function, can be achieved through step-by-step integration. One possible numerical approximation method is the Newmark method, which approximates the variability of accelerations with a linear trend:

$$\ddot{x}(t) = \ddot{x}_j + \frac{t-t_j}{\Delta t}(\ddot{x}_{j+1} - \ddot{x}_j) \quad (2.7)$$

By integrating equation (2.7) and through successive algebraic steps, the unknown quantities to be substituted into equations (2.3) and (2.4) are obtained.
It should be noted that in equations (2.3) and (2.4) the term $\ddot{u}_g(t)$ is a known term at each time step *j* of the integration. In fact, the choice of the forcing function is completely arbitrary and depends on the specific case and the limit state to be analyzed. One way to consider different time histories of ground motion, as provided in the technical standards, is to refer to seismic hazard through a response spectrum. From this response spectrum, any number of

compatible ground motion histories can be obtained and used in step-by-step integration.
In this initial part of the study, the selected response spectrum is the one provided in Eurocode 8 for rigid outcrop (soil type A) with a PGA of 0.15 g, and from this, 100 compatible accelerograms with a duration of 20 seconds each were obtained. The generation of ground motion histories was performed using the software Simqke [30], setting the compatibility conditions as provided in the standards of Eurocode 8 [31].
Figure 2.2 shows the original spectrum and the average spectrum of the 100 accelerograms.

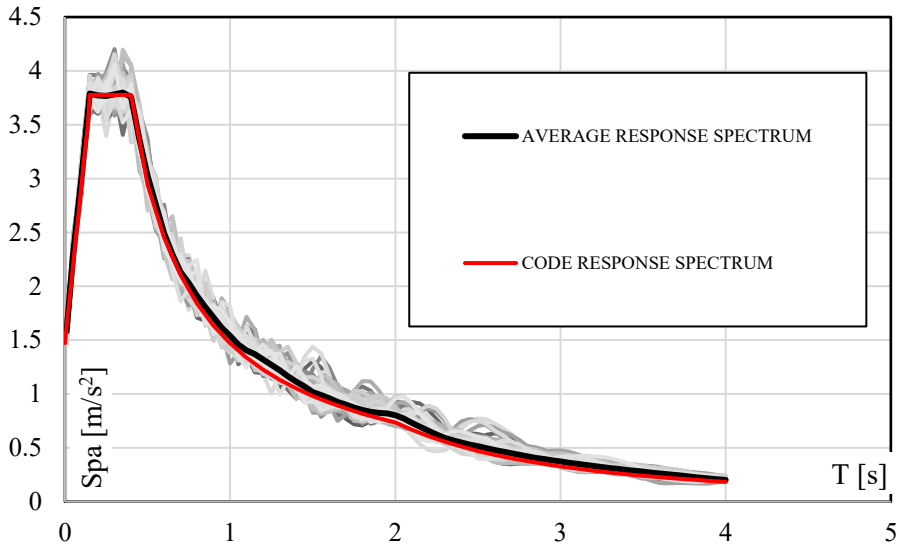


Figure 2.2 – Average response spectrum and code response spectrum

2.2 Parametric analysis

By using a simple model that describes the dynamic behavior of a structure-TMD system, it is possible to search for optimal solutions that minimize the structural response. To achieve this, a parametric analysis was conducted, considering the variability of all the quantities involved in the previously described two-degree-of-freedom model. By selecting different vibration

periods for the structure and the TMD, different mass ratios, and damping values, unique configurations are obtained and analyzed.
By comparing the response of the same structure equipped with different TMDs, it is possible to evaluate the efficiency of each combination and identify the optimal solution, aiming to reduce relative displacement (structural drift) or absolute acceleration (inertial forces). Table 2.1 provides a legend of the combinations considered in the parametric analysis.

Table 2. 1 – Combinations adopted for the parametric analysis

T_b	0.1→4.0 step 0.1	[s]
T_{tmd}	0.04→4.0 step 0.04	[s]
$\overline{m}$	0.1, 0.2, 0.3, 0.4	[-]
ξ_{tmd}	0.15, 0.20, 0.25	[-]

The terms T_b and T_{tmd} of Table 2.1 represent the fundamental period of the main system and TMD, respectively, considered with fixed base. The quantities are related at ω_b and ω_{tmd} through the expressions:

$$T_b = \frac{2\pi}{\omega_b} \tag{2.8}$$

$$T_{tmd} = \frac{2\pi}{\omega_{tmd}} \tag{2.9}$$

The complete interpretation of the results of the parametric analysis, varying all considered quantities, must be sought in a four-dimensional space. Since 100 ground motion histories were used, for each combination of the parameters in Table 2.1, there are as many time histories of the displacements and accelerations of the masses in the 2DOF system. As is customary, the spectral value of displacement and acceleration, i.e., the maximum (in absolute value) over the entire duration, is of interest in these time histories. Given the large number of solutions due to the multiplicity of seismic events, the results were treated statistically to obtain values with a 95% fractile.

For a reasonable representation of the results of the parametric analysis, it is convenient to fix some quantities, such as the mass ratio and damping, to represent the solutions in three-dimensional space. Fixing these two quantities reveals an extension of the classical response spectra to the case of 2 degrees of freedom. While the typical representation is that of spectral displacement/acceleration as a function of the fundamental period of the single-degree-of-freedom system, the presence of a second mass means that this spectral quantity is a function of both periods. This representation can be easily interpreted from Figs. 2.3-2.4, noting how it is possible to obtain the classical spectrum when the condition $T_{tmd} = 0$ is met.

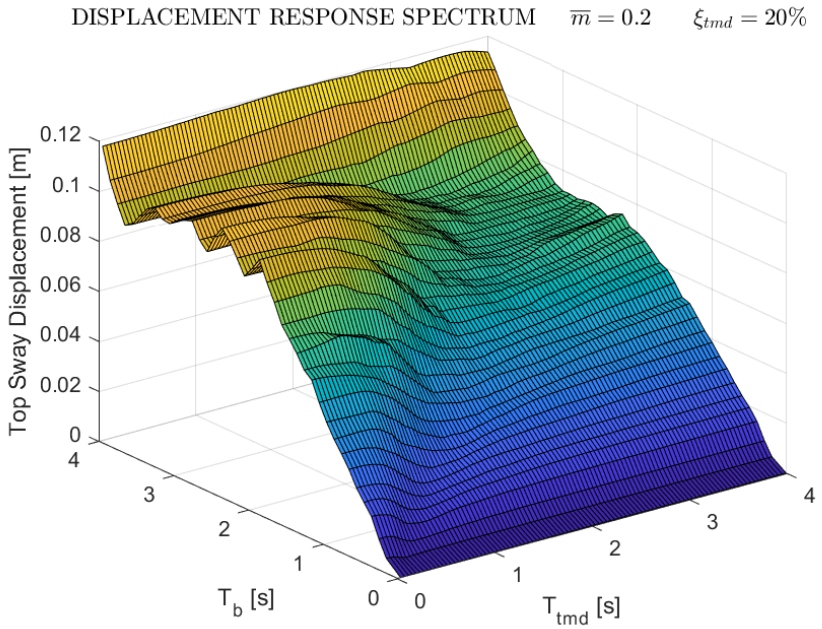


Figure 2.3 – Displacement response spectrum of the base bass

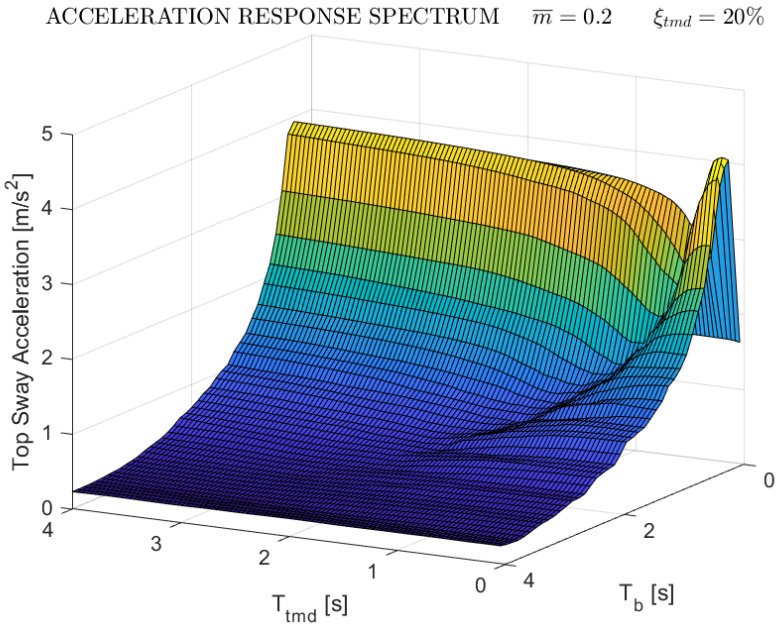


Figure 2.4 – Acceleration response spectrum of the base bass

By observing the surfaces in Figs. 2.3-2.4, regions corresponding to the minima of the structural response can be identified. It is important to identify these optimal solutions as the fundamental period of the structure and the mass ratio vary, in addition to the damping of the TMD (which, as will be seen, plays a less decisive role). For this purpose, it is useful to represent sections of these surfaces, varying the involved quantities.

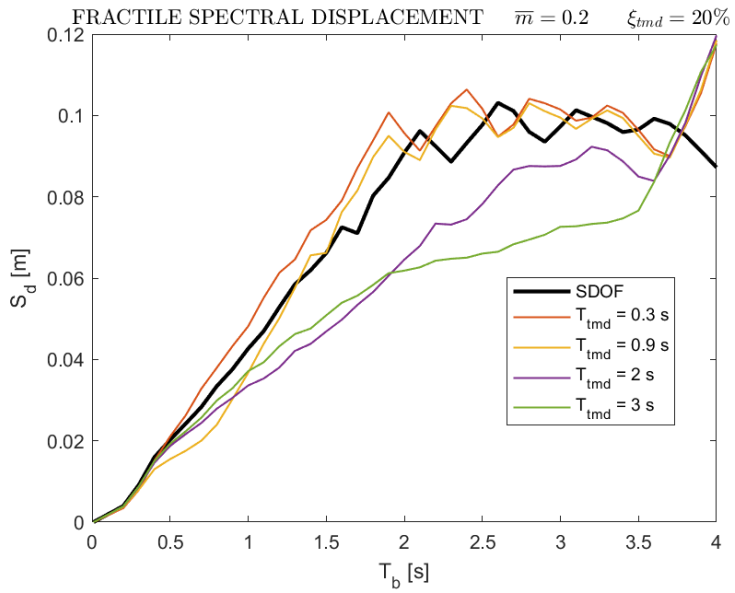


Figure 2.5 – Sections of displacement response spectrum for different period of TMD, T_{tmd}

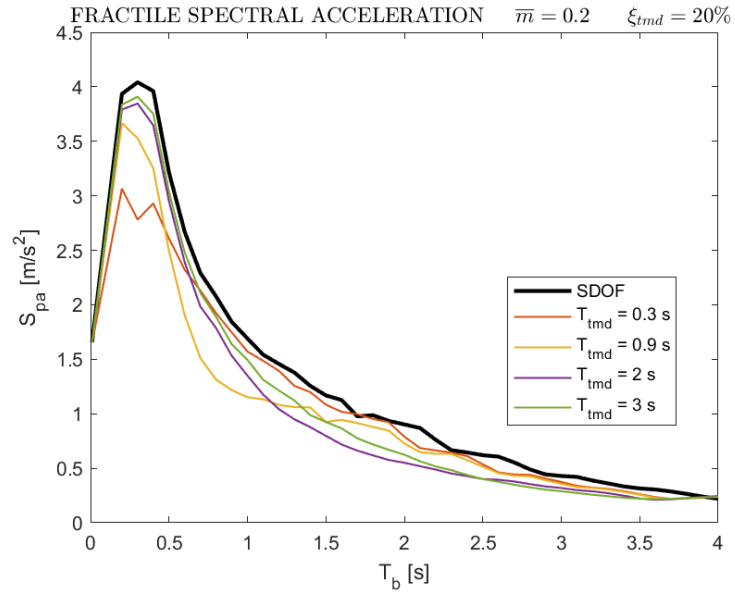


Figure 2.6 – Sections of acceleration response spectrum for different period of TMD, T_{tmd}

Figs 2.5-2.6 show the trend of spectral displacement and acceleration as a function of the fundamental period of the structure. The thick black curve represents the SDOF, i.e., the structure not equipped with a TMD. The other curves represent systems with a variable fundamental period equipped with TMDs of a fixed period. By comparing the figures, the effectiveness of a high mass ratio TMD in reducing accelerations in the low-period regions (0-0.5 s) and in reducing displacements in the range of long periods (1.5-3 s) can be observed. It is also possible to make sections of the surfaces in Figs 2.3 and 2.4 at fixed values of the system's base period. In this way, the variability of the spectral quantities allows for identifying the optimal TMD solutions for each base period value.

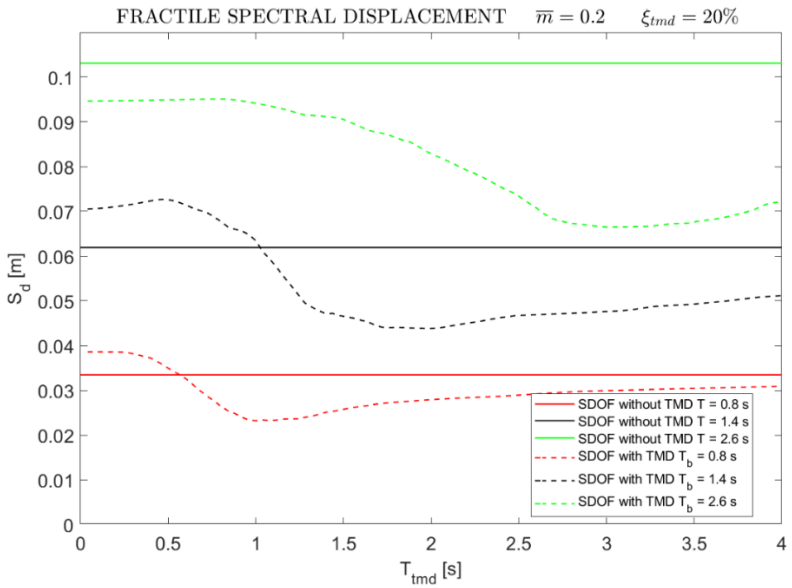


Figure 2.7 – Sections of acceleration response spectrum for different period the base, T_b

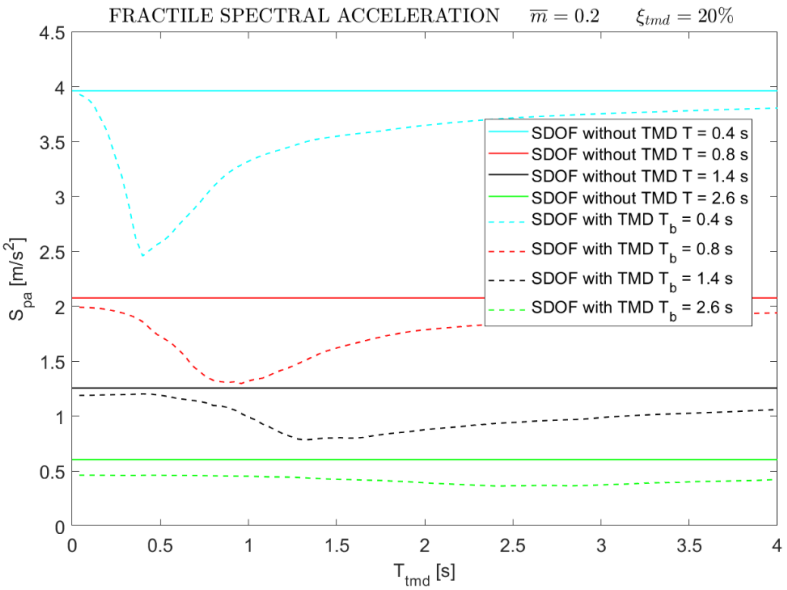


Figure 2.8 – Sections of acceleration response spectrum for different period the base, T_b

In Figures 2.7 and 2.8, the solid horizontal lines represent the value of the spectral quantity evaluated on an SDOF with a fixed period, while the dashed lines represent the spectral trend of systems with a fixed base period and a TMD with a variable period. The optimal configurations are clearly positioned, aligning with what is known from the scientific literature on the subject, and are found in systems where the TMD period is close to that of the main system. Although the figures shown above are clearly interpretable, they have the disadvantage of presenting the results in dimensional terms, which can obscure the actual benefit in terms of displacement and acceleration reduction.
To get a comprehensive view and quantify the variability of these quantities, the spectral quantities can be normalized as follows:

$$d = \frac{S_{d,SDOF+TMD}}{S_{d,SDOF}} \tag{2.10}$$

$$a = \frac{S_{pa,SDOF+TMD}}{S_{pa,SDOF}} \tag{2.11}$$

These normalized quantities represent the ratio between the spectral quantity considered in the two-degree-of-freedom system (i.e., structure + TMD) and that recorded on the same structure without a TMD. By adopting discrete values for the fundamental period of the structures and overlaying the results of analyses with different damping values of the TMD, a design chart useful for identifying optimal regions is obtained.

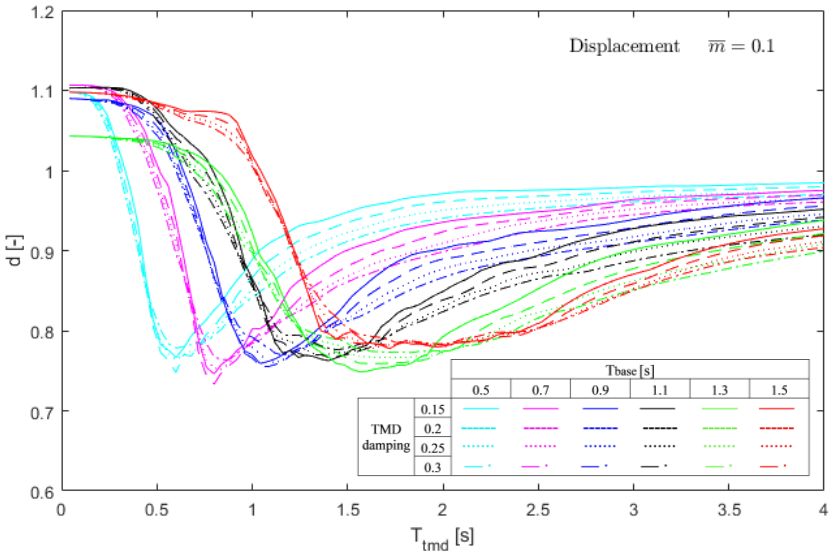


Figure 2.9 – Normalized displacements of 2DOF with 10% mass ratio

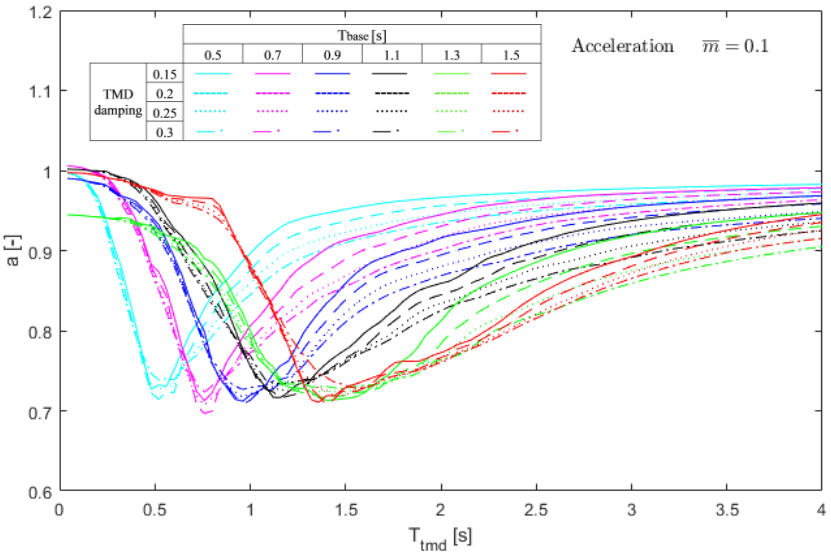


Figure 2.10 – Normalized accelerations of 2DOF with 10% mass ratio

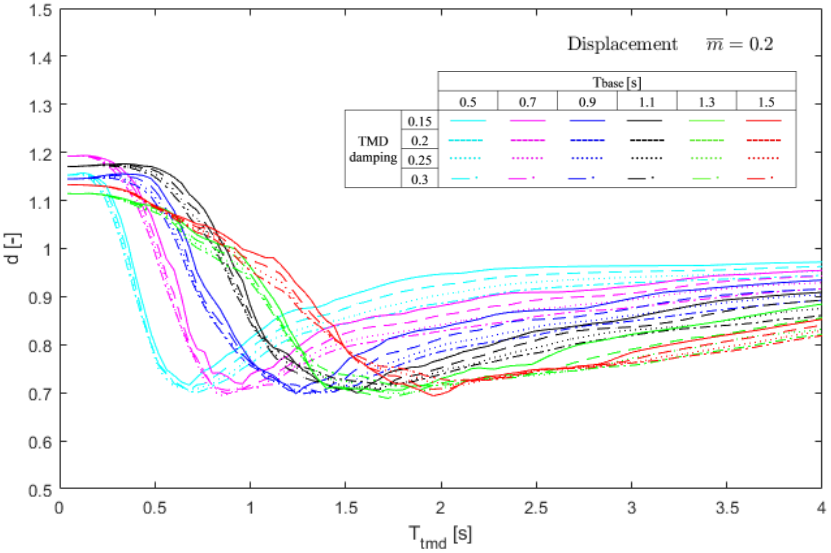


Figure 2.11 – Normalized displacements of 2DOF with 20% mass ratio

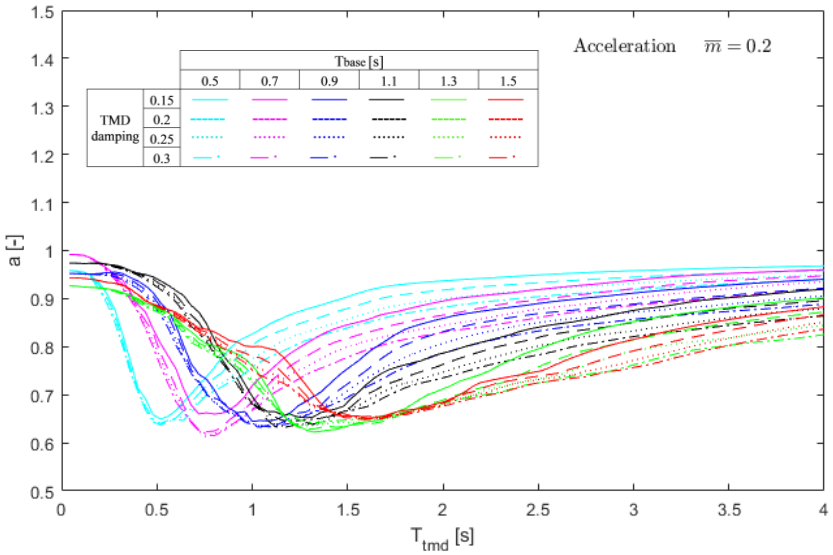


Figure 2.12 – Normalized accelerations of 2DOF with 20% mass ratio

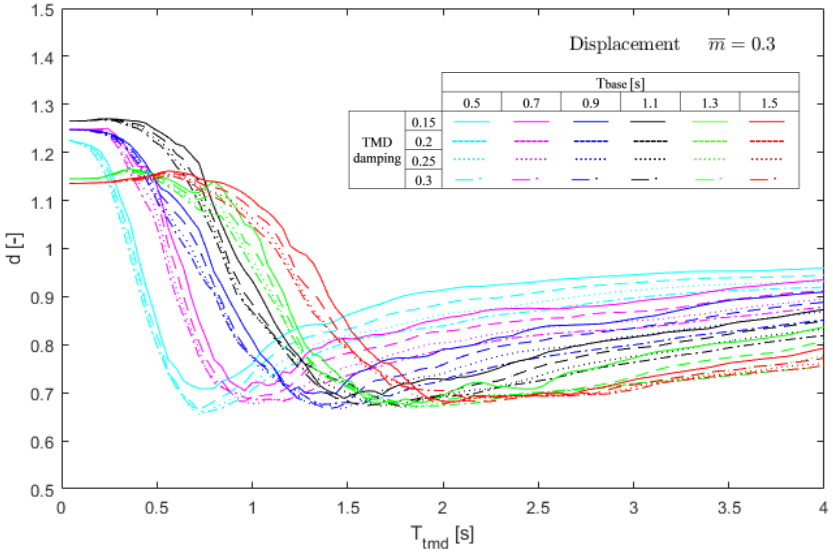


Figure 2.13 – Normalized displacements of 2DOF with 30% mass ratio

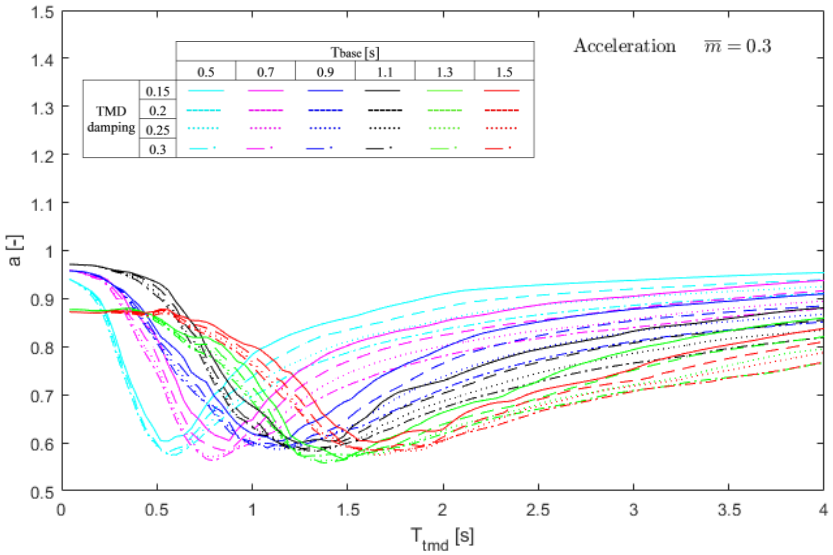


Figure 2.14 – Normalized accelerations of 2DOF with 30% mass ratio

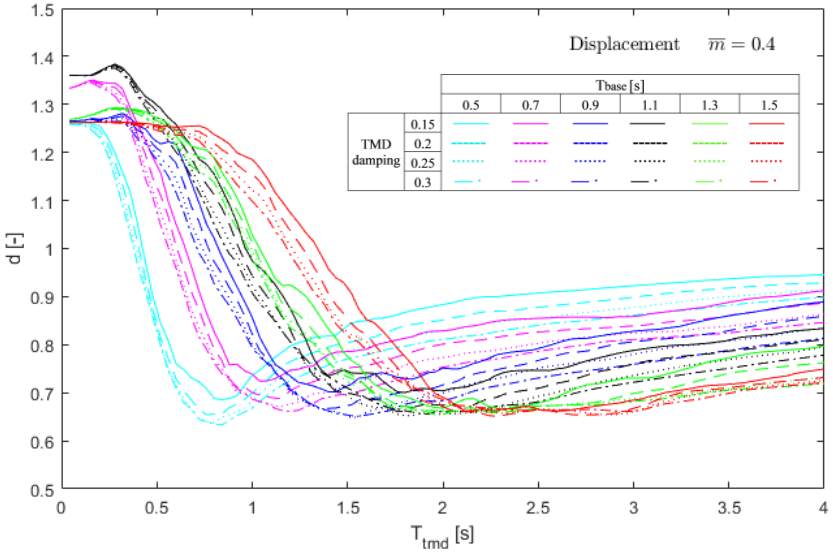


Figure 2.15 – Normalized displacements of 2DOF with 40% mass ratio

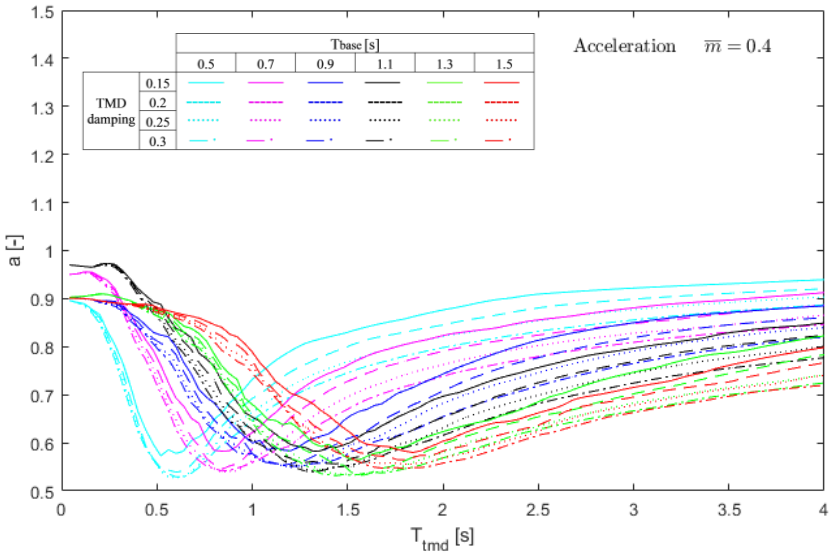


Figure 2.16 – Normalized accelerations of 2DOF with 40% mass ratio

From the curves in Figures 2.9 – 2.16, a common trend can be observed in all cases. The normalized spectral quantity, obtained as the ratio between that of the SDOF + TMD system and that of the SDOF system, assumes a value around unity for null TMD periods, a condition corresponding to a mass perfectly constrained to the existing one. The starting value is not and cannot be unitary because that condition corresponds to an SDOF with a greater mass, and thus a different period.

$$\omega = \sqrt{\frac{k}{m_{tot}}} = \sqrt{\frac{k}{m(1+\overline{m})}} \tag{2.12}$$

The trend of the considered quantities then decreases more as the mass ratio increases, rise and tend towards unity for high values of the TMD period. The damping factor of the TMD, represented by lines with different dash patterns, only causes noticeable variations in the normalized quantities starting from the optimal region onwards, with an effect that tends to remain constant even with high values of Ttmd. The curves show a general improvement as the

TMD damping increases. The quantity most correlated with efficiency, however, is the mass ratio.
The benefit of TMDs with a high mass ratio is not limited to the greater reduction of spectral quantities: if the same spectral quantities but referred to different mass ratios are compared, it can be seen that as this ratio increases, the range of optimal periods also broadens. This characteristic of high mass ratio TMDs, which represents greater robustness, is well-known in the scientific literature. Such TMDs can preserve their efficiency even in the presence of phenomena not considered during the design phase: structural detuning due to the excursion into the inelastic range of structures, soil-structure interaction that alters dynamic behavior compared to fixed-base conditions, etc.

2.3 Application to Fixed Base structures

The results shown in the previous section, obtained on a simplified two-degree-of-freedom system, can be applied to the case of real structures. The approximation is in the fact that, by considering a 2DOF system, it is possible to reduce the dynamic response to a single-mode response. The vibration mode on which to tune the TMD can be chosen once the dynamic characterization of the structure under examination is carried out. In the case of a structure that is regular in plan and elevation and has a limited number of floors, it is possible to obtain a good percentage of mass participating at the fundamental mode. For this purpose, to apply the results obtained in the previous section, a case study that meets the above requirements was selected. The case under examination consists of an existing reinforced concrete frame structure with 4 stories. The building has a rectangular plan with dimensions of approximately 22.5 x 24.5 meters and an interstory height of 3.3 meters (total height of 13.2 meters) and is located in a medium seismicity zone. The geometric and mechanical characteristics of the members were obtained from a simulated design carried out in accordance with a non-seismic code [32], and thus only gravitational actions were considered during the design phase. For the concrete, a cubic compressive strength of 25 MPa was adopted, and for the steel, an ultimate strength of 375 MPa (FeB38k). As is customary for existing buildings, factors such as aging and uncertainties in strength were considered through a confidence factor.

It is also noted, as shown in Figure 2.17, that the building does not have continuous frames in all directions. As was common practice in the construction era referenced for the building, except for the perimeter frames, beams connecting the columns were not always provided if they did not serve as support for the slabs. It is common to find in older frame buildings that floor beams protrude from the slab only to close the slab fields.
Despite these peculiarities regarding frames and their positioning, slabs possess a sufficiently thick superior concrete topping to ensure rigid diaphragm behaviour. In other words, the inertial forces can be distributed in plan according to the stiffness of the structural elements; therefore, the degrees of freedom associated with each floor level are three: the two horizontal translations and the rotation about the building's vertical axis.
The floors have a permanent load of 6.14 kN/m² and a variable load of 2 kN/m², as provided in the Italian code for residential environments, with a concurrency coefficient for seismic loads of 0.3. The total seismic mass of the building is 3305.6 tons.
Since the structure is doubly symmetric in plan, the dynamic response is translational, and the mass involved in the two horizontal directions is the same or very similar (mode 1 and mode 2). The approximation of the system to a 2DOF model in this case is therefore sufficient, as shown in the table of modal properties of the structure (Table 2.2).

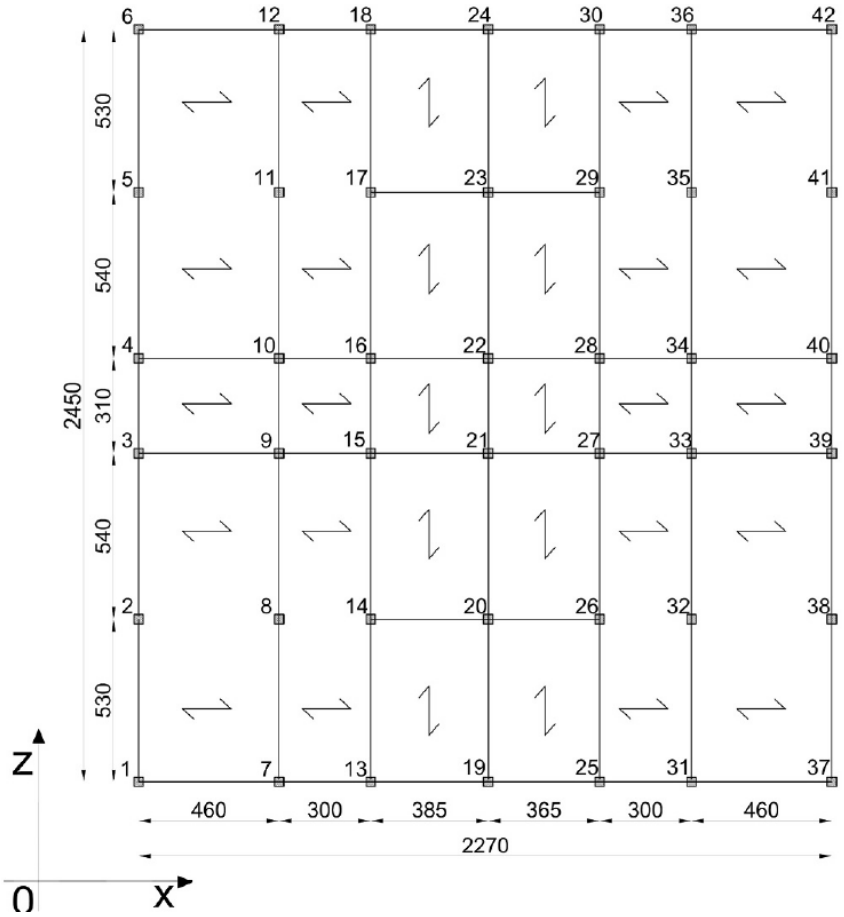


Figure 2.17 – Plan scheme of the reference building

Table 2.2- Modal characterization of the structure

Mode [-]	Period [s]	U_x [%]	U_y [%]	U_z [%]	R_x [%]	R_y [%]	R_z [%]
1	0.947	77.74	0	0	0	5.24	0.03
2	0.862	0	78.33	0	4.41	0	0.45
3	0.855	0.03	0.44	0	0.02	0	80.76

4	0.346	15.57	0	0	0	12.12	0
5	0.314	0	14.4	0	10.74	0	0.34
6	0.313	0	0.36	0	0.28	0	13.13

To apply the results of the parametric study to the case study and thus design the elevation system that acts as a TMD, once the desired mass ratio $\overline{m}$ has been chosen, it is sufficient to use the following formulation:

$$k_{tmd} = 4\pi^2 \frac{m_{tmd}}{T_{tmd}} \tag{2.13}$$

Where m_{tmd} is evaluated through the product of the mass ratio $\overline{m}$ and the modal mass of the mode taken as a reference. The period T_{tmd} can be determined from the charts in Figures 2.9-2.16.
A mass ratio of 20% was chosen as a reference; therefore, from Figure 2.11, looking at the blue curves (T_{base}=0.90), the optimal period of the TMD is around 1.3 seconds. The damping value, was set to 0.2. Using the formula 2.12, with m_{tmd} equal to 513.6 tons and T_{tmd} equal to 1.3 seconds, an overall stiffness of 15563 kN/m is required for the system.
Once the connection system between the existing structure and the elevated part is designed in terms of stiffness and damping, the next step is to determine the arrangement of the devices in the plan. This operation can depend on various requirements:

- Costs
- Availability of compatible devices in the market
- Overall mechanical properties required for the elevation system

Regarding the last two points, it is worth noting that, since the devices function in parallel, the total stiffness will be the sum of the individual stiffnesses, and the maximum displacement (in translational terms, neglecting torsional rotation) will be common to all. Therefore, the choice of the number of devices must necessarily meet displacement requirements (maximum

stroke that can be supported by a single device), while the arrangement must ensure sufficient torsional stiffness of the elevation system.
In the case under examination, 22 elastomeric devices were used along the outer perimeter, and 20 flat sliding devices were placed at the internal columns. The elastomeric devices are characterized by a force-displacement relationship that is well approximated by a bilinear relation, while the sliding devices follow a perfectly plastic relationship (Coulomb friction law). The isolators used have an initial stiffness of 647 kN/m and a secondary stiffness of 184 kN/m.
The modeling of the structure and the TMD and subsequent analyses were performed in the SeismoStruct environment [33], which allows fiber modeling for structural elements and includes elements such as sliders and elastomeric isolators in its library.
To ensure correspondence between the dynamic analyses and the parametric study, the response spectrum used as input is the same. For the analyses, however, as provided in the technical standards [31], 7 compatible accelerograms are used. The average spectrum of the 7 artificial events is shown below.

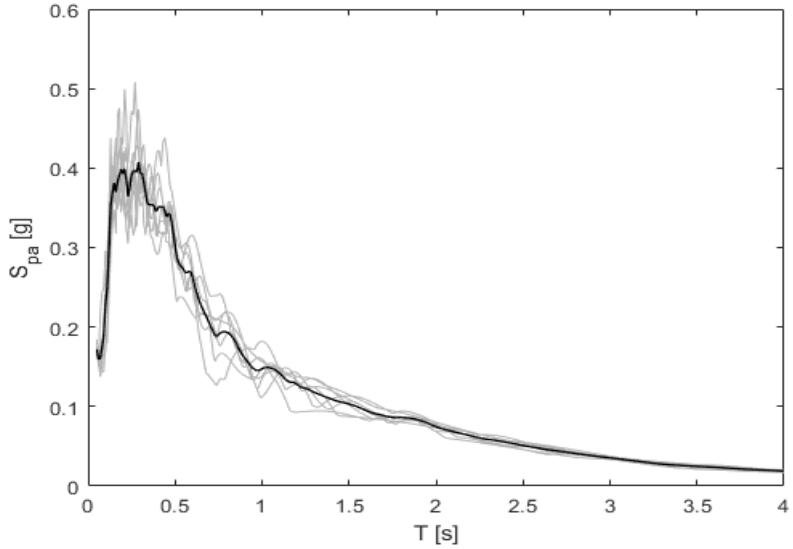


Figure 2.18 – Average response spectrum of the 7 events

The analyses carried out on the existing structure are incremental dynamic analyses (IDA) to consider the different limit states provided by the standards. Starting from a PGA of 0.15 g up to a value of 0.285 g, Figures 2.19 and 2.21 show the average results in terms of maximum interstory drift ratio (MIDR) and the number of damaged elements, comparing the existing structure and the structure equipped with a TMD with a mass ratio of 20%.

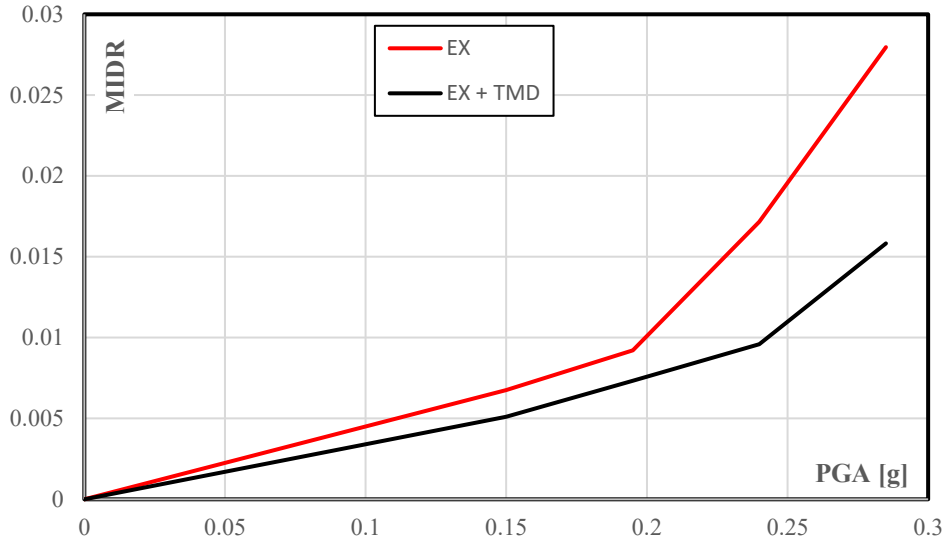


Figure 2.19 – MIDR comparison between existing structure and structure with a 20% mass ratio TMD, as function of PGA

A general decrease in the maximum interstory drift ratio (MIDR), i.e., the maximum floor drift divided by the interstory height, can be observed. From a certain value of the PGA onwards, the existing structure clearly enters the inelastic range, while the structure equipped with a TMD maintains an elastic or slightly post-elastic behavior. Figure 2.20 shows the average MIDR (among the 7 accelerograms) evaluated at various floors corresponding to the maximum considered PGA. The maximum reduction, in correspondence with the soft story mechanism between the second and third floors, is around 40%.

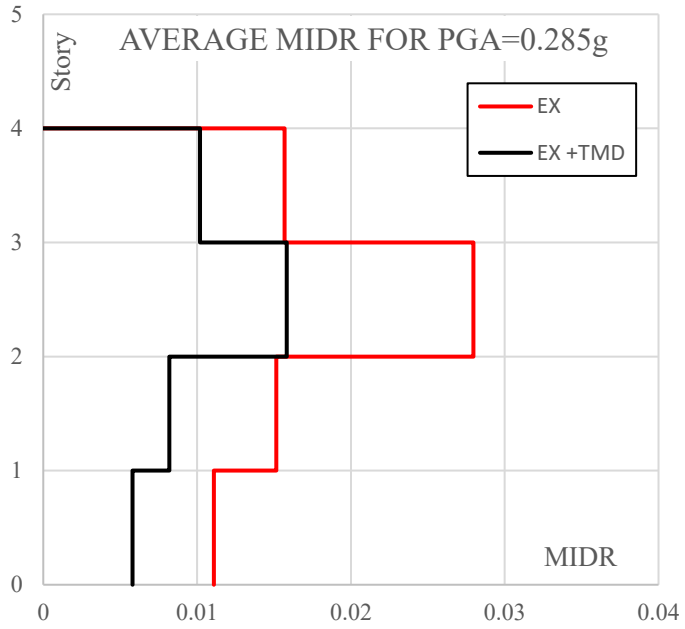


Figure 2.20 – MIDR comparison between existing structure and structure with a 20% mass ratio TMD, for a 0.285g PGA

The presence of the LM-TMD therefore raises the elastic threshold of the structure, resulting in a decrease in overall damage, for the same PGA. It can be seen that the average percentage of damaged elements at the end of seismic events is generally lower in the case of the structure with a TMD, and this decrease is greater in the case of low-intensity events. When the structure is subjected to high-intensity events that cause damage, this leads to changes in the distribution of seismic forces and, in general, in the dynamic properties that impact the efficiency of the TMD. At the maximum PGA, the percentage of damaged elements is comparable between the two structures, but it remains positive in favor of the structure with the TMD, as reported above the black bars. The difference between the two structures starts at a value of 62.35 in the case of a PGA of 0.15 g and decreases (while still remaining favorable) with increasing intensity to a value of 11.17 in the case of a PGA of 0.285 g.

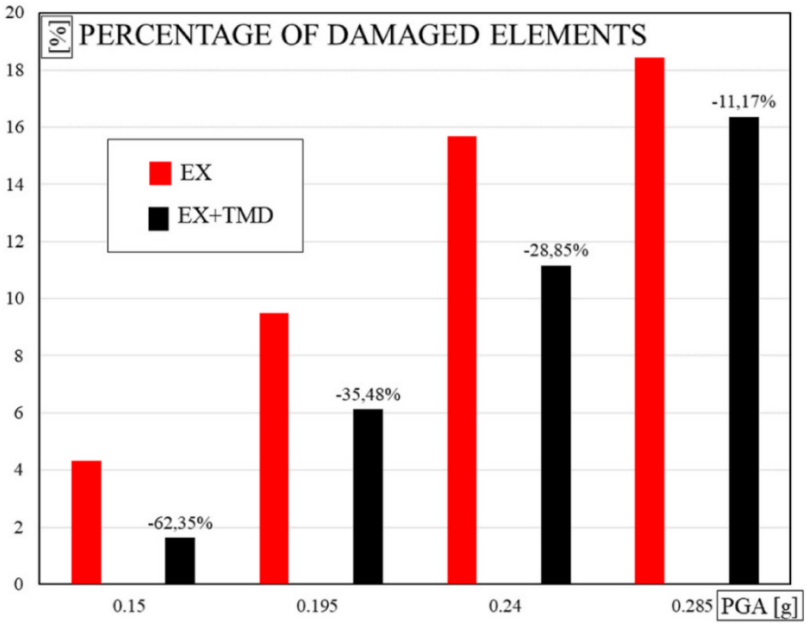


Figure 2.21 – Comparison of damaged elements ad the end of the analyses, average values between the 7 events

It is important to remember that, in addition to looking at and quantifying the effects of the TMD on the structure, attention must also be paid to those relating to the elevation system itself. As previously mentioned during the TMD design phase, it is essential to verify the compatibility of the maximum stroke required by the devices with their capacity. Figure 2.22 shows the maximum relative displacements experienced by the elevation system for all intensities, with the dashed horizontal line representing the limit value of the relative displacement between the two ends of the device.

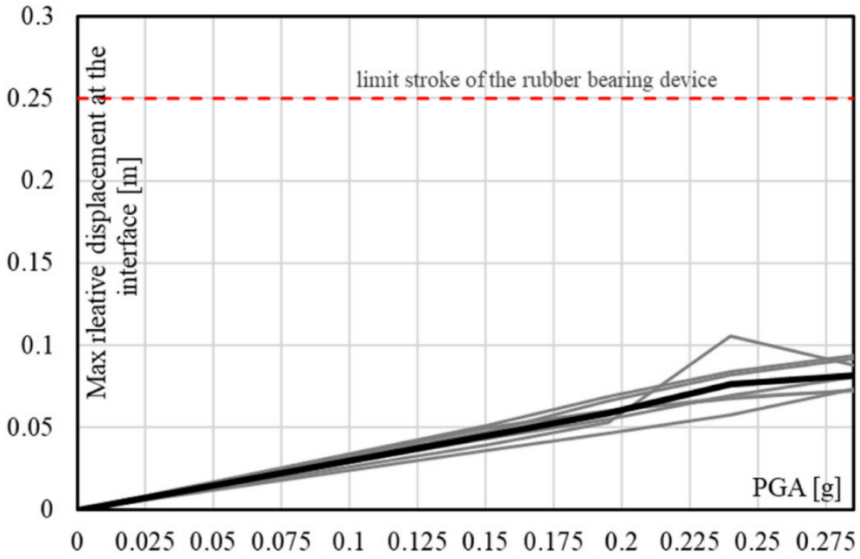


Figure 2.22 – Max stroke of the superelevation as function of PGA

In the case under examination, the elevation system functions as a TMD but can it consist of an additional floor with functionality and usage equivalent to the lower floors. Therefore, it is important to also evaluate the maximum acceleration to which the elevation system is subjected, ensuring that it does not compromise habitability or functionality. Very high values of absolute acceleration, which are responsible for inertial forces, could pose a danger to objects and potential occupants in the event of seismic events. It can be seen from Figure 2.23 that even at the maximum PGA, the elevation system experiences an absolute acceleration of less than 0.15 g, which is the lower value used in the incremental dynamic analyses.

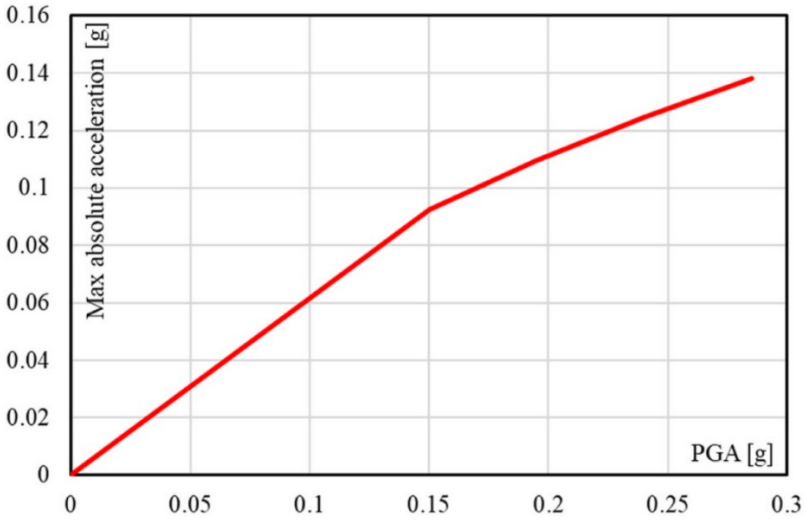


Figure 2.23 – Absolute acceleration of the TMD as function of the PGA

It is worth noting that, despite the positive effects induced by the TMD on the structure, evident in the reduction of damage and seismic risk, it is inevitable that the adoption of high mass ratios leads to increases in the axial forces of the vertical elements. In the case of existing structures, this condition cannot be overlooked, and a strength verification must always be performed.
Some considerations, however, can be made:

- Existing structures, even if designed without seismic codes, generally have good safety margins against vertical loads.
- In the case of medium-low-rise structures, the sizing of vertical members may be dictated by construction considerations rather than static ones, which means that overly small sections cannot be used, resulting in reduced static demand.
- If checks for vertical loads are negative, the reinforcement to be carried out remains limited to the vertical elements and for vertical loads. Such reinforcements are minimally invasive and quick to execute.

The design and verification procedure for the retrofitting/upgrading system using TMDs illustrated in this chapter can be schematized as shown in Figure 2.24.

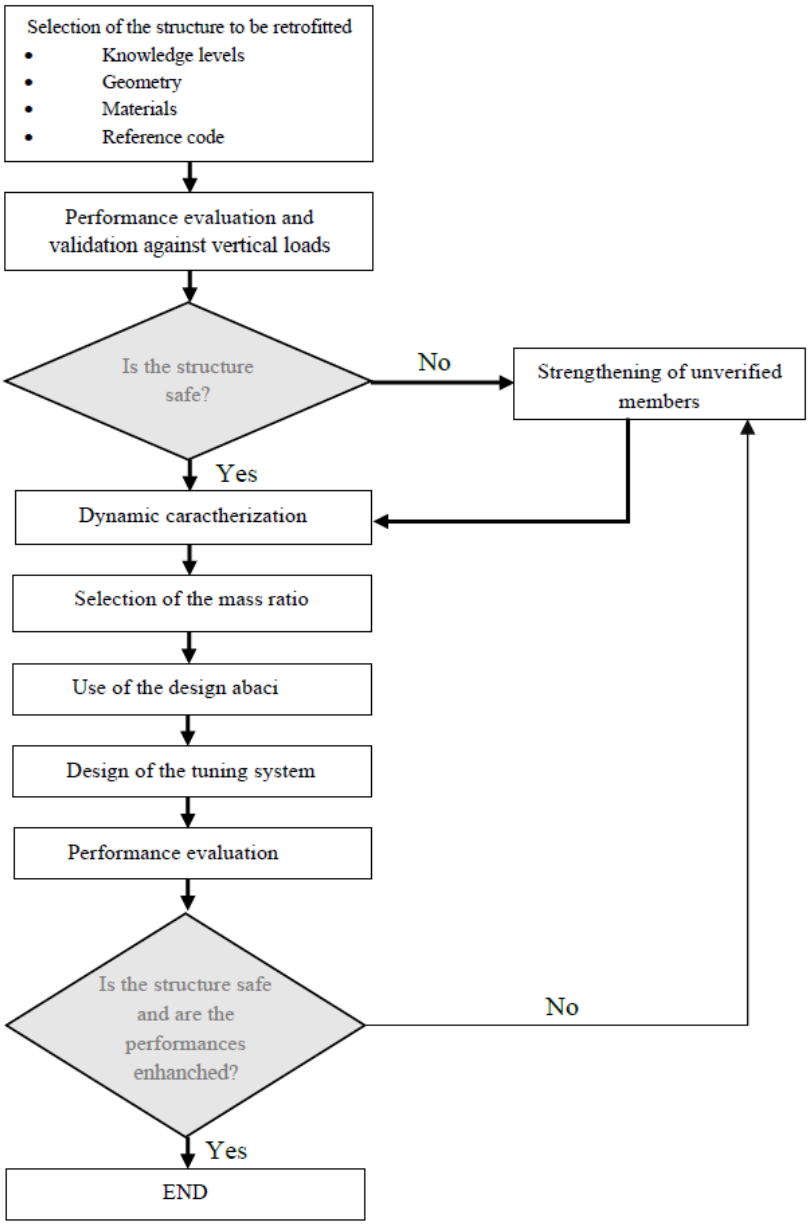


Figure 2.24 – Proposed design procedure for TMD to be installed on existing structures

3 CHAPTER 3 BENCHMARK SOIL-STRUCTURE-TMD SYSTEM: FROM HIGH-FIDELITY NUMERICAL MODELLING TO PERFORMANCE

3.1 Introduction

The dynamic behavior of structures equipped with TMDs can be negatively affected by two aspects if they are not considered during the design phase. The first aspect is the so-called "detuning" caused by the inelastic response of the structure: the TMD, initially tuned to the dynamic properties of the structure in the elastic range, loses its coupling when, during severe seismic events, the structure begins to sustain damage (formation of plastic hinges, etc.) and alters its response during the event. As seen in the previous chapter, a high mass ratio can partially limit detuning due to the greater robustness offered by LM-TMDs.

However, any structure is found on some type of soil, whose presence inevitably influences its structural response. The soil modifies the characteristics of seismic waves depending on its properties, and phenomena of amplification or damping of seismic actions can occur, which, if not properly accounted for, lead to inaccurate evaluations of structural response. These effects also impact the efficiency of TMDs, if the structures are equipped with them, leading to erroneous assessments of behavior.

Gorini and Chisari (2022) [29] studied the effect of soil-structure interaction on classically designed TMDs, i.e., under fixed-base assumptions, identifying certain performance regions. The authors identified significant quantities which, if not considered during the design phase, can cause the actual behavior to deviate from that predicted according to classical assumptions.

To understand the coupled behavior of soil-structure-TMD systems, this chapter will illustrate the simulations carried out on a complete model, where the soil, structure, and TMD were accurately modeled. The dynamic analyses were performed in the OpenSees software framework [34] using natural seismic events compatible with the referenced site as input. Subsequently, the

interpretative model of Gorini and Chisari was employed in an extensive parametric analysis aimed at formulating an integrated design law for TMDs. Most of the information and results in this chapter are also contained in a journal article by Gorini et al. [35].

3.2 Soil response and record selection

The case study under consideration is an ordinary reinforced concrete building located in the Pantano region in the south of Italy. The site has been the subject of numerous studies [36–37] and is therefore well characterized geologically and geotechnically. The structure belongs to use class 2, according to the Italian technical standards [38], and four limit states have been identified. Among these, two are serviceability limit states, the operational limit state and the damage limit state, with return periods of 30 and 50 years respectively, and two ultimate limit states, the life safety limit state and the collapse limit state, with return periods of 475 and 975 years.
Starting from the seismic demand of the Pantano region, given by the response spectrum on rigid outcrop, eight compatible natural seismic events were selected. From the PEER database (https://ngawest2.berkeley.edu/), events that meet the seismo-tectonic compatibility of the Pantano region according to Italian standards were identified, with reference to the life safety limit state (Intensity Measure IM=1). These scenarios are listed in Table 3.1, along with all the main properties.

Table 3.1- Modal characterization of the structure

No.	Record	Event name	I_A (m/s)	T_s (s)	T_m (s)	$Vs_{,30}$ (m/s)	M_w (-)	R_{jB} (km)
1	RSN 765	Loma Prieta	1.7	11.4	0.33/0.49	1428	6.93	8.84
2	RSN 1011	Northridge, Wonderland Ave.	0.2	12.7	0.44/0.33	1223	6.69	15.11
3	RSN 1091	Northridge, Vasquez Rocks Park	0.4	15.4	0.51/0.52	996	6.69	23.1
4	RSN 1165	Kocaeli	0.8	21.0	0.72/0.81	811	7.51	3.62

5	RSN 3925	Tottori, OKYH07	0.3	3.98	0.14/0.15	940	6.61	15.23
6	RSN 3954	Tottori Japan, SMNH10	0.5	16.13	0.65/0.41	967	6.61	15.58
7	RSN 4083	Parkfield	0.2	19.75	0.44/0.37	907	6.0	4.66
8	RSN 5618	Iwate	1.4	25.77	0.79/0.70	826	6.9	16.26

In Table 3.1, the quantity I_a represents the Arias intensity, T_s the significant duration, T_m the mean period, $V_{s,30}$ the average shear wave velocity in the top 30 meters of depth, M_w the moment magnitude, and R_{jb} the Joyner and Boore distance.

Due to the complexity and size of the model, the computational burden of the nonlinear analyses is substantial, and it was therefore necessary to limit the duration of the seismic events used as input. The effective duration of the scenarios was appropriately reduced to an effective duration by considering an indicator that quantifies the energy content, in this case, the Arias intensity [39].

$$I_A = \frac{\pi}{2g}\int_{t_0}^{t_f} a(t)^2 dt \tag{3.1}$$

With t_0 and t_f as the initial and final instants of the event and $a(t)$ the acceleration at instant t.

Referring to a specific scenario, the effective duration is reached at the instant when the Arias intensity is equal to 95% of the total.

In Figures 3.1 and 3.2, as an example, some quantities characterizing scenario no. 2 (Northridge, Wonderland Ave) in the two horizontal directions are shown, and in Figures 3.3 and 3.4, the same signals are reduced to the effective duration and filtered at 20 Hz. The application of the filter was intended to avoid or reduce convergence problems during dynamic analyses.

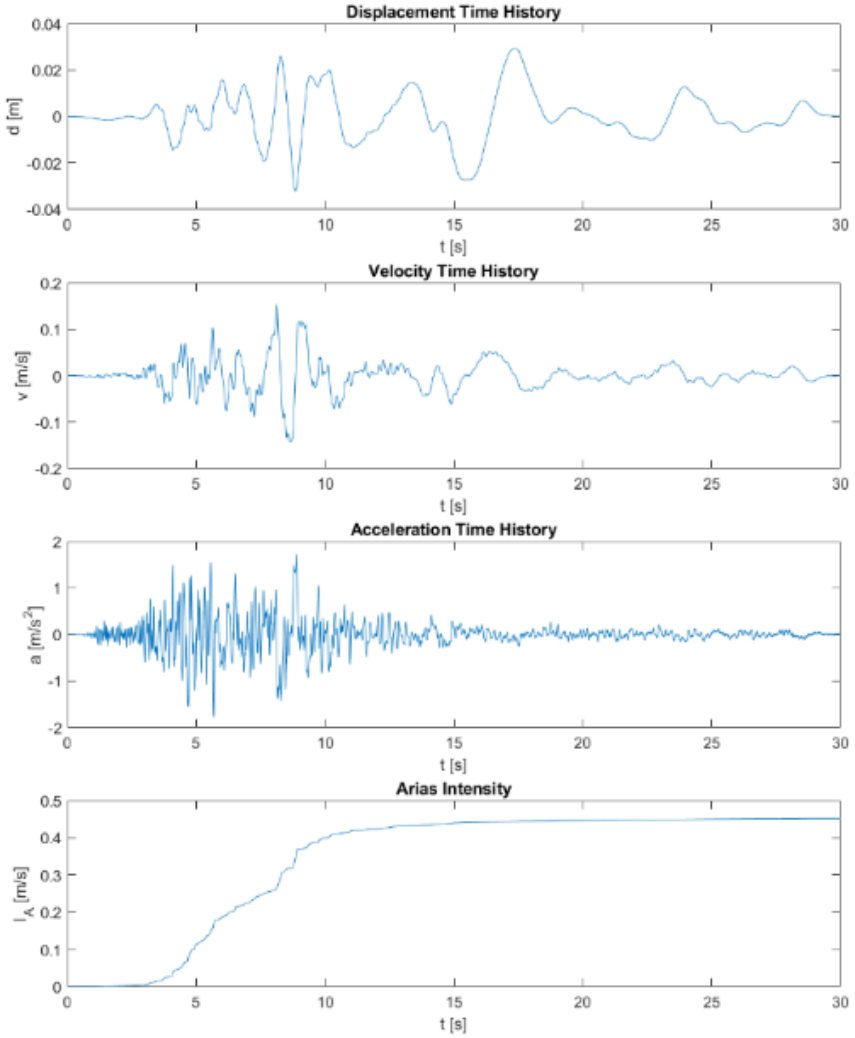


Figure 3.1 – Northridge Worderland Ave horizontal component X:displacement time history, velocity time history, acceleration time history, Arias Intensity

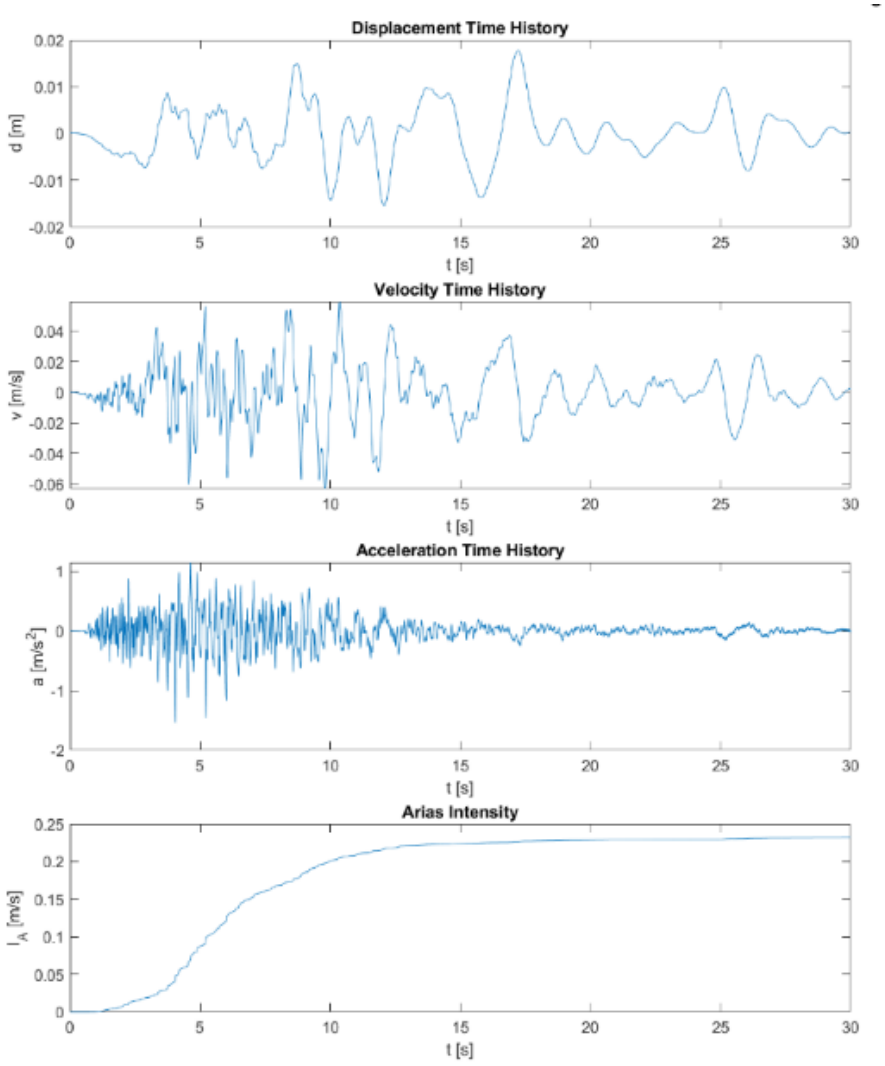


Figure 3.2 – Northridge Worderland Ave horizontal component Z: displacement time history, velocity time history, acceleration time history, Arias Intensity

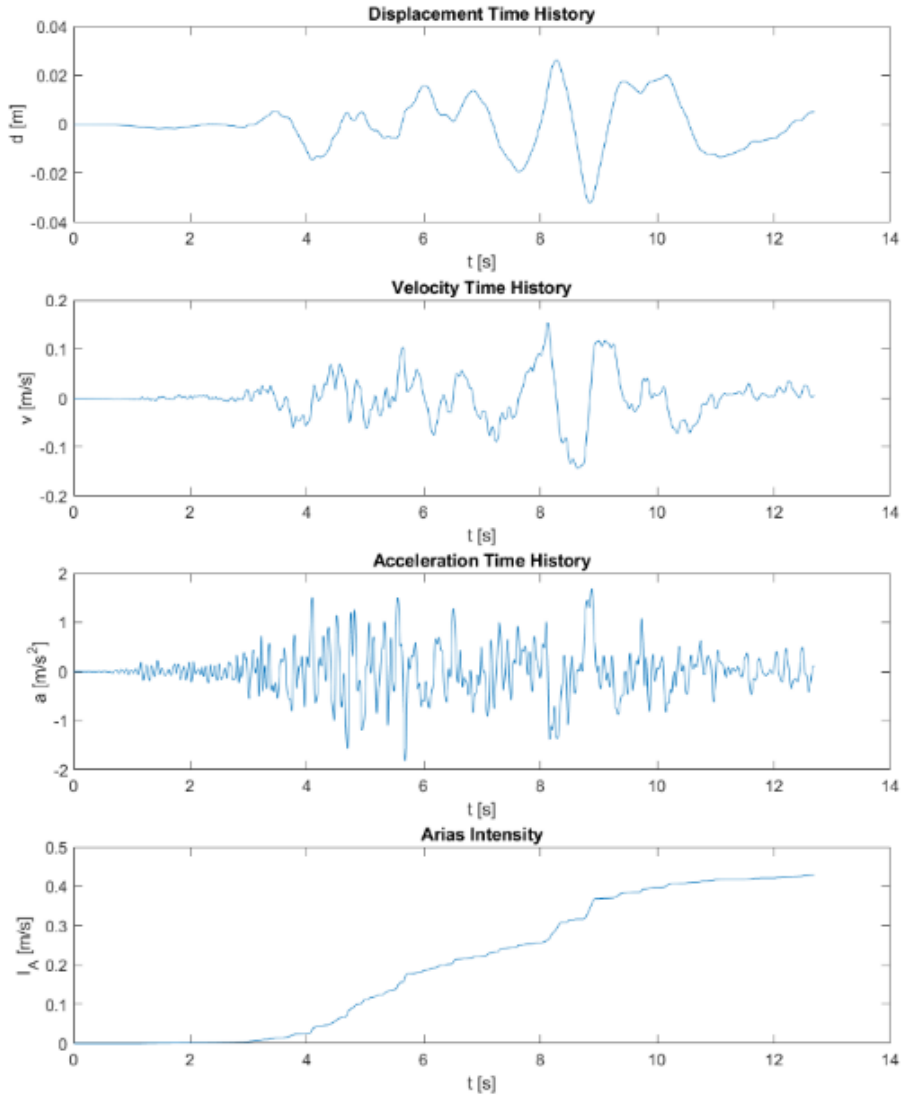


Figure 3.3 – Northridge Worderland Ave horizontal component X reduced at its effective duration: displacement time history, velocity time history, acceleration time history, Arias Intensity

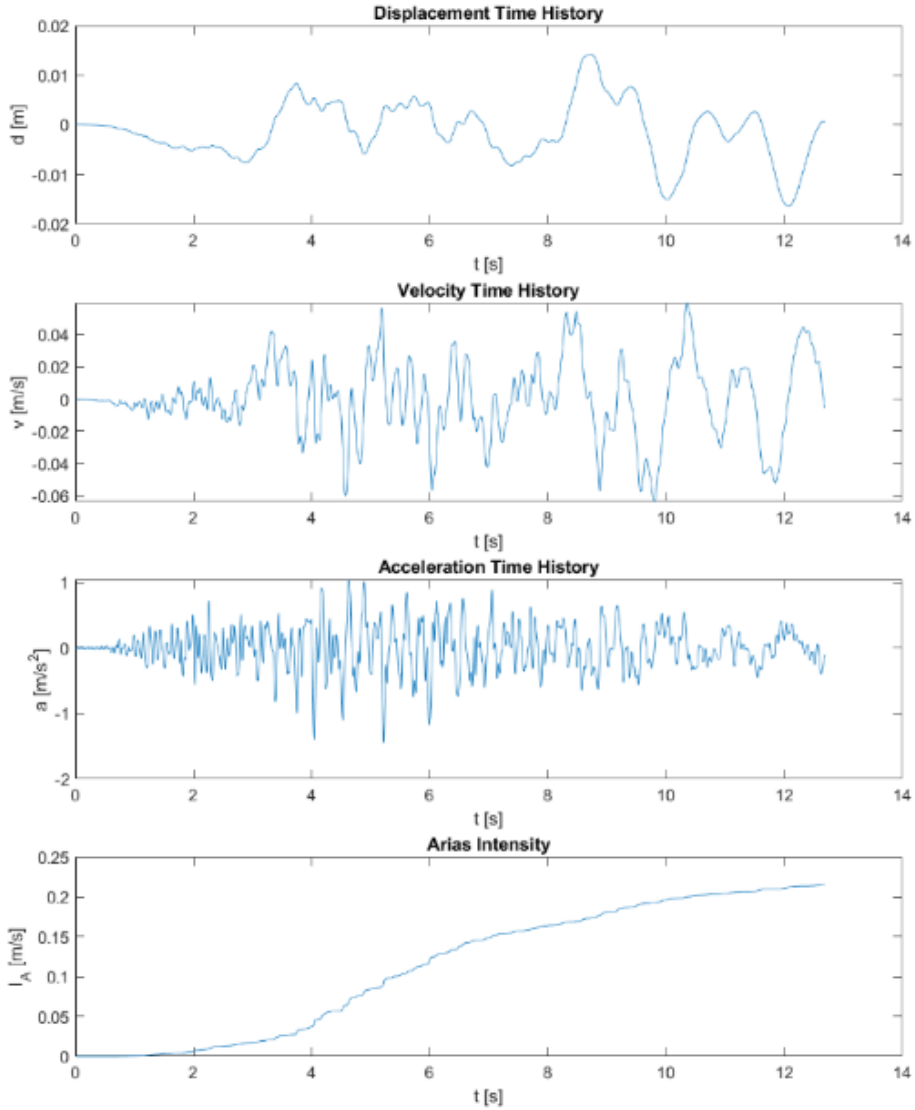


Figure 3.4 – Northridge Worderland Ave horizontal component Z reduced at its effective duration: displacement time history, velocity time history, acceleration time history, Arias Intensity

Figures 3.3 and 3.4 show the filtered signal reduced to the effective duration, as it was subsequently considered for the analysis. It should be specified that

the analyses were performed on the entire filtered signals and were considered valid only when the duration reached at least the effective duration.
These signals, obtained with reference to the life safety limit state (SLV), were scaled to reproduce the intensity of the various limit states. The intensity measure (IM) scaling factor, set to one for the SLV, is 0.5, 0.75, and 1.25 for the operational limit state (SLO), damage limit state (SLD), and collapse limit state (SLC), respectively. The above IM are chosen to reproduce the same peak ground acceleration of Messina site suggested by Italian Technical Standards [38] for each limit state.
To consider a reasonable volume of soil and thus reduce the vertical extent in the coupled model, the convolution procedure performed by Gorini [36] was referenced, as the bedrock in this region is found at a depth of 475 meters. Through a sensitivity study conducted on a soil column with nonlinear behavior under free-field conditions, the depth beyond which the soil can be considered linear was identified, which resulted to be 32 meters. The propagation of seismic waves from the bedrock to this identified depth occurs under free-field conditions, and then the motion is directly applied to the base nodes of the model.

3.3 Modeling in the Finite Element analysis framework OpenSees

The reference structure for the seismic analyses in this chapter is the same as considered in the previous section but with 8 storeys. Consequently, the members of the top 4 storeys are exactly the same as in the previous case, while the vertical members of the first 4 storeys were designed following the same procedures, i.e., considering only gravitational actions.

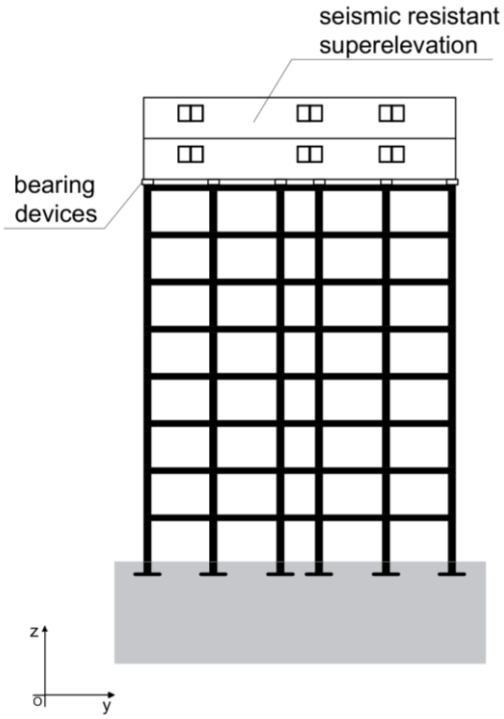


Figure 3.5 – Elevation scheme of the structure and superelevation

Materials and loads are the same as in the fixed-base case of the previous chapter, except for the roof deck, which has a permanent load of 5.06 kN/m² and a variable load of 0.48 kN/m².
Structural elements such as beams and columns were modeled using force-based beam-column elements [40–41] with fiber sections. The constitutive relationship of the concrete fibers is that of Kent-Scott-Park [42], while the relationship for the fibers corresponding to the reinforcement bars is an elastoplastic relationship with kinematic hardening.
The beam-column elements have 10 integration points, and the geometric transformations are linear for the beams and P-Delta for the columns, to account for second-order effects.

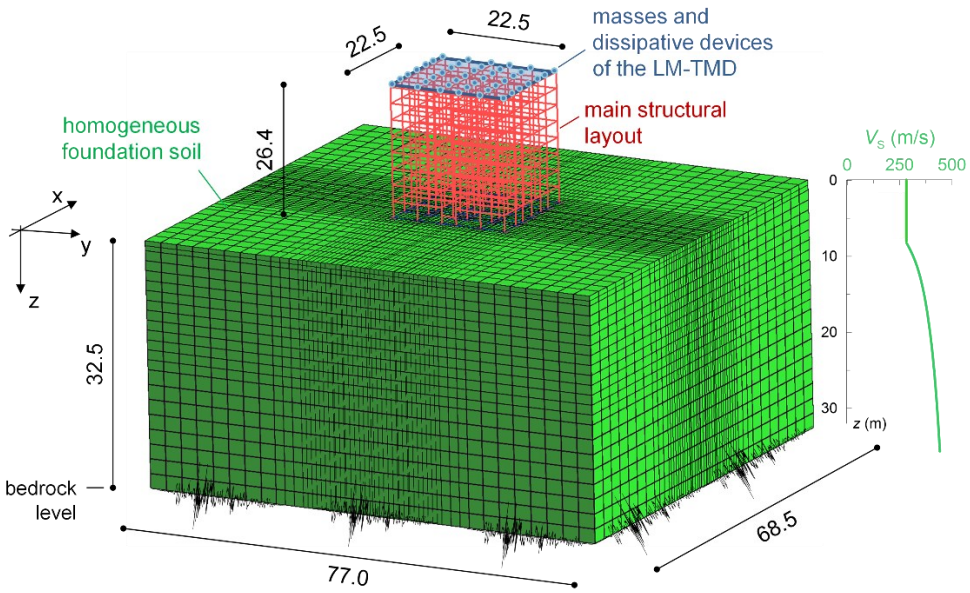


Figure 3.6 – Visualization of the coupled model's mesh by GID pre/post-processor [35]

Rigid diaphragms are applied at the various floors, and the masses are applied at the structural nodes, taking into account their constituent components: structural elements, non-structural elements, and a portion of the variable loads present in the seismic combination. Table 3.2 shows the masses applied to each node for the various floors.

Table 3.2- Nodal masses applied to the structural model. Values in [Mg]

	x1y1	x2y1	x3y1	x4y1	x1y2	x2y2	x3y2	x4y2	x1y3	x2y3	x3y3	x4y3
1	10.22	17.14	10.87	13.2	14.55	24.19	18	27.26	15.79	23.71	15.61	20.33
2	10.09	16.89	10.75	12.95	14.22	23.86	17.67	26.69	13.77	23.22	15.36	20.04
3	9.97	16.65	10.62	12.71	13.89	23.53	17.34	26.11	13.52	22.72	15.11	19.75
4	9.84	16.4	10.5	12.46	13.69	23.03	17.13	25.61	13.4	22.39	14.99	19.34
5	9.72	16.15	10.37	12.21	13.48	22.54	16.92	25.12	13.28	22.06	14.86	18.92
6	9.72	16.03	10.37	12.09	13.23	22.21	16.68	24.58	13.03	21.73	14.62	18.55
7	9.72	15.9	10.37	11.96	12.99	21.88	16.43	24.05	11.01	21.4	14.37	18.18
8	6.23	11.23	7.17	8.24	8.63	16.53	12.65	18.24	8.82	16.35	10.36	12.38

To clarify the $x_i y_j$ caption, Figure 3.7 shows the plant alignment (red lines), with the green lines representing the symmetry axes of the building

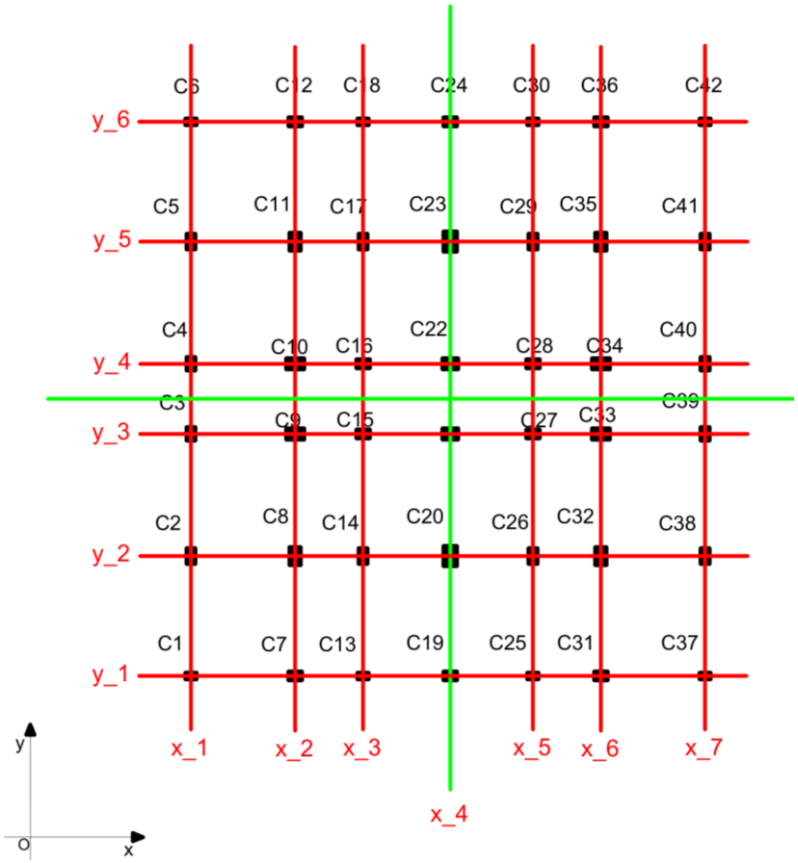


Figure 3.7 – Plan alignment of nodes (and masses)

For the double symmetry the mass applied at node x_1-y_1 is equal to the one applied to nodes x_7-y_1, x_1-y_6, x_7-y_6 etc.
The foundation system of the building consists of rectangular footings with a support plane at a depth of -1 meter, connected by tie beams. The entire foundation system was assigned a concrete class of C20/25. The tie beams, like the elevated elements, were modeled with force-based beam-column

finite elements, while the footings were modeled with shell elements, ShellMITC4 from the OpenSees library.

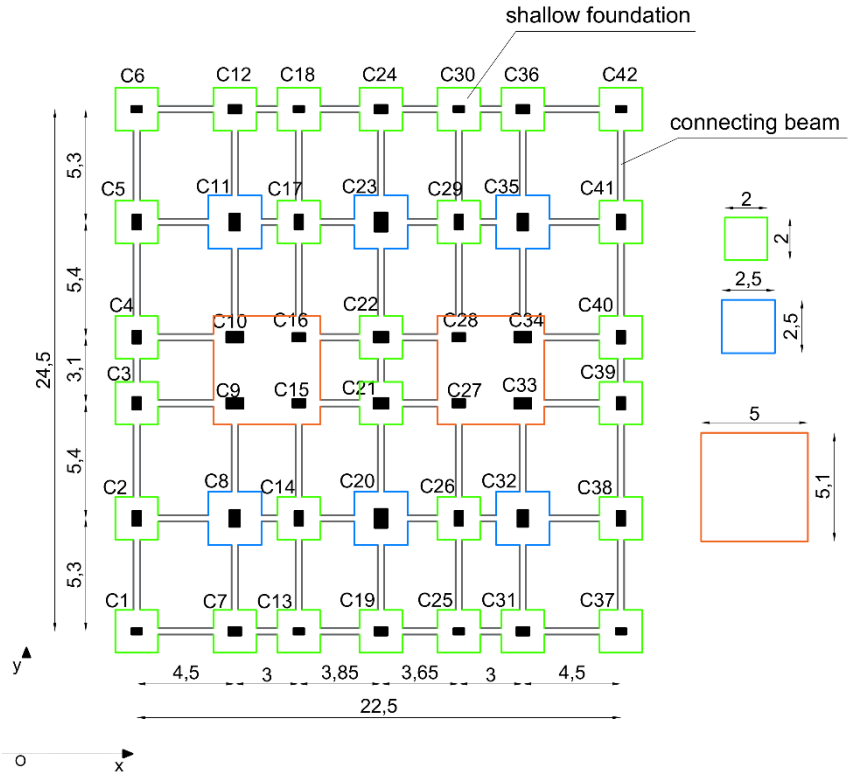


Figure 3.8 – Foundation layout [35]

The soil domain considered in the model has transverse dimensions of 77 m x 68.5 m and a depth of 32.5 m. These transverse dimensions were determined as the minimum sizes above which the effect of boundary conditions becomes negligible.

In this case, different boundary conditions were set for purely gravitational analyses and seismic analyses. For the gravitational analyses, the nodes at the boundary were constrained to move only vertically, while the nodes at the base were set to perfect fixed conditions.

For the seismic analyses, the boundary nodes were internally constrained kinematically from one face to the opposite (equalDOF), as these nodes can be assumed to have free-field conditions. Therefore, nodes at the same depth are kinematically connected to those on the opposite face for each horizontal direction.
Through a sensitivity analysis, the effects of different boundary conditions on the spectral accelerations and maximum displacements of two reference points were compared: the first located at a central node of the domain and the second on the boundary. Specifically, Figure 3.9 shows the comparison for these two nodes of the ratio between the spectral acceleration at the fundamental period in the reference case and that recorded at the same point in an enlarged domain with triple the size. The reference case was then compared by varying boundary conditions such as: domain with Lysmer & Kuhlemeyer absorbing boundary, massive columns at the boundary and free-field columns at the boundary.

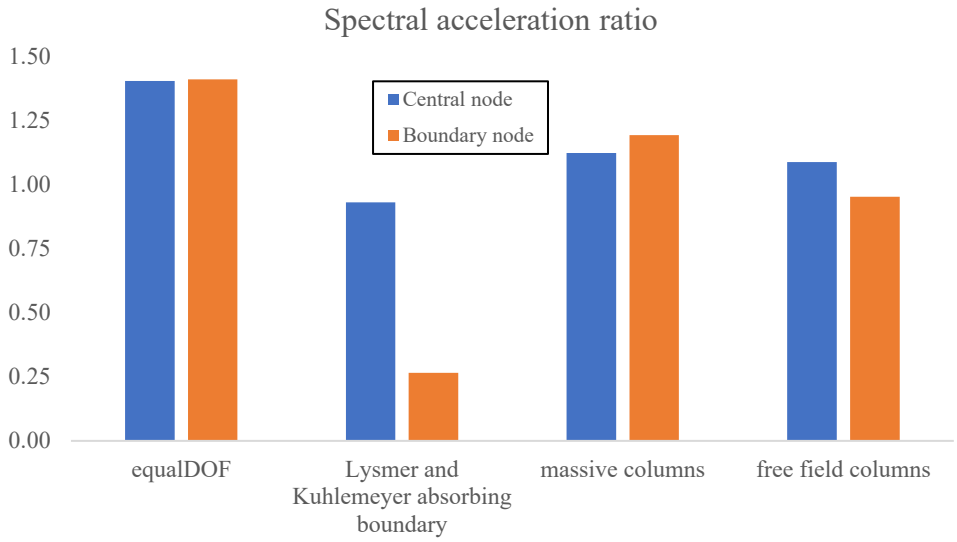


Figure 3.9 – Comparison between different boundary condition on spectral acceleration

The soil in this domain replicates that of the Messina gravels, which are coarse-grained deposits. The finite element type used for the modeling is the SSPbrick hexahedral [43], whose behavior is described by the Pressure

Dependent Multi-Yield (PDMY) hardening behaviour [44]. The calibration of this soil model was carried out in the works of Gorini 2019 [36] and Gorini et Al [45–46]. Table 3.3 provides all the quantities that characterize its mechanical behavior, as set during the calculation phase.

Table 3.3- Parameters of the PDMY model [35]

Variable	Description	Soil
ρ Mg/m^3	mass density	2.243
G_r (kPa)	elastic shear modulus at p_r'	1.3×10^5
n	Poisson's ratio	0.2
p_r' (kPa)	reference mean pressure	80.0
d	pressure dependent coefficient	0.5
$\gamma_{d,max}$	peak shear strain	0.1
φ_{PTL}	phase transformation angle	26°
C	contraction parameter	0.195
d_1	dilation parameters	0.6
d_2		3.0
M	critical stress ratio	1.54
λ_c	Critical State Line param.	0.022
e_0		0.448
ζ		0.7
N	number of yield surfaces	40

The discretization of the soil domain, as shown in Figure 3.6, was differentiated with a denser mesh in the central zones that encompass the building's footprint. Additionally, the finite elements have a vertical dimension that increases with depth.
Regarding the design of the TMD, the same procedure outlined in Chapter 2 was followed, but this time considering the 8-story reference building previously described. After performing the dynamic characterization of the structure through modal analysis and identifying the mass participation percentages for the various modes, the charts proposed in Figures 2.9-2.16 were used to determine the optimal period of the TMD. Table 3.4 presents the main modal properties of the reference structure.

Table 3.4- Modal properties of the reference structure

Mode [-]	Period [s]	U_x [%]	U_y [%]	U_z [%]
1	1.51	74.3	0	0
2	1.21	0	73.9	0
3	1.14	0	2.7	0
4	0.56	12.5	0	0
5	0.46	0	2.0	0
6	0.45	0	10.9	0
7	0.32	5.1	0	0

With the first 7 modes, 90% of the seismic mass is involved in the two horizontal directions, with significant periods ranging from 0.32 s for the seventh mode to 1.51 s for the first. The first mode, used as the reference for the design with a period of 1.51 s, corresponds to the red curves in Figures 2.9-2.16.

In the following sections, TMD configurations with various mass ratio values, ranging from 5% to 30%, will be analyzed (Table 3.5). Higher values would be impractical due to the considerable mass of the reference building, which has 8 floors. The total seismic mass of the building is 5240.6 tons, with 74% participating in the first mode.

Table 3.5- TMD properties

System	Mass [Gg]	Stiffness [MN/m]	Damping Coefficient [MN·s/m]
Bulding	3.893	67.418	1.296
LM-TMD, $\bar{m}$=5%	0.194	1.483	0.214
LM-TMD, $\bar{m}$=10%	0.389	3.326	0.455
LM-TMD, $\bar{m}$=20%	0.778	6.184	0.885
LM-TMD, $\bar{m}$=30%	1.168	8.818	1.283

In this application, as in the previous chapter, 22 elastomeric devices were distributed on the perimeter columns and 20 flat slider devices on the internal ones. The TMD was modeled by applying concentrated masses at the nodes of the top floor and connecting them to these nodes using zero-length elements of the elastomeric bearing plasticity and flat slider bearing type. The elastomeric devices were then assigned characteristics to reproduce the stiffness and damping derived from the design, while the flat sliders were given a friction coefficient of 0.01. The elastomeric devices were assigned damping according to Rayleigh's formulation, assuming a damping ratio of 0.18 and 0.30 at periods of 0.44 s and 2.32 s, respectively, to match the damping curve proposed in the FIP catalog [47].

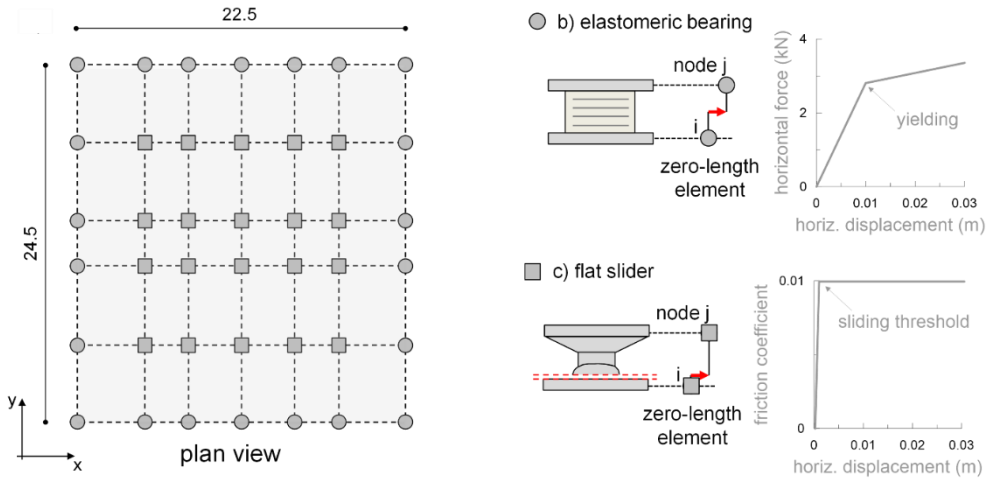


Figure 3.10 – Devices and plan arrangement [35]

The analysis procedure was implemented step-by-step to simulate the various construction phases (Table 3.6). An initial elastic analysis was conducted on the soil domain alone to reproduce the stress state before the construction of the building, after which the soil's behavior was considered elastoplastic. During the construction of the foundation system, the soil elements affected by the excavation were removed and replaced with shell elements representing the footings, followed by the insertion of the tie beams. A gravitational analysis was then performed, and the construction sequences, floor by floor, were taken into account, each followed by a gravitational

analysis, up to the completion of the seismic resistant superelevation that acts as the TMD.

Table 3.6. Construction sequence and staged analysis

Stage	Description
0	Initialization of effective stress in the soil
1	Activation of the elastic-plastic behaviour in the soil
2	Soil element removal (escavation) and appearance of foundation shell elements
3	Definition of the connecting-beams and first floor
4-10	Definition of 2nd to 8th floors
11	Realization of the TMD

3.4 Results

Analyses were performed on the coupled soil-structure-TMD model, considering different input signals, with intensities ranging from IM = 0.5 to IM = 1.25 and with TMDs having a variable mass ratio from 0 (absence of TMD) to 0.30. The same analyses were then repeated on a model without soil interaction, i.e., a fixed-base structure, to compare their performances. In the fixed-base model, the seismic signals were obtained from a local seismic response under free-field conditions and then directly applied to the base nodes.

Since the volume of results and representations would be excessive, only the results related to recording 2, which is used as a reference, will be detailed. A comprehensive comparison between all the recordings will be made at the end.

Evaluating the maximum interstory drifts (MID) that occur in the fixed-base structure, as shown in Fig. 3.11, a clear formation of a soft-story mechanism can be observed, which tends to manifest between the sixth and seventh floors. This characteristic, typical of existing buildings, is a consequence of design without seismic precautions. At the transitions between floors

(specifically, every two floors), there are reductions in the column sections, which, being designed solely for vertical loads, are meant to respond to axial forces decreasing toward the top. Such kinematic mechanisms are very dangerous due to the limited displacement capacity they induce, further exacerbated by the low ductility of these elements, a trait that is more pronounced in existing buildings.

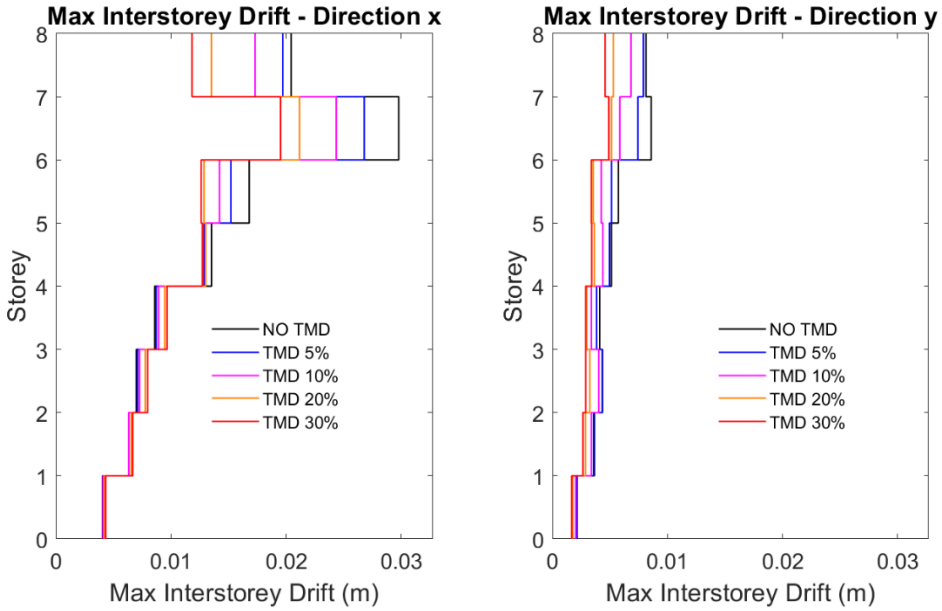


Figure 3.11 – Max Interstorey drift in the two horizontal directions, recorded on the Fixed Base structure. IM=0.5, Rec n.2

This phenomenon is also observed for seismic events of modest intensity (IM = 0.5) but is mitigated by the TMDs, whose effectiveness increases with the mass ratio. Looking at the resulting MID, a reduction of around 30% can be observed for mass ratios of 0.2. High mass ratio TMDs can generate greater inertial forces, which partially counteract the formation of the soft-story mechanism, resulting in an overall positive effect. On the lower floors, the interstory drift is comparable to that of the existing building, and it may be increased or decreased depending on the floor being observed.

It is important to note that in the graphs in Figure 3.12, the resulting MID values do not correspond to the combination of those in Figure 3.11. Instead, they were obtained at the instant when the combination of the two components produces the

maximum value, rather than the combination of the maximum values in the two directions which occur at different, not necessarily coinciding, instants.

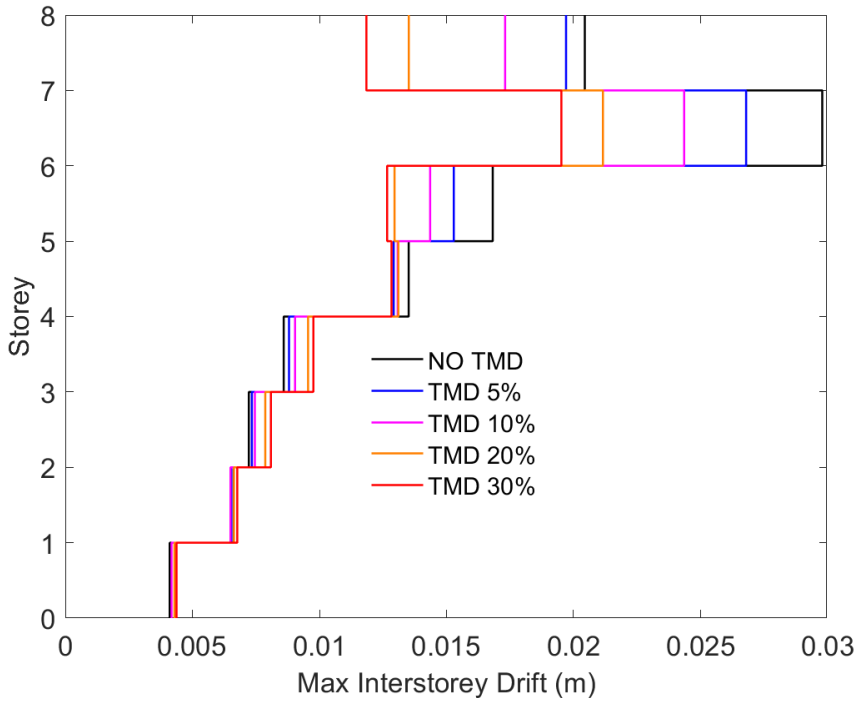


Figure 3.12 – Max resultant Interstorey drift recorded on the Fixed Base structure. IM=0.5, Rec n.2

It is useful to introduce an efficiency parameter for the TMD, which can be directly linked to the reduction in structural drift or, alternatively, to the reduction in the maximum absolute acceleration observed across the various floors of the structure:

$$\eta_{drift} = \frac{max\{MID_{noTMD}\} - max\{MID_{LM-TMD}\}}{max\{MID_{noTMD}\}} \tag{3.2}$$

$$\eta_{acc} = \frac{max\{acc_{noTMD}\} - max\{acc_{LM-TMD}\}}{max\{acc_{noTMD}\}} \tag{3.3}$$

The quantities with the subscript "noTMD" evidently refer to the existing structure. η_{drift} is therefore a measure of the reduction in the maximum drift observed across

all floors, while η_{acc} is a measure of the reduction in the maximum absolute acceleration due to the effect of the TMD.
Once the efficiencies are defined as in eqs. 3.2-3.3, they can be directly correlated to the mass ratio of the TMDs.

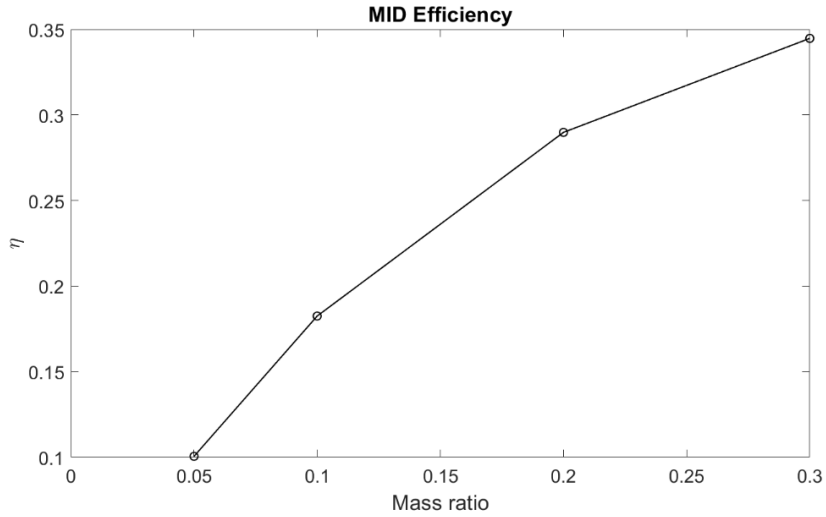


Figure 3.13 – Effectiveness in the reduction of the MID as a function of the mass ratio. FB model, IM=0.5, Rec n.2

As expected, the efficiency curve increases, albeit with a downward concavity.
It is also interesting to show the time history of the displacement of a node at the top of the building, on the uppermost floor, where the reduction in displacements is obviously greater in structures equipped with TMDs with high mass ratios.

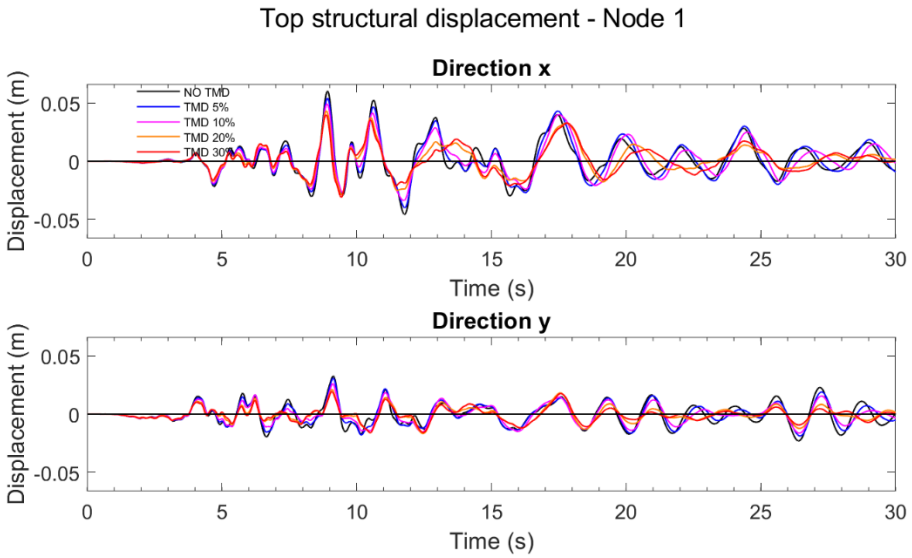


Figure 3.14 – Horizontal top displacement time histories

Focus now move on to illustrate the results obtained for the structure modeled together with the interacting soil, corresponding to the same event with equal intensity (Northridge, Wonderland Ave, IM = 0.5), and then compare some of the differences.

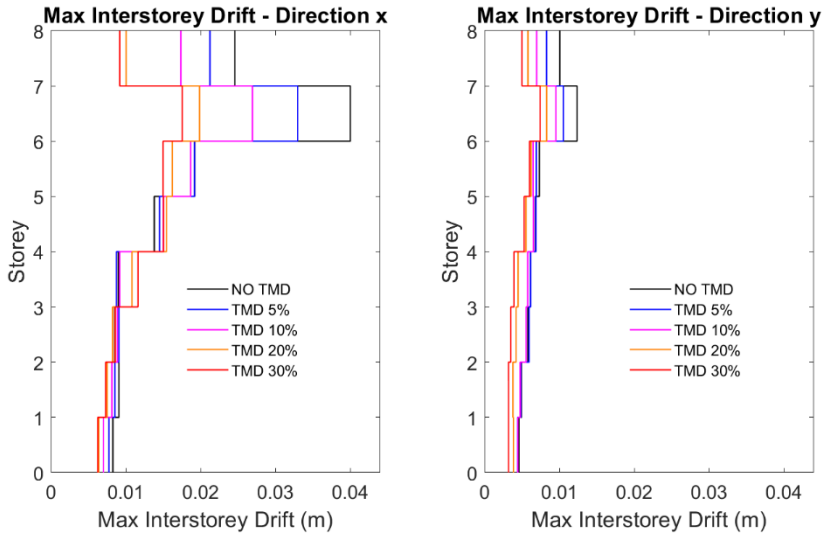


Figure 3.15 – Max Interstorey drift in the two horizontal directions, recorded on the structure in the Coupled Model. IM=0.5, Rec n.2

Similarly to the fixed-base structure, the presence of a soft-story mechanism between the 6th and 7th floors is observed. Due to the greater severity of the horizontal component in the X direction, this mechanism is more pronounced in that direction than in the other. Examining the MID values across the various floors, a generally higher value is found compared to the counterpart evaluated on the fixed-base structure. This increase is due to dynamic effects induced by the interacting soil, which amplifies the structural response.
In the resulting drift, the effect of the TMD is more evident even on the lower floors compared to the fixed-base cases. The effectiveness of high mass ratio TMDs is confirmed, and for low-intensity seismic events, such as the one considered in this example (IM = 0.5), the efficiency is even greater than in the fixed-base case (with a maximum of 0.57 compared to 0.34 in the previous case).

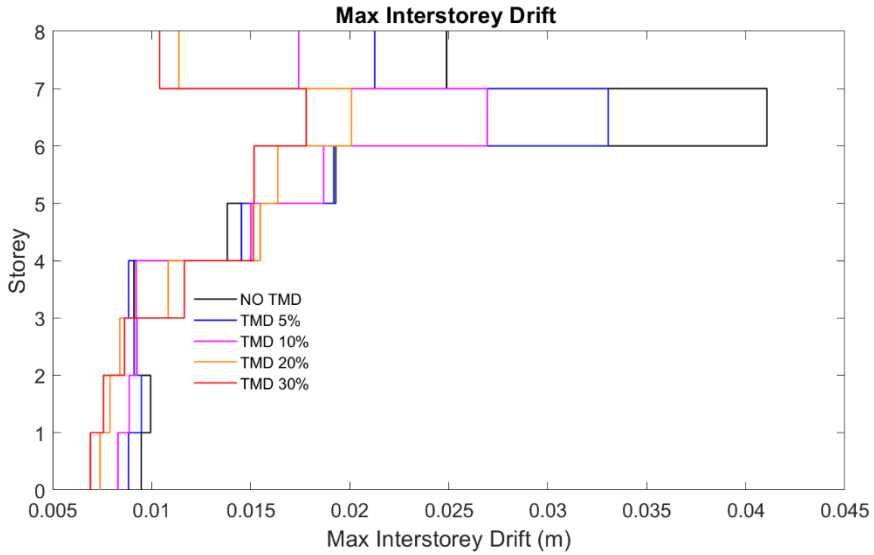


Figure 3.16 – Max resultant Interstorey drift , recorded on the structure in the Coupled Model. IM=0.5, Rec n.2

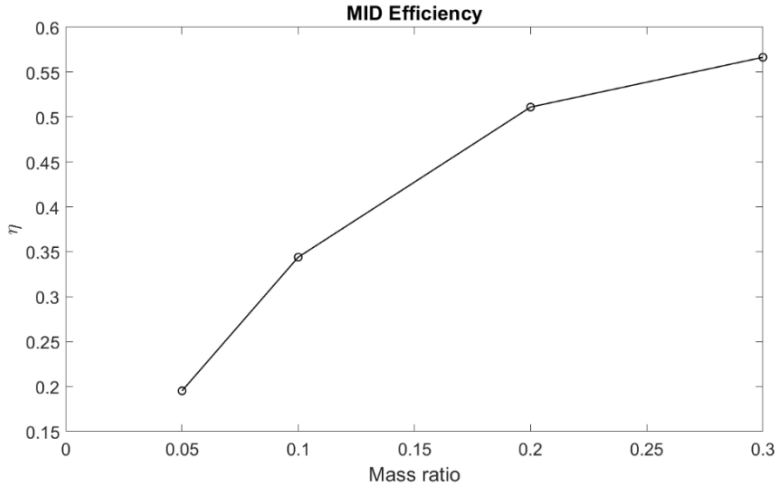


Figure 3.17 – Effectiveness in the reduction of the MID as a function of the mass ratio. CM model, IM=0.5, Rec n.2

Similarly to efficiency, and as a function of the TMD mass ratio, the maximum acceleration of the elevation system can be monitored. As previously mentioned, this acceleration must not compromise the functionality or safety of potential occupants. A positive observation with the increase in the mass of the elevation system is the reduction in the maximum absolute acceleration, which decreases by more than 50% when moving from conventional TMDs (MR = 0.5%) to LM-TMDs.

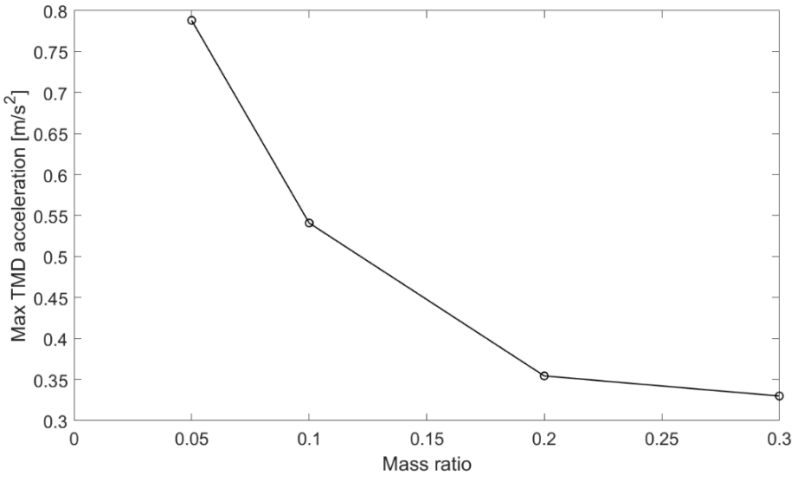


Figure 3.18 – Max absolute acceleration in the different mass ratio superelevations

It is also interesting to monitor other quantities that may be influenced by the presence of TMDs, such as settlements and rotations in the foundation. A high mass contribution could dynamically, or even just statically, lead to an increase in the stress state in the soil, which could impact the aforementioned quantities. In Figure 3.19, almost negligible variations can be observed in the horizontal displacements (x and y) of the reference footing, as well as in the vertical displacements (z direction), where more significant settlements might be expected due to the high mass contribution and, consequently, the increased weight; these remain almost identical.

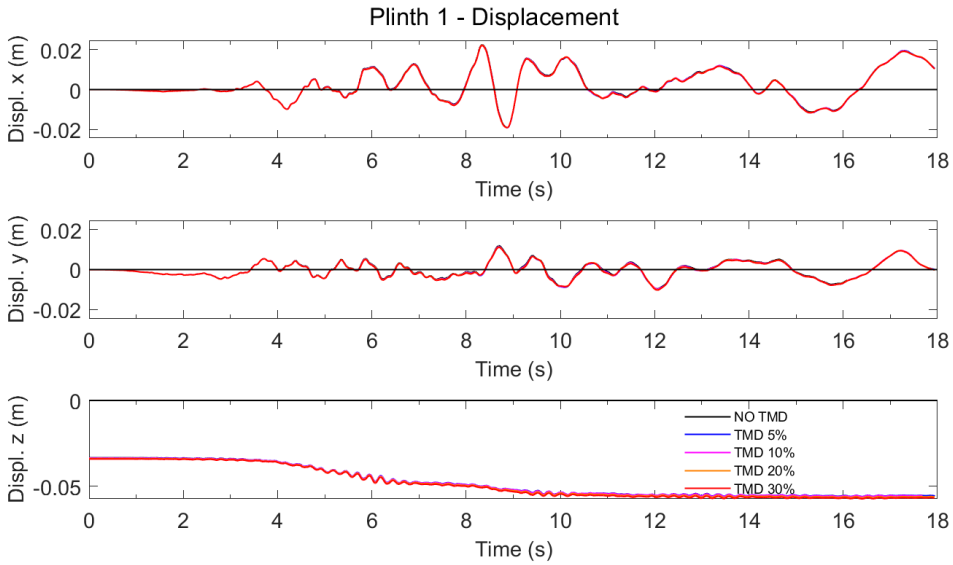


Figure 3.19 – Horizontal displacements and settling in the foundation Plinth

For a further quantification of the effects induced by the TMDs, particularly those related to the considered mass ratios, the displacements of two nodes within the soil domain were monitored: one node at the center and one at the boundary. The central node of the domain represents an area strongly influenced by the presence of the structure, while the boundary node represents free-field conditions. Figure 3.20 shows the displacements in the two horizontal directions and the vertical direction, plotted over the duration of the seismic event, for the two reference nodes.
The horizontal components remain almost unchanged by the presence of the TMD, even at the central node, while a noticeable increase is observed in the vertical displacement history of the central node, as expected due to the behavior of the vertical stresses. These displacement representations are confirmed by the graphs in Figure 3.21, which show the response spectra in terms of accelerations for these two

nodes. From Figure 3.21, a clear distinction can be seen for each horizontal direction between the response spectra corresponding to: the seismic motion at the site (green line), the seismic motion of the central node (solid line), and that of the boundary node (dashed line). Insignificant variations are found in each node with changing mass ratios of the elevation system.

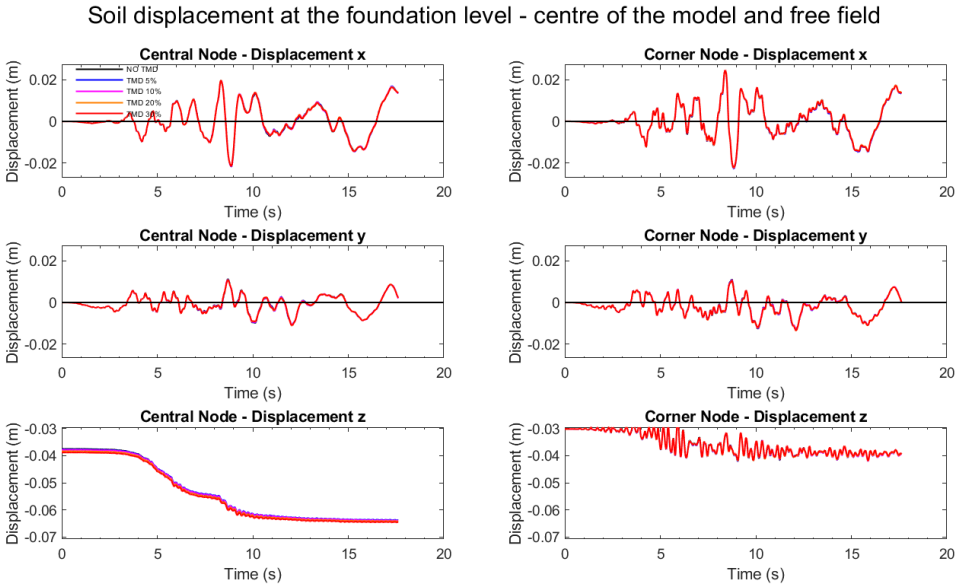


Figure 3.20 – Horizontal and vertical displacements of nodes in a central node and in free-field conditions

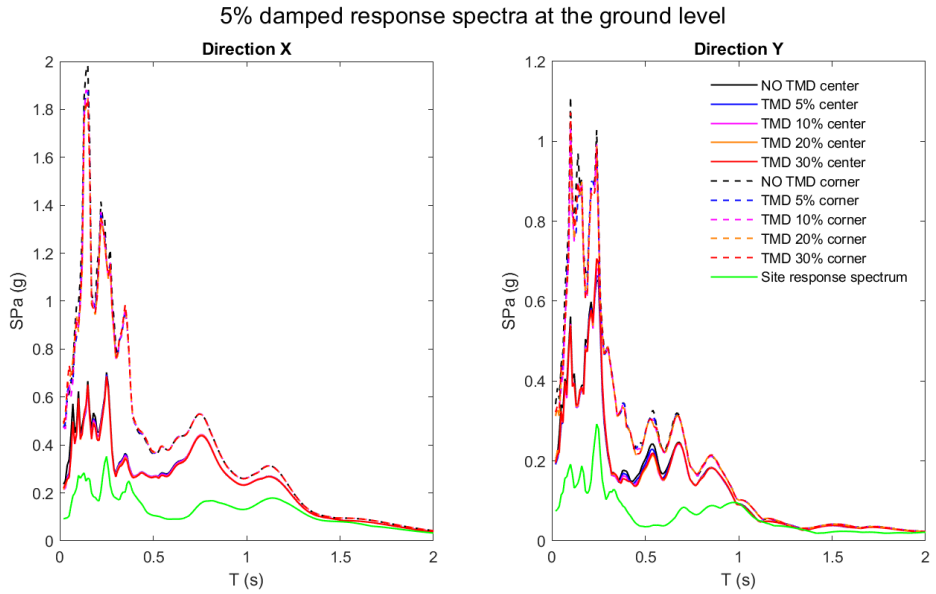


Figure 3.21 – Acceleration response spectra of the nodes at the center and at corner

Once illustrated the general effects of the TMD on the main structural and geotechnical quantities, focus now move on to the comparison graphs between the fixed-base models and the coupled models. For greater clarity, in Figure 3.22 the reference for the structure with a TMD is set at a mass ratio of 20% only. The intensity of the seismic events considered here corresponds to the life-safety limit state (IM = 1), and the reference models are denoted as follows: FB-noTMD and FB-TMD20 refer to the fixed-base structure without and with a TMD at a 20% mass ratio, respectively; CM-noTMD and CM-TMD20 refer to the coupled models without and with a TMD at a 20% mass ratio, respectively.

At higher intensity levels, the soil exhibits a different response, which in turn affects the structural response: it becomes roto-translational due to foundation rocking, altering the shape of the fundamental mode of structural vibration. This effect results in lower TMD efficiency compared to the cases with reduced intensity, as the TMD design assumptions were based on a purely translational seismic response.

The comparison between the fixed-base models and the interaction models reveals a similar structural response among all models for the first four floors. Differences become apparent in the upper floors near the soft story. The TMD's effect is detrimental only on the 5th floor and in the coupled models, while it is comparably favorable between the two models on the top two floors. The TMD's efficiency in terms of drift reduction is comparable between the two models, but in absolute terms,

the MID is greater in the interaction model. This effect, due to the soil's non-linearity, can be seen in the permanent deformations of the foundation system illustrated in Table 3.7.
Notably, there are translational-type permanent settlements affecting the foundation, which are incremental relative to static conditions, confirming the impact attributable to the intensity of the seismic event. These permanent foundation deformations also influence the configuration of post-seismic permanent deformations in the structure as depicted in Figure 3.23, resulting in a rotation at the base node, which subsequently affects the displacement profile in elevation.
It is also interesting to observe the TMD's effect on the displacement profile in the CM model, showing how the inertia forces induced by the TMD cause a reduction in displacements near the top, close to the elevation itself. In contrast, in the interaction model without the TMD, the permanent effects increase with height, also due to the lower resistance offered by the members on the upper floors.

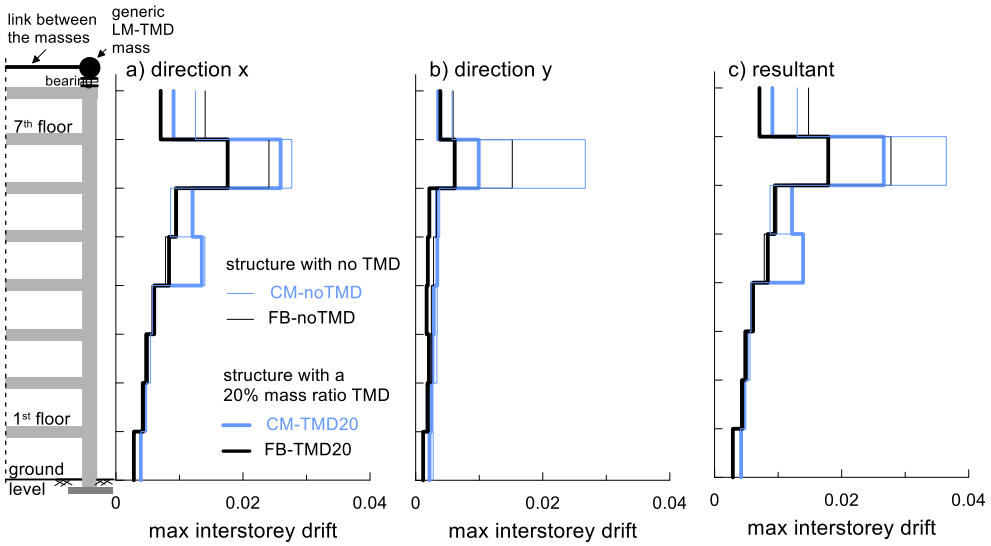


Figure 3.22 – MID comparison in the CM and FB models in absence of TMD and with a 20% mass ratio TMD [35]

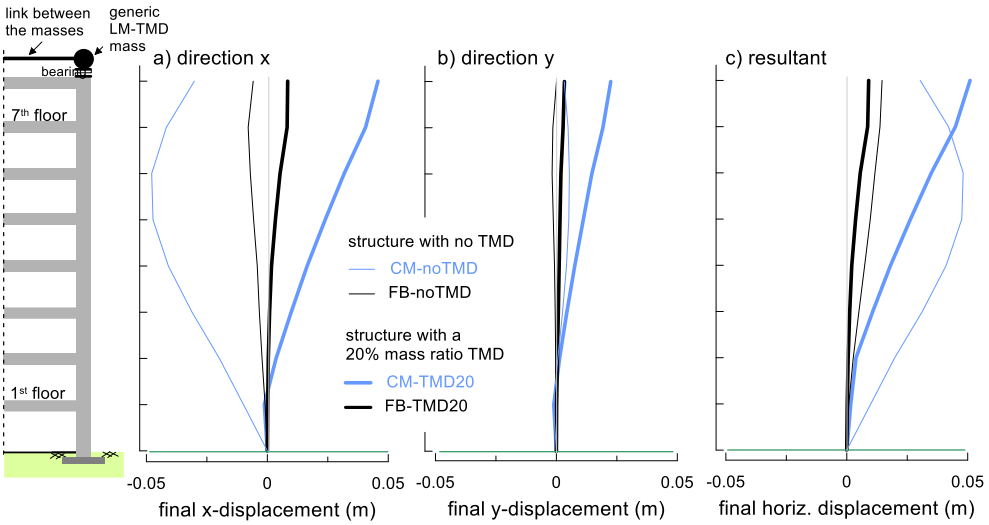
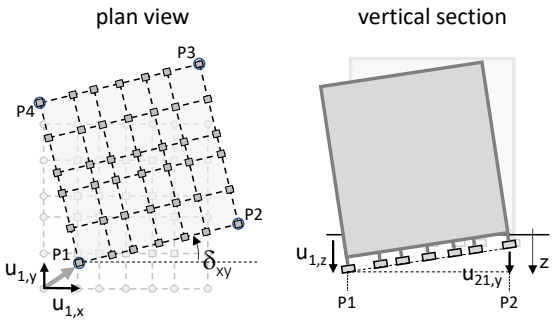


Figure 3.23 – Permanent deformed configurations at the end of the event [35]

Table 3.7- Permanent displacements and rotations of the foundation system [35]

Quantity	no TMD	LM-TMD
$u_{1,x}$ (m)	0.036	0.035
$u_{1,y}$ (m)	0.026	0.026
$u_{1,z}$ (m)	0.081	0.084
δ_{xy} (°)	0.003	0.003
$u_{21,z}$ (m)	0.002	0.001
$u_{41,z}$ (m)	0.003	0.003



The spectral response (in terms of accelerations) of the top floor and the elevation is shown in Figures 3.24 (a) and (b), respectively. These figures demonstrate a greater involvement at the top floor in structures without a TMD, depicted with a thin line. This trend is reduced by the presence of the TMD, particularly in the spectral region of the structure, making the response comparable between the two models with and without soil interaction, with a slight increase in the fundamental periods when soil interaction is considered.

Looking at the spectrum related to the elevation, a higher expected acceleration is noted in the CM models, which generally holds across the entire range of periods, with the maximum excursion at the fundamental period. This aspect suggests that

greater attention should be given to the functionality of the elevation and the non-structural elements, as they are subject to increased inertial forces due to soil deformability.

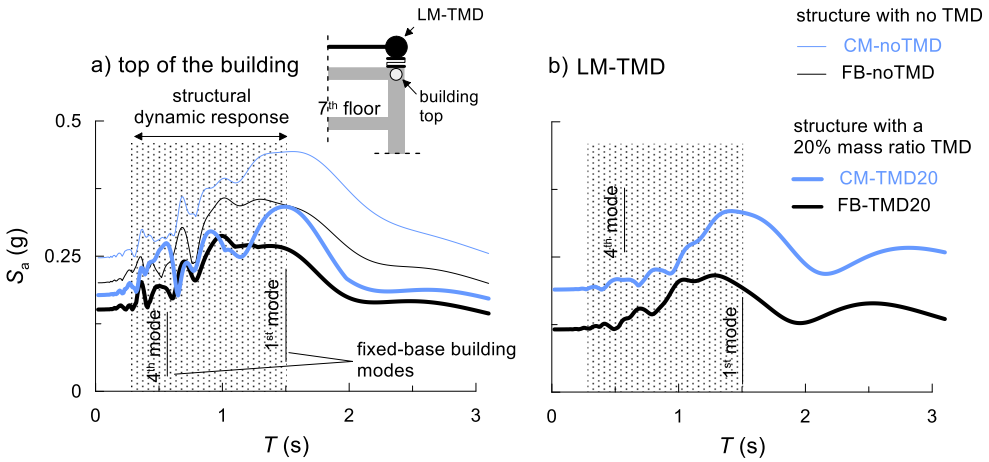


Figure 3.24 – Acceleration response spectra of the a) top of the structure and b) seismic-resistant superelevation [35]

The effect of the different mass ratios considered is now examined in the seismic scenario under reference. Analyzing the maximum interstory drift, a similar trend can once again be observed on the lower floors, which are less affected by the inertial forces induced by the elevation. On the upper floors, the effect of the different mass ratios becomes evident: the efficiency of the TMD increases with its mass, leading to drastic reductions in the MID on the top two floors (45% and 50%) when looking at the upper limit considered (MR = 30%). In this scenario, the TMD can be effectively considered as an intervention solution only if equipped with mass ratios greater than or equal to 20%, as its effectiveness in mitigating the MID is almost negligible for lower values.

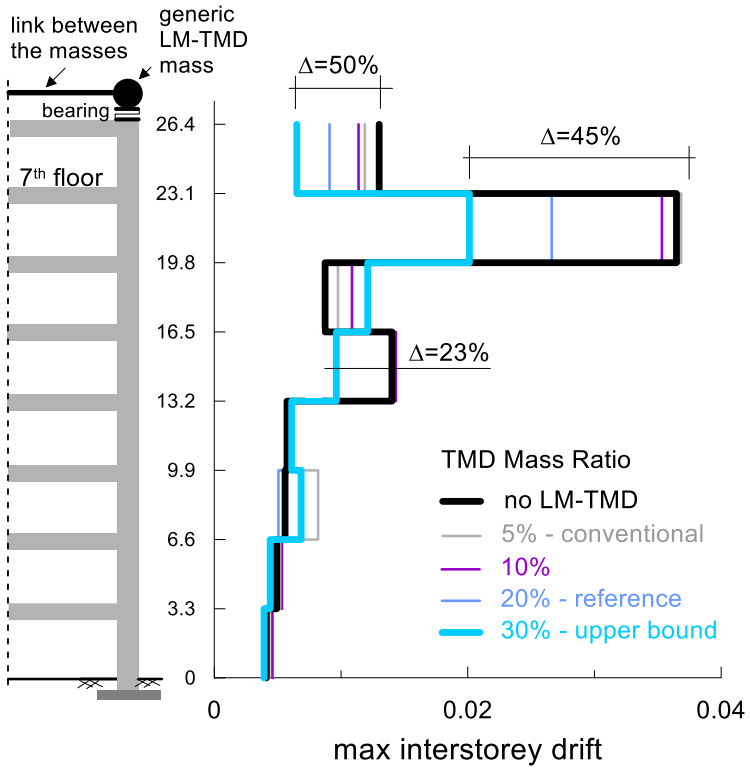


Figure 3.25 – Max interstorey drifts for different mass ratios [35]

Converting in terms of efficiency in drift reduction, a monotonically increasing trend can be observed in both the fixed-base models, plotted in Figure 3.25 with a black line, and in those with interaction. For low MR values, the efficiency is negative (5% MR) or almost negligible (10% MR) in the coupled models, before increasing and becoming comparable to that recorded in the fixed-base model when MR reaches 30%. Figure 3.26 (b) shows the efficiency curves for the reduction in the maximum absolute acceleration recorded across all floors, displaying a completely different trend than that of the drifts. In the floors affected by the elevation, higher absolute accelerations are generated with higher mass ratios, resulting in overall lower efficiency, with a very similar trend between the FB and CM models.

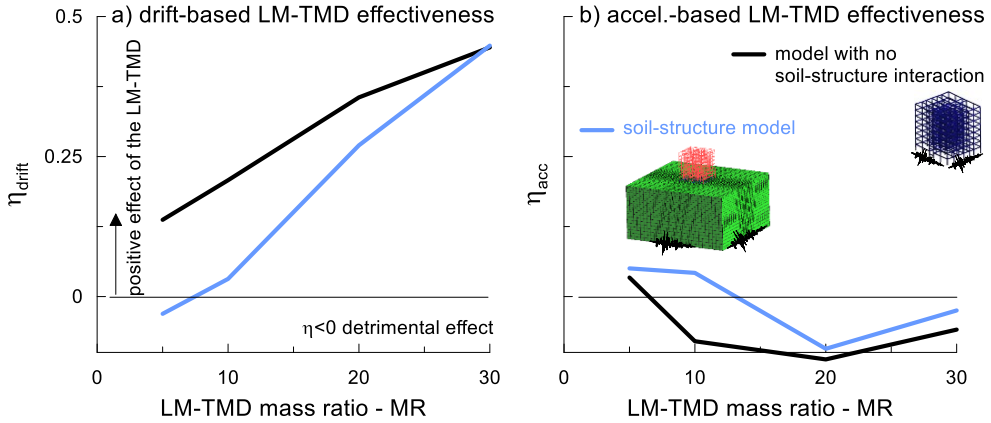


Figure 3.26 – Effectiveness of the LM-TMDs in the reduction of a) max interstorey drift and b) max absolute acceleration [35]

In Figure 3.27, the efficiency trends for the different mass ratios considered and for all limit states are summarized, parameterized by the IM coefficient ranging from 0.5 to 1.25. For each limit state, the curves for the FB and CM models are compared. The trend of η_{drift} is the same in all cases: the curve increases with MR and reaches high values at the maximum mass ratio, almost 60% in the FO limit state for the CM model, exceeding the 35% of the FB model.
For low intensities, positive efficiencies are observed, even in the interaction model, which are also higher than those of the FB model. However, in the more severe limit states, LS and NC, a sharp decrease in efficiency is observed in the CM models, due to the nonlinear behavior of the soil, which is not mitigated by TMDs with modest mass ratios. Under these conditions, a worsening of the structural response may also occur, which is only improved by higher mass ratios.

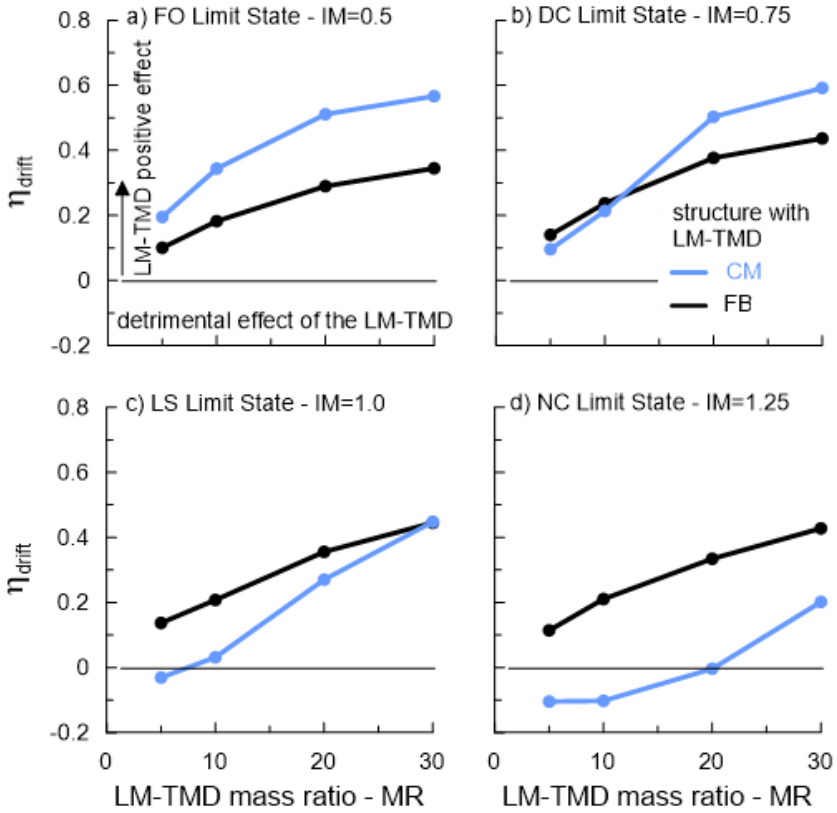


Figure 3.27 – Effectiveness of the LM-TMDs in the reduction of the max interstorey drift for each limit state: a) Full Operational (FO), b) Damage Control (DC), c) Life Safety (LS) and d) Near Collapse (NC) [35]

The efficiency trends in fixed-base models are barely affected by the different intensities considered. As shown in Figure 3.28 (a), which displays the efficiencies of the FB models, they are strongly influenced by the mass ratio but not at all by the intensity of the seismic event.

By contrast, when looking at the curves in Figure 3.28 (b) for the CM models, a clear distinction in behavior is evident, with a decreasing trend as the intensity of the event increases, compromising the performance when soil nonlinearity is pronounced.

This aspect emphasizes once again the importance of accounting for soil-structure interaction effects, both as a general criterion and particularly when designing seismic devices that operate based on structural behavior, such as TMDs.

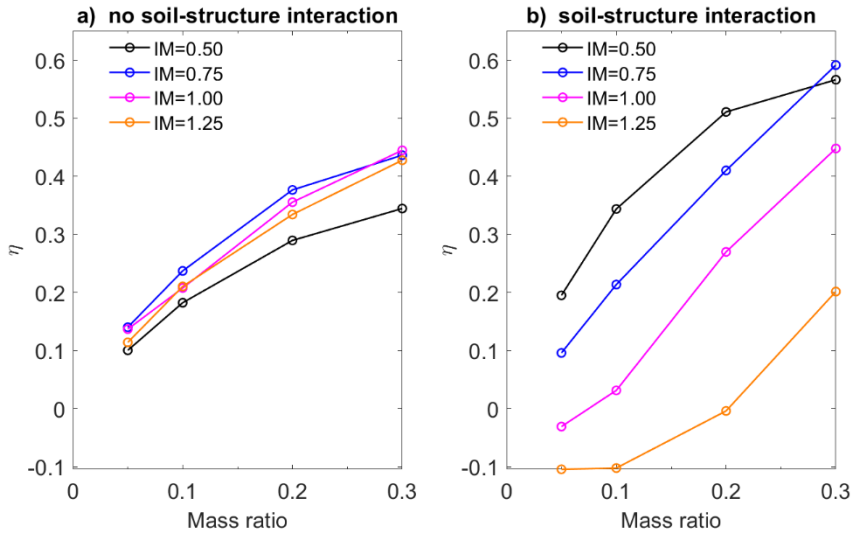


Figure 3.28 – Effectiveness of the LM-TMDs in the reduction of the max interstorey drift for each limit state in a) no soil-structure interaction conditions and b) soil-structure interaction conditions

A final interesting comparison can be made, in statistical terms, between all the events selected earlier. Similarly to Figure 3.27, Figure 3.29 presents the average values of TMD efficiencies recorded for each limit state in the CM models, along with their respective standard deviations.

What can be observed is that, at moderate intensities, the dispersion of efficiency among the different seismic events is limited, as it is only influenced by the variability of the seismological characteristics between events, rather than by soil-structure interaction phenomena. In contrast, the dispersion becomes significant in the more intense events, confirming the influence of the soil on the structural response and, consequently, on the TMDs.

Looking at the trend of the mean efficiency value in the NC limit state, there is no apparent dependence on the mass ratio, confirming that, despite the previously mentioned robustness benefits derived from high mass ratios, the design of classical TMDs is inadequate when interaction phenomena cannot be neglected.

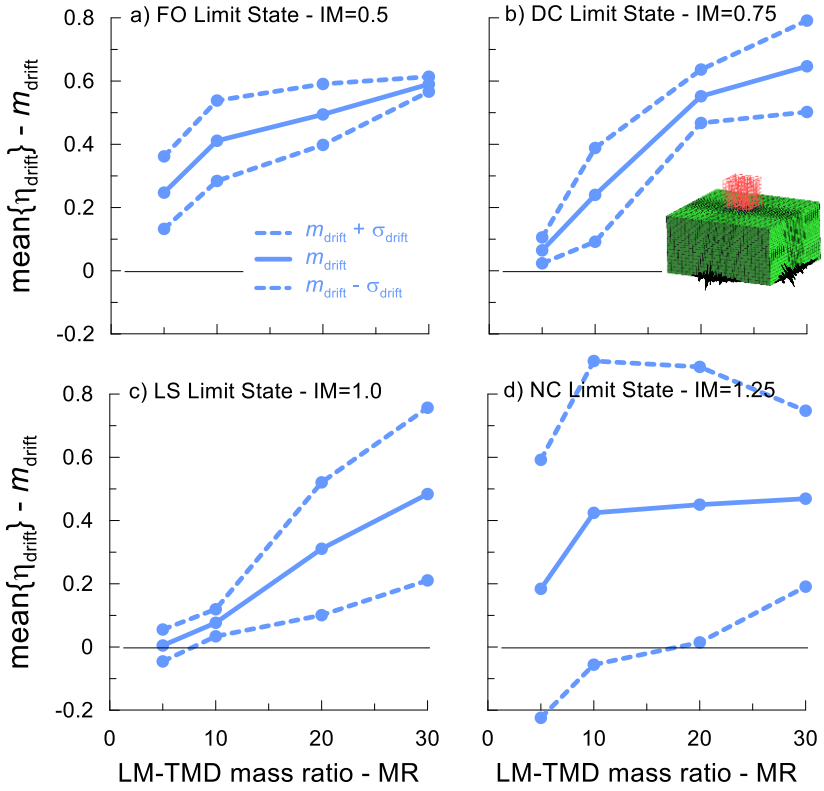


Figure 3.29 – Variability of the effectiveness mean of LM-TMDs for all seismic scenarios, and relative standard deviations for each limit state: a) Full Operational (FO), b) Damage Control (DC), c) Life Safety (LS) and d) Near Collapse (NC) [35]

4 CHAPTER 4
AN INTEGRATED DESIGN CRITERION FOR TMDs ACCOUNTING FOR SSI

4.1 Introduction

In the previous chapters, the dynamic response of structure-TMD and soil-structure-TMD systems has been discussed, showing that the classical design of Tuned Mass Dampers is generally based on the assumption of a fixed-base structure. Although this assumption may be acceptable when soil-structure interaction effects are negligible, it may become inadequate when foundation compliance significantly alters the dynamic characteristics of the overall system. In such cases, the interaction with soil modifies the natural frequencies, the modal properties, and the relative contribution of translational and rotational components of motion, so that a TMD designed for the fixed-base configuration may become partially detuned, or even ineffective, when applied to the actual soil-structure system. These aspects highlight both the importance of properly accounting for soil-structure interaction in seismic analyses and the limitations of conventional fixed-base design assumptions for TMDs.

The works of Gorini and Chisari [29–48] provide a physically consistent interpretation of the problem. In a first work [48], the effect of soil deformability on TMD performance was investigated through a parametric study on a reference timber building, and the results were expressed by means of non-dimensional performance curves relating the efficiency of the device to the structure-to-soil relative stiffness. Such representation clearly showed that the effectiveness of a classically designed TMD progressively decays as the influence of soil-structure interaction increases. In particular, three response regions were identified (Figure 4.1): a first region, corresponding to negligible soil-structure interaction effects, in which the fixed-base design remains appropriate; an intermediate region, characterised by coupled soil-structure behaviour, in which the TMD still provides a beneficial effect but with decreasing efficiency; and a third region, in which the soil acts as a natural isolator and the contribution of the TMD becomes negligible.

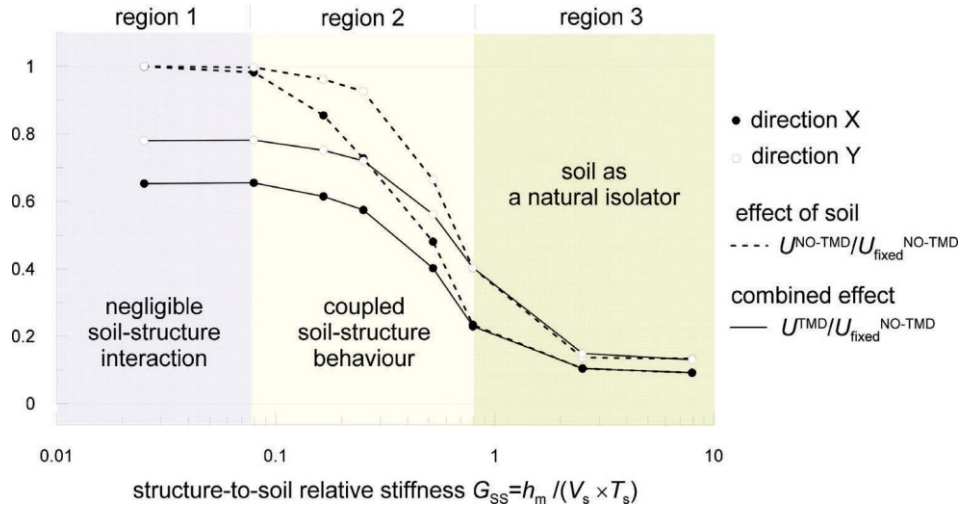


Figure 4.1 – Effect of TMD and soil deformability on the maximum structural displacement [48]

Gorini and Chisari [29] subsequently proposed an interpretative linear soil-structure-TMD model, herein referred to as the SimilSDOF model and schematically shown in Figure 4.2. The model represents the structure through an equivalent first-mode system, while explicitly accounting for the mass and rotational inertia of the foundation, the horizontal and rocking impedance functions of the soil, and the translational TMD connected to the structure at a given elevation. Despite its reduced form, the model retains the essential ingredients governing the coupled dynamic response, namely structural deformability, foundation compliance, rocking effects, modal mass distribution, and TMD position.

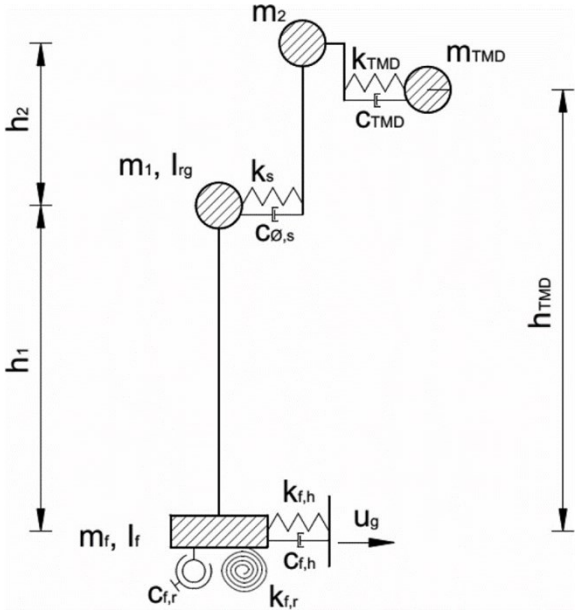


Figure 4.1 – SimilSDOF interpretative model [29]

A non-dimensional formulation of the problem has been made. Starting from the physical quantities describing the structure, the TMD, the structure and the soil systems, the authors derived a complete set of 19 non-dimensional groups, of which 15 are input parameters and 4 are output response quantities. This formulation allows to express the behaviour of the system independently of the dimensional scale of the specific case study and provides a general framework in which different soil-structure-TMD configurations can be interpreted in a unified manner. In particular, the input groups include first the classical TMD design parameters, which are the mass ratio (G_1), the frequency ratio (G_2), and damping ratio (G_3). In addition, the SimilSDOF include also structural and soil-foundation features: the normalised TMD height (G_4), the foundation embedment ratio (G_5), the structure-to-soil relative stiffness (G_6), the structural slenderness (G_7), the soil-structure relative mass (G_8), the foundation aspect ratio (G_9), the structural damping ratio (G_{10}), the effective modal mass ratio (G_{11}), the parameters governing rocking height (G_{12}) and mass distribution(G_{13}), the normalised foundation mass density (G_{14}), and the normalised input frequency (G_{15}). The

corresponding output groups describe the normalised structural deformation, the normalised TMD displacement, the normalised foundation displacement, and the normalised foundation rotation.
Among these quantities, the structure-to-soil relative stiffness plays a central role, as it accounts for the relative deformability of the structure and the supporting soil. In the preliminary study on the timber building, this parameter was already shown to govern the transition from negligible soil-structure interaction to coupled soil-structure behaviour and, finally, to the condition in which the soil behaves as a natural isolator. The subsequent non-dimensional formulation extends this interpretation to a more general class of linear soil-structure-TMD systems and makes it possible to distinguish, within a rigorous theoretical framework, the contribution of soil compliance from that of the TMD itself.
On this basis, Gorini and Chisari carried out a global sensitivity analysis by means of the Elementary Effects method, with the aim of evaluating the influence of each non-dimensional group on the effectiveness of the TMD, measured in terms of reduction of the maximum base shear. The analysis was performed over broad ranges of variability of the input groups, so as to cover a wide spectrum of structural and geotechnical configurations, and was repeated for both a TMD designed according to Den Hartog's criterion and a TMD designed according to the modified approach based on the coupled soil-structure frequency. The results showed that the response is not controlled by the full set of non-dimensional parameters, but rather by a limited number of dominant groups. For the classical Den Hartog-type design, the most influential parameters were found to be the TMD mass ratio, the structure-to-soil relative stiffness, the structural slenderness, the foundation aspect ratio, the structural damping ratio, and the normalised radius of gyration. This result is particularly significant because it shows that the loss of effectiveness of a translational TMD is governed not only by the relative deformability of soil and structure, but also by those quantities that control the rocking contribution of the foundation response.
Building on the model proposed by Gorini and Chisari, and focusing on the groups considered significant for the TMD's response, a parametric analysis and subsequent interpolation of the results are proposed with the aim of developing a comprehensive and integrated design formulation.

4.2 Parametric analysis

The parametric analysis was conducted in the OpenSees environment [34], appropriately modeling the interpretative model presented above. A total of 4 distinct models were defined: 2 of them, referred to as CM (Coupled Models), include the soil response, and 2 referred to as FB (Fixed Base models). The CM and FB models can be either equipped with a TMD or not, leading to further distinctions such as CM-TMD, CM-NO_TMD, etc. The modeling in OpenSees is outlined in Figure 4.2, which shows the nodes defined in the 4 models.

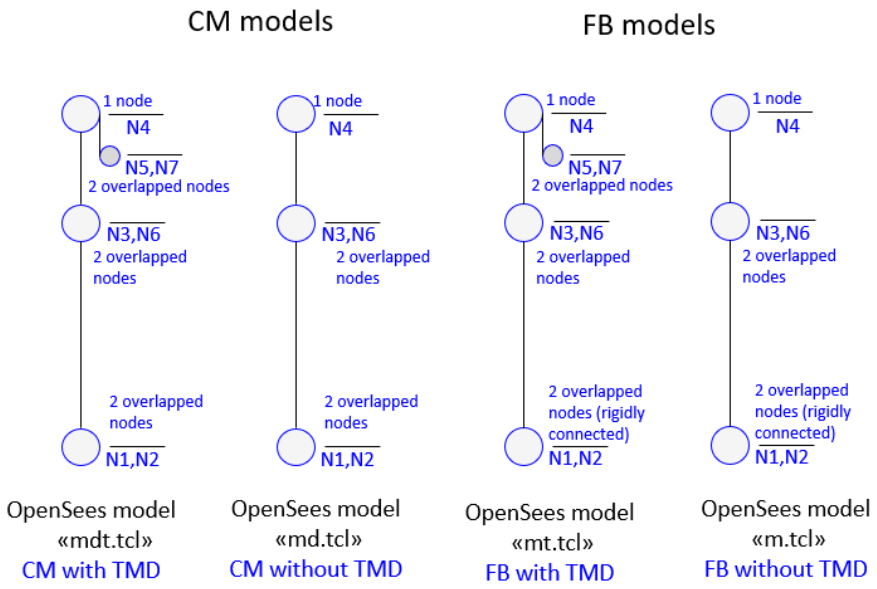


Figure 4.2 – SimilSDOF modeled in the OpenSees software framework

The base nodes are rigidly connected in the FB models, while they are connected through a parallel combination of a spring and a damper (Voigt-Kelvin model) in the CM models, with the forcing applied at node 1. There is a rigid link between nodes 2 and 3, as well as between nodes 6 and 4. Nodes 3 and 6 are also connected with a zero-length element featuring Voigt-Kelvin material, where the stiffness and damping correspond to those of the main mass. Finally, the models with a TMD include an additional node, node 5,

which is connected to node 7 and assigned the mass, stiffness, and damping properties of the TMD.
The various quantities characterizing the models are derived from the values of the groups in the parametric analysis. The groups under analysis were set to cover a wide range of soil-structure-TMD systems. The remaining groups, which were classified as non-relevant for TMD performance, were fixed with reference to the structure presented in Chapter 3.
Table 4.1 lists the groups under analysis and the corresponding ranges of values considered in the parametric analysis. For the TMD mass ratio (group G_1), a range referring to TMDs with high mass ratios (LM-TMD) was considered. The most important group, which is the frequency ratio of the TMD (G_2), is the focus of the analysis as it serves as the design parameter. By identifying the optimal values of the frequency ratio, it becomes possible to design the TMD while considering all other characteristics of the structure. In contrast to the typical tuning values of classical TMDs, which are around unity, a broader range was considered in this case.
The soil-structure interaction effects are encapsulated in group G_6, defined as the relative soil-structure stiffness. Very low values correspond to negligible interaction conditions, while high values (over 0.5) lead to a deterioration in the performance of classically designed TMDs.
The geometric properties of the structure are included in groups G_7, G_9, and G_{13}, representing, respectively, the structural slenderness, the aspect ratio of the foundation, and the mass distribution in plan.

Table 4.1 – Groups of the parametric analysis and relative ranges

Non-dimensional group	**Definition**	**Lower value**	**Upper value**
G1. Mass ratio of the TMD	m_{TMD}/m_m	0.1	0.4
G2. Frequency ratio of the TMD	$1/\omega_s(k_{TMD}/m_{TMD})^{0.5}$	0.4	2
G3. Damping ratio of the TMD	$c_{TMD}/2(m_{TMD}k_{TMD})^{0.5}$	0.15	0.25
G6. Structure to-soil relative stiffness	$h_m/(V_sT_s)$	0.07	0.8
G7. Slenderness ratio	$h_m/L_{f,x}$	0.5	2
G9. Foundation aspect ratio	$L_{f,x}/L_{f,y}$	0.5	1

G10. Damping ratio	$c_{\phi s}/(2\omega_s m_m)$	0.03	0.05
G13. Normalized radius of gyration	$h^2_m m_m/(r^2_G m_s)-(h_{G,s}m_s-h_m m_m)^2/[r^2_G m_s(m_m-m_s)]$	0.1	0.5

As mentioned above, the complete definition of the interpretative model requires 15 input groups, of which 8 were subjected to parametric analysis, while the remaining groups were fixed. Table 4.2 lists the values adopted for these fixed groups, which correspond to the existing framed building that was extensively analyzed and presented in the previous section.

Table 4.2 – Fixed groups

Non-dimensional group	**Value (fixed)**
G4. Normalized TMD height	1.5
G5. Foundation embedment ratio	0.0533
G8. Soil-structure relative mass	2.2
G11. Effective mass ratio	0.736
G12. Normalized rocking height	0.1016
G14. Normalized foundation mass density	1.5362
G15. Normalized frequency	Variable

The base quantities chosen in the dimensional analysis according to the Buckingham theorem are the structural mass, indicated as m_2 in Figure 4.1, the structural stiffness represented by the spring with stiffness k_s, and the modal height h_m. These fixed values were also evaluated based on the 8-story reference building.

Table 4.3 – Base quantities

Base quantity	**Value (fixed)**
m_2 [Mg]	3893
k_s [Kn/m]	67418
h_m [m]	18.58

The modal height evaluated with reference to the fundamental period of vibration, with the following formulation:

$$h_m = \frac{\{h\}^T[M]\{\phi\}}{\{\phi\}^T[M]\{I\}} \tag{4.1}$$

With h the vector that include the effective storey height, M the mass matrix, ϕ the eigenvector of the first mode (normalized) and I the identity vector
The total number of permutations across the groups is 186624. Each permutation corresponds to a specific soil-structure-TMD configuration, and for each one, the 4 models described above are recreated.
A routine in OpenSees determines the values to assign to all the dimensional quantities necessary for defining the models and allocates them to the various elements. Once the models are recreated, the base motion is applied through a series of harmonic forces with varying frequencies. A total of 31 different forces were defined, with periods ranging from 0.1 to 4 times the fundamental frequency of the main model. This fundamental period is fixed as it is determined by the base quantities k_s and m_2.
During the analyses, the main characteristics of the motion were recorded using a recorder: displacements and accelerations of the various nodes and forces mobilized in the springs. The results of the analyses were subsequently interpreted in a post-processor in the Matlab environment, which allowed for the quantification of the TMD efficiency for each analysis performed. The effectiveness of the TMD is defined as in Eq. 4.2 and refers to the reduction in structural drift ($u_{3\text{-}6}$, i.e., the relative displacement between nodes 3 and 6).

$$\eta_i = \frac{u_{3-6}(NoTMD) - u_{3-6}(TMD)}{u_{3-6}(TMD)} \tag{4.2}$$

u_{3-6} represents the maximum displacement between the nodes of the reference model (with and without TMD) across all the harmonic forces considered as input. The subscript i indicates the permutation number, and the efficiency refers to the maximum reduction in drift, providing an indication of the specific soil-structure-TMD system.
For this reason, the efficiency depends solely on the values of the groups considered as variables in the parametric analysis:

$$\eta = \eta\,(G_1, G_2, G_3, G_6, G_7, G_9, G_{10}, G_{13}) \tag{4.3}$$

Among the various groups on which efficiency depends, there are two that serve as design parameters. Identifying the values of G_2 and G_3 that yield the maximum efficiency, while keeping all other parameters constant, corresponds to determining the optimal parameters of the TMD.
Therefore, the goal of this analysis is not to find the law that describes efficiency itself, but rather the law that describes the behavior of the groups G_2 and G_3 that maximize it. These optimal functions for the TMD can be denoted as $G_{2,opt}$ and $G_{3,opt}$:

$$G_{2,OPT} = G_{2,OPT}\,(G_1, G_3, G_6, G_7, G_9, G_{10}, G_{13}) \tag{4.4}$$

$$G_{3,OPT} = G_{3,OPT}\,(G_1, G_2, G_6, G_7, G_9, G_{10}, G_{13}) \tag{4.5}$$

These two functions depend on the remaining groups and provide the tuning values: the frequency ratio ($G_{2,opt}$) and the damping ratio ($G_{3,opt}$)of the TMD, which maximize the efficiency for the specific soil-structure system characterized by those groups.

4.3 Design correlations

Frequency ratio G_2

For a reasonable understanding of these functions, it is possible to fix certain variables and visualize the effectiveness of the TMD as a function of others. For example, in Figure 4.3, the function η from Eq. 4.3 is shown in the G_2 and G_6 space, with all other quantities held constant.

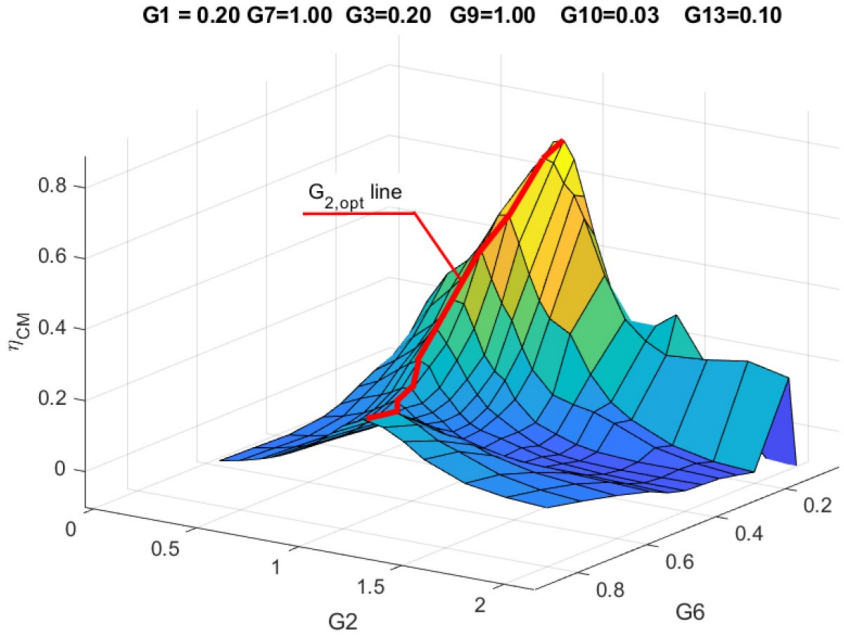


Figure 4.3 – Visualization of the effectiveness variability within the frequency ratio G_2 and the structure to soil relative stiffness G_6.

It is evident that by enveloping the maxima of this surface, the function $G_{2,opt}$ is obtained, which will depend solely on the variable G_6. As expected and consistent with the scientific literature on this topic, the optimal tuning values between the TMD and the structure, represented by the values taken by $G_{2,opt}$ (red line in Figure 4.3), are close to unity. It also aligns with known literature that efficiency is maximal for values of the soil-structure relative stiffness that approach zero, i.e., when the interaction is negligible, allowing these systems to be conveniently studied as fixed-base. Efficiency then decreases as interaction effects increase, eventually reaching an almost constant value when the soil behaves like a natural isolator (high values of G_6).
The variability of $G_{2,opt}$ can be represented in space as a function of two groups, with all others fixed. In Figures 4.4-4.7, for example, the groups G_6 and G_7 are shown with increasing values of the mass ratio (G_1). It can be observed that on the plane where $G_6 = 0$ (no interaction effects), there is a constant tuning value between the structure and the TMD, which is therefore not affected by structural slenderness. All surfaces are characterized by a

reduction in $G_{2,opt}$ for intermediate values of the soil-structure relative stiffness, followed by an increase at higher values. An increase in structural slenderness generally leads to a decrease in the value of $G_{2,opt}$. The effect of an increasing mass ratio manifests as a general lowering of the tuning values.

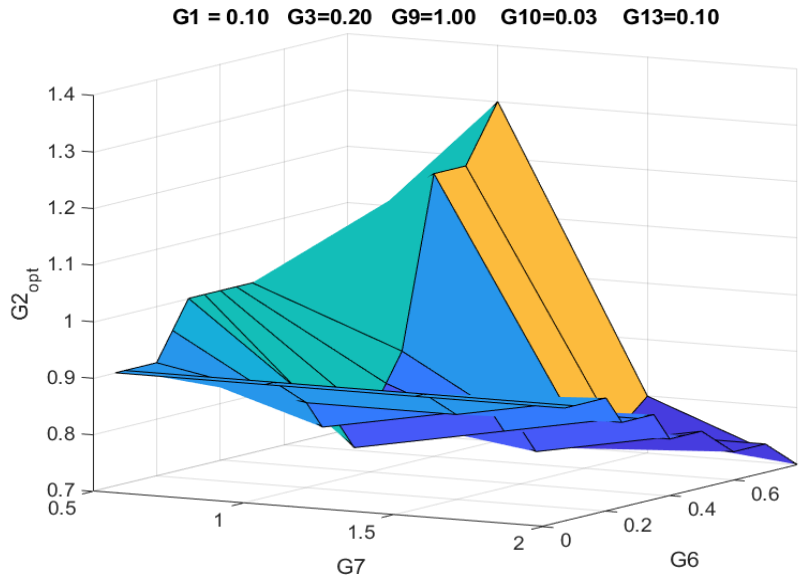


Figure 4.4 – G2,opt plotted as function of the structure to soil relative stiffness G_6 and structural slenderness G_7, for a TMD with 10% mass ratio

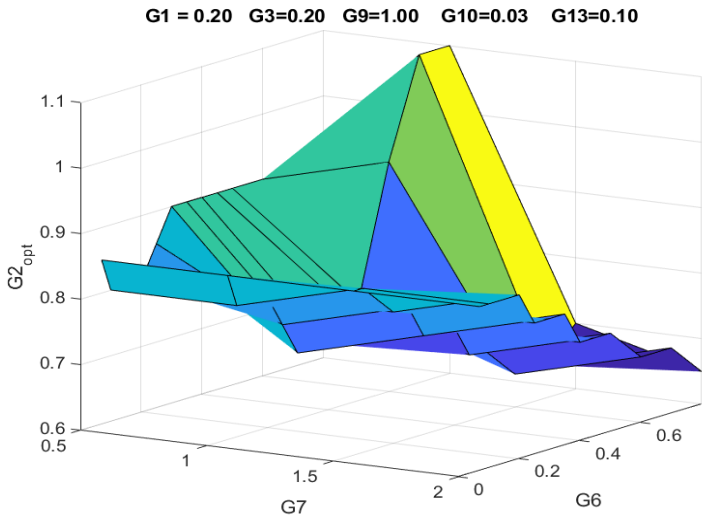


Figure 4.5 – G2,opt plotted as function of the structure to soil relative stiffness G_6 and structural slenderness G_7, for a TMD with 20% mass ratio

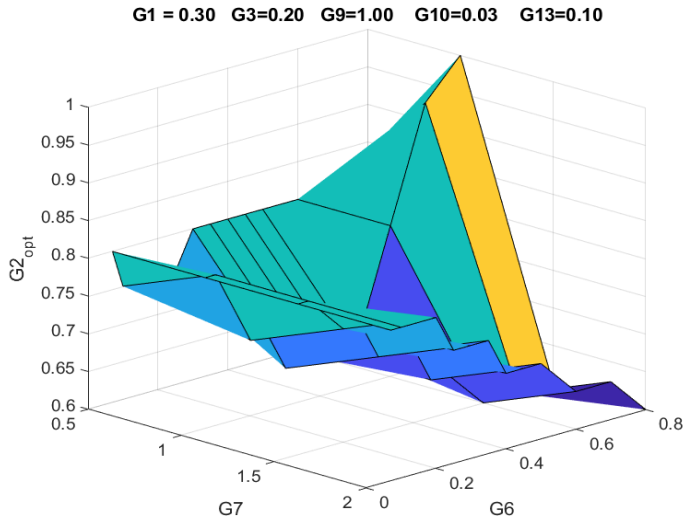


Figure 4.6 – G2,opt plotted as function of the structure to soil relative stiffness G_6 and structural slenderness G_7, for a TMD with 30% mass ratio

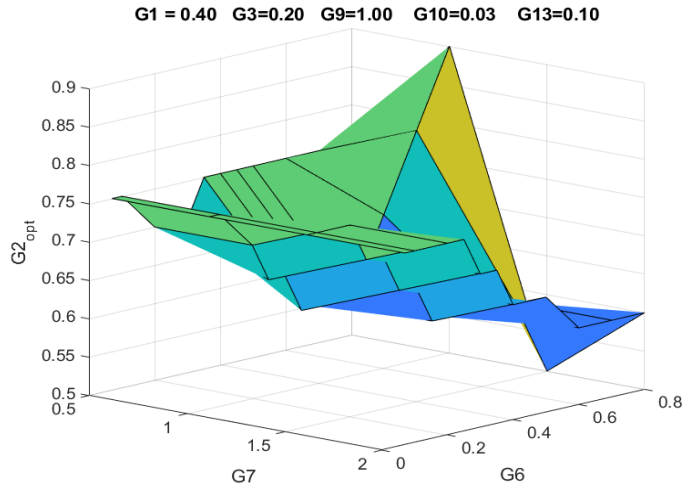


Figure 4.7 – G2,opt plotted as function of the structure to soil relative stiffness G_6 and structural slenderness G_7, for a TMD with 40% mass ratio

The interpolation process of the results began with the groups G_6 and G_7, and thus with the surfaces described above. For defining the interpolating function, the "curve fitting toolbox" in Matlab was used, which allows data interpolation with various functions for up to 2 variables. The functions provided by the toolbox enable data interpolation with R^2, coefficient of determination, values close to unity. However, the disadvantage of using these functions is that they require numerous coefficients for their definition, even in the R^3 space.

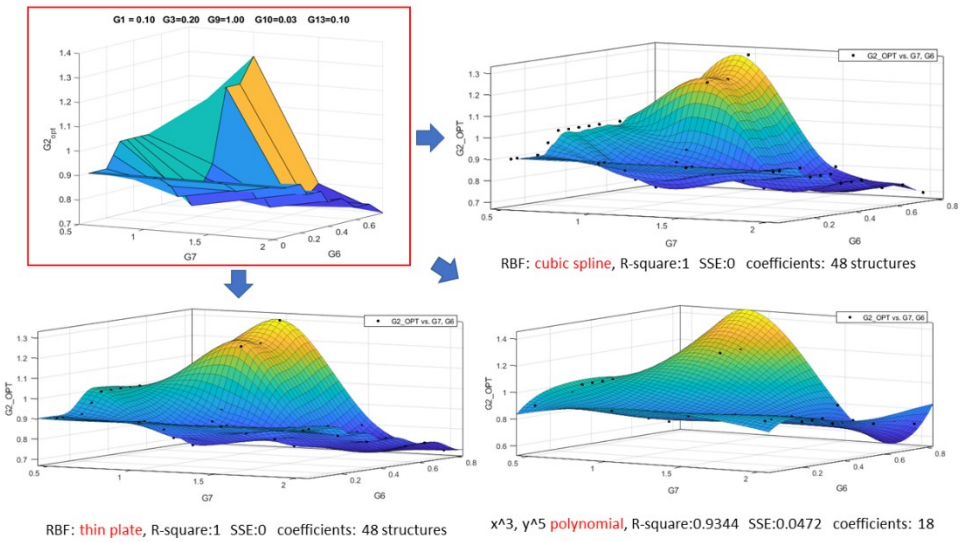


Figure 4.8 – Interpolation of the analysis results with Radial Basis Functions (RBF)

These functions, such as radial basis functions, require coefficient structures for each point to be interpolated, making them inconvenient when dealing with a large number of points, as in this case.
Thus, the interpolation process was carried out step-by-step, introducing variables one at a time into a general function. By examining planar sections of the surface in Figures 4.9-4.10, at fixed values of G_7, the resulting curves were found to be well interpolated by a Gaussian function.

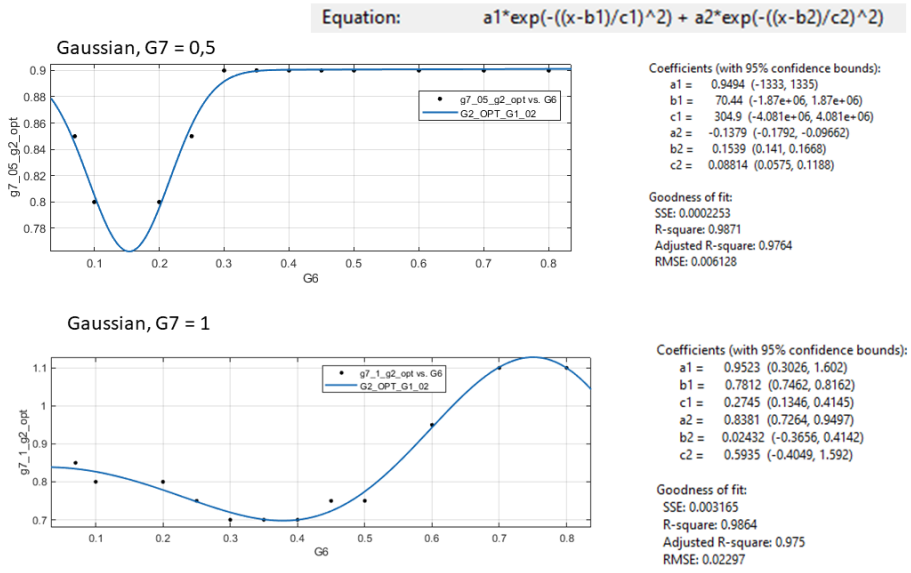


Figure 4.9 – Interpolation of the analysis results with a Gaussian Functions Slenderness fixed at 0.5 and 1

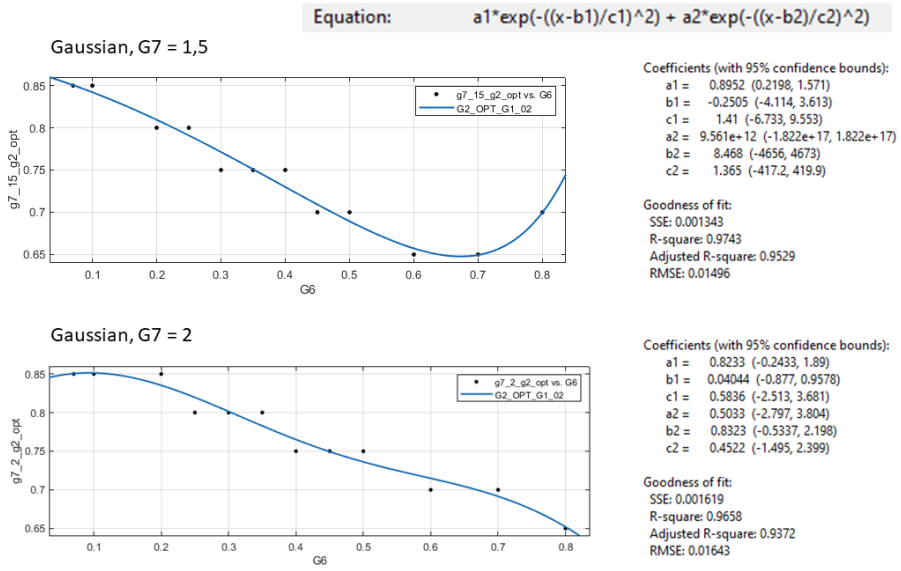


Figure 4.10 – Interpolation of the analysis results with a Gaussian Functions Slenderness fixed at 1.5 and 2

The Gaussian function, in fact, yielded a very high coefficient of determination (0.96–0.98). This observation allowed the use of a custom function defined within the toolbox, which automatically determines the coefficients that maximize the R^2 value.
A custom composite function was then defined, consisting of the sum of the equations of a plane, a 3D Gaussian, and a quartic:

$$z = A + B \cdot y + C \cdot x + D \cdot e^{-\left[\frac{(x-1)^2}{0.1} + \frac{(y-0.8)^2}{0.05}\right]} + E \cdot x \cdot y + F \cdot x \cdot y^3 + H \cdot y \cdot x^2 + L \cdot y \cdot x^3 \quad (4.6)$$

The coefficients *A, B, C, D, E, F, H, L* are unknowns to be determined, while the variables z, x, and y represent $G_{2,opt}$, G_7, and G_6, respectively. The internal coefficients of the Gaussian function were also determined using the toolbox. Therefore, the function can be rewritten in the form:

$$G_{2,OPT} = A + B \cdot G_6 + C \cdot G_7 + D \cdot e^{-\left[\frac{(G_7-1)^2}{0.1} + \frac{(G_6-0.8)^2}{0.05}\right]} + E \cdot G_7 \cdot G_6 + F \cdot G_7 \cdot G_6^3 + H \cdot G_6 \cdot G_7^2 + L \cdot G_6 \cdot G_7^3 \quad (4.7)$$

By keeping the values of the various groups fixed and repeating the interpolation process for different values of group G_1 (mass ratio), 4 sets of coefficients are obtained, each of which interpolates a different surface. Figures 4.11-4.14 show these surfaces along with the values of the 8 coefficients required for the best interpolation.

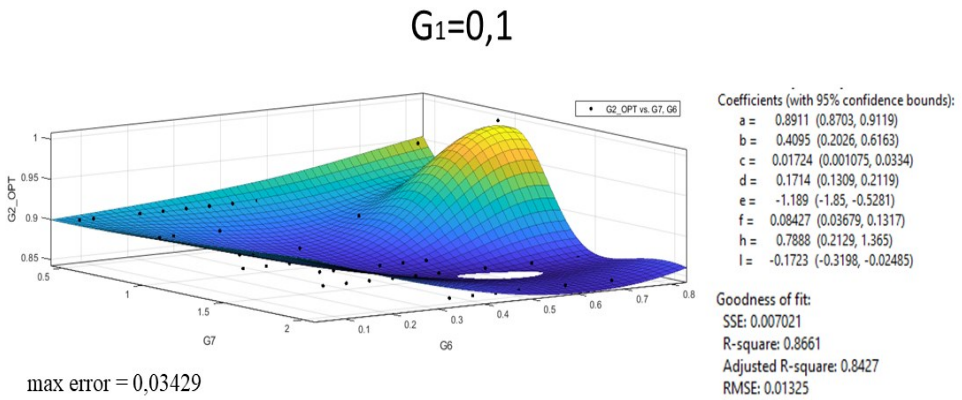


Figure 4.11 – Interpolation of the analysis results with the custom function and determination of the coefficients for a mass ratio of 10%

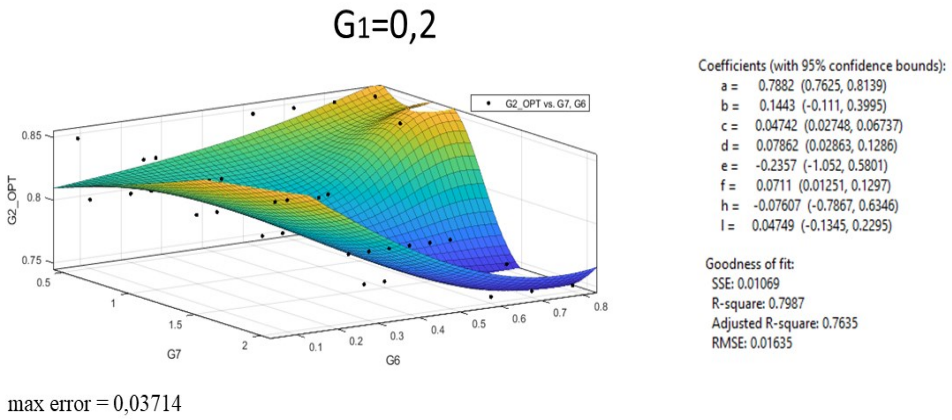


Figure 4.12 – Interpolation of the analysis results with the custom function and determination of the coefficients for a mass ratio of 20%

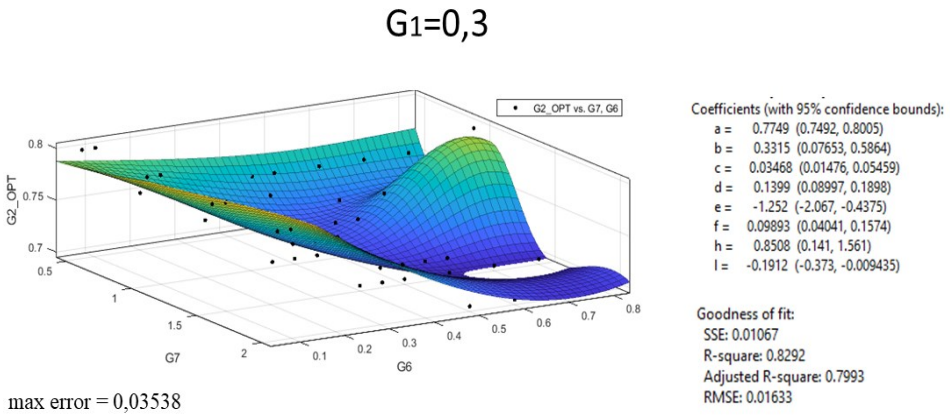


Figure 4.13 – Interpolation of the analysis results with the custom function and determination of the coefficients for a mass ratio of 30%

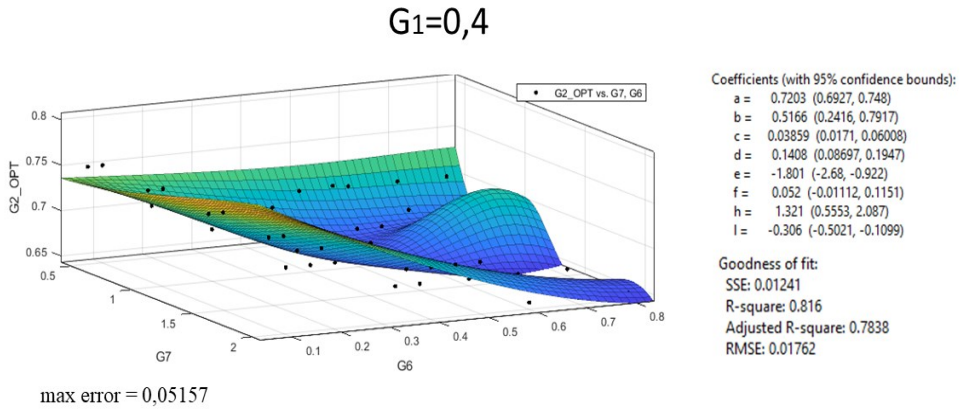


Figure 4.14 – Interpolation of the analysis results with the custom function and determination of the coefficients for a mass ratio of 40%

To incorporate the group G_1 into the general formulation of $G_{2,opt}$, an interpolation was performed on the coefficients. This interpolation was carried out for each of the 8 coefficients in the generic plane with G_1 as the abscissa, and a second-degree polynomial function was found to be sufficiently accurate.

Naturally, the use of a second-degree function introduced 3 coefficients for each of the main function's 8 coefficients, resulting in a total of 24 coefficients. Figure 4.15 presents the interpolations for the 8 coefficients, along with their respective trend curves.

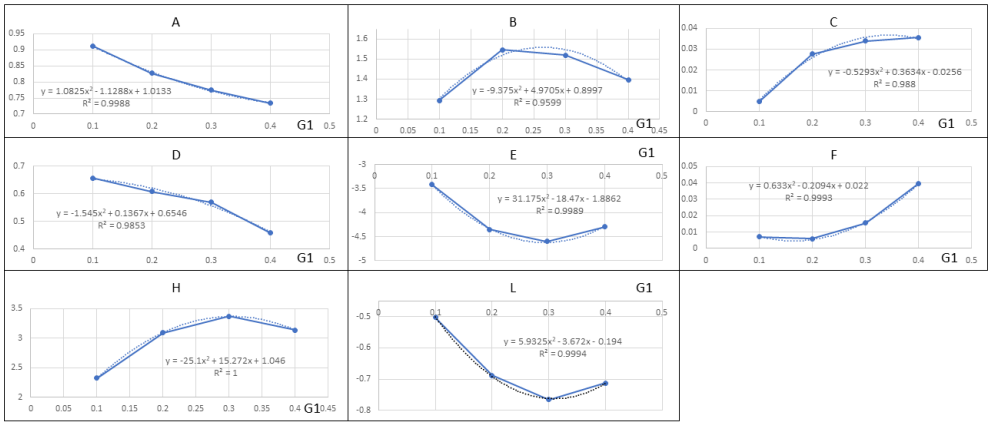


Figure 4.15 – Interpolation within G1

In this way, the coefficients in Eq. 4.7 themselves become functions, in this case, of group G_1. The equation for the coefficients remains the same, with only the subscript i varying to distinguish the different coefficients.

$$G_{2,OPT}\,(G_1, G_6, G_7) = \\ = A + B \cdot G_6 + C \cdot G_7 + D \cdot e^{-\left[\frac{(G_7-1)^2}{0.1} + \frac{(G_6-0.8)^2}{0.05}\right]} + E \\ \cdot G_7 \cdot G_6 + F \cdot G_7 \cdot G_6^3 + H \cdot G_6 \cdot G_7^2 + L \cdot G_6 \cdot G_7^3 \tag{4.8}$$

$$A, B, C, D, E, F, H, L = C_{i,1} \cdot G_1^2 + C_{i,2} \cdot G_1 + C_{i,3} \qquad i = A..L \tag{4.9}$$

Table 4.4 lists the coefficients of Eq. 4.9

Table 4.4 – Coefficients defining the variability due to the mass ratio G1

	A	B	C	D	E	F	H	L
$C_{i,1}$	1.0825	-9.375	-0.5293	-1.545	31.175	0.633	-25.1	5.9325
$C_{i,2}$	-1.1288	4.9705	0.3634	0.1367	-18.47	-0.2094	15.272	-3.672
$C_{i,3}$	1.0133	0.8997	-0.0256	0.6546	-1.8862	0.022	1.046	-0.194

Similar procedures were applied to introduce the other groups into the general function. For the sake of brevity, the intermediate steps are omitted, and the final formulation, which includes all the groups, is presented:

$$G_{2,OPT}(G_1, G_6, G_7, G_9, G_{13}, G_{10}) = A + B \cdot G_6 + C \cdot G_7 + D \cdot e^{-\left[\frac{(G_7-1)^2}{0.1} + \frac{(G_6-0.8)^2}{0.05}\right]} + E \cdot G_7 \cdot G_6 + F \cdot G_7 \cdot G_6^3 + H \cdot G_6 \cdot G_7^2 + L \cdot G_6 \cdot G_7^3 + M \cdot G_{10} \quad (4.10)$$

And coefficients defined as follows:

$$A, B, C, D, E, F, H, L, M = C_{i,1} + C_{i,2}G_1 + C_{i,3}G_9 + C_{i,4}G_1^2 + C_{i,5}G_1G_9 + C_{i,6}G_9^2 + C_{i,7}G_1^3 + C_{i,8}G_1^2G_9 + C_{i,9}G_1G_9^2 + C_{i,10}G_{13} + C_{i,11}G_{13}G + C_{i,12}G_{13}G_9 + C_{i,13}G_{13}^2G_1 + C_{i,14}G_{13}^2G_9 \quad (4.11)$$

The table of coefficients is thus provided, which, in the final formulation, consists of 116 coefficients.

Table 4.4 – Coefficients defining the functions A,B,C,D,E,F,H,L,M

	A	B	C	D	E	F	H	L	M
C1	1.095	-1.3	-0.096	-0.141	2.472	-0.128	-1.53	0.3501	-0.602
C2	-1.563	-0.365	0.688	-0.696	8.383	0.435	-10.11	2.7788	-1.88
C3	-0.219	4.748	0.24	0.684	-11.03	0.62	7.85	-1.905	0
C4	3.268	1.852	-1.476	3.382	-28.48	2.445	29.89	-8.15	8.676
C5	0.044	-1.746	-0.319	-0.727	-3.549	-1.684	6.221	-1.715	0
C6	0.217	-2.612	-0.217	0.149	6.571	-0.502	-5.117	1.3294	0
C7	-3.333	19.62	1.499	-0.468	-36.24	-3.982	24.93	-5.407	-14.46
C8	0.478	-26.07	-0.352	-3.883	85.59	0.283	-72.1	17.861	0
C9	-0.283	9.682	0.405	1.023	-26.68	1.048	20.75	-5.075	0
C10	0.055	-0.102	-0.051	0.047	0.188	-0.077	-0.178	0.0751	0
C11	0.065	-0.761	-0.402	-0.212	3.007	-2.115	-0.227	-0.146	0
C12	-0.194	0.61	0.323	-0.017	-1.662	0.539	0.854	-0.232	0
C13	-0.109	1.303	0.502	0.408	-4.57	2.622	0.706	0.1526	0
C14	0.245	-0.876	-0.471	-0.165	2.341	-0.91	-0.569	0.0659	0

It can be observed that, compared to Eq. 4.7, which included only the groups G_6 and G_7, the final function explicitly introduces group G_{10} through the coefficient M. In the definition of M coefficients, only the multiplicative coefficients of group G_1 are non-zero, making it effectively dependent solely on G_1. The final formulation also demonstrated an excellent fit with the actual values of $G_{2,opt}$ obtained from the analyses (Table 4.5).

Table 4.5 – Statistical indicators of the fitting

R-square	0.9294
SSE	2.1306
SST	30.18
MSE	0.0087
RMSE	0.0934
Average error	0.0189

Damping ratio G_3

All formulations related to TMDs provide a similar law for evaluating the optimal value of the damping ratio of the TMD, referred to as G_3 in this study. Thus, assessments were also conducted for this parameter. The results showed that variability in the optimal damping values exists only when the mass ratio is low (0.10). For higher mass ratios, the optimal damping consistently corresponded to the maximum available value.
When examining structure-TMD systems with a mass ratio of 0.1 and determining the efficiency at the optimal tuning ($G_{2,opt}$), it can be seen that the efficiency may be greater or lesser depending on the value of group G_3. Figures 4.16 and 4.17 illustrate the efficiency values of the TMD evaluated at the optimal G_2 and the different damping ratio values considered. The former shows the ratio of the output effectiveness obtained between the lowest value considered for the damping ratio of TMD (0.15) and the reference value (0.2), and the latter the ratio between the highest (0.2) and the reference one. The ratio of efficiencies, evaluated in the G_6, G_7 space, will form a surface that takes on values either greater or less than one, depending on the two variables considered.

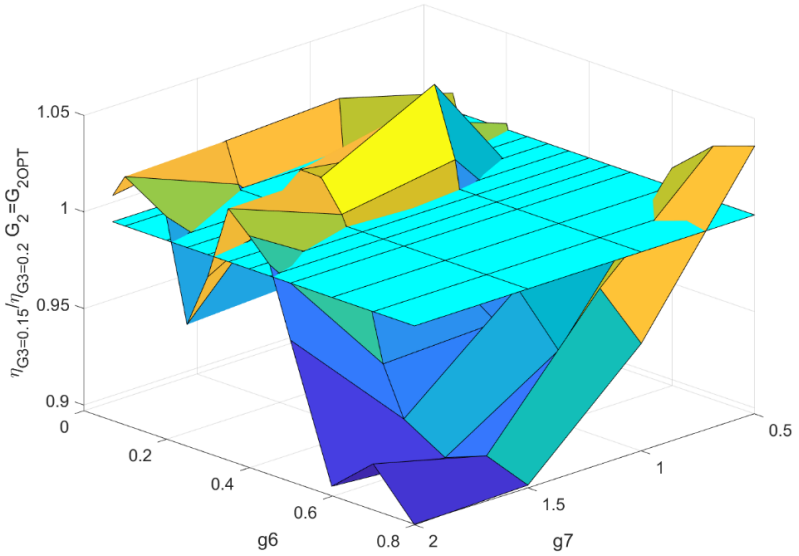


Figure 4.16 – Effectiveness ratio between models with different TMD damping ratio. 15% and 20% damping ratio in the G_6 and G_7 space. TMDs with 10% mass ratio

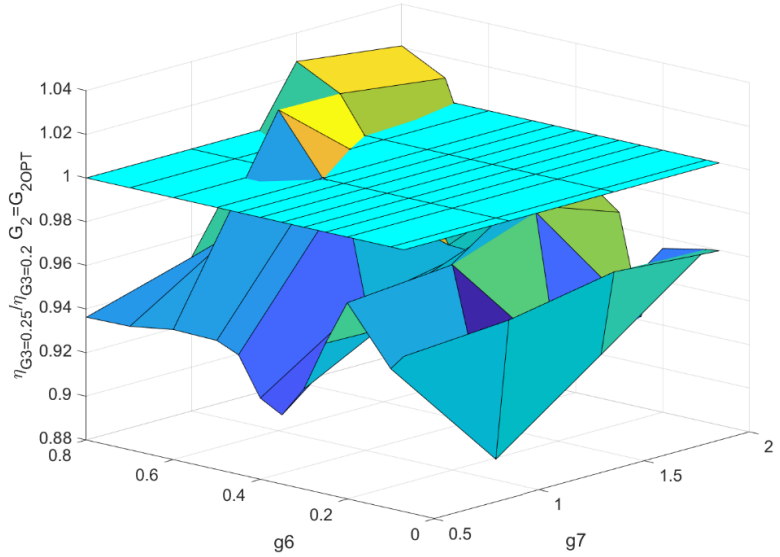


Figure 4.17 – Effectiveness ratio between models with different TMD damping ratio. 25% and 20% damping ratio in the G_6 and G_7 space. TMDs with 10% mass ratio

From these surfaces, it becomes clear that the determination of the optimal G_3, i.e. $G_{3,opt}$, should be done on a case-by-case basis, considering all other groups, just as was done for $G_{2,opt}$.
However, when looking at higher mass ratios (0.2 in Figures 4.18 and 4.19), it can be observed that effictiveness is consistently greater in TMDs with a higher damping ratio. In fact, the ratio $\eta_{G3=0.15}/\eta_{G3=0.2}$ is always less than one, while the ratio $\eta_{G3=0.25}/\eta_{G3=0.2}$ is always greater than one.

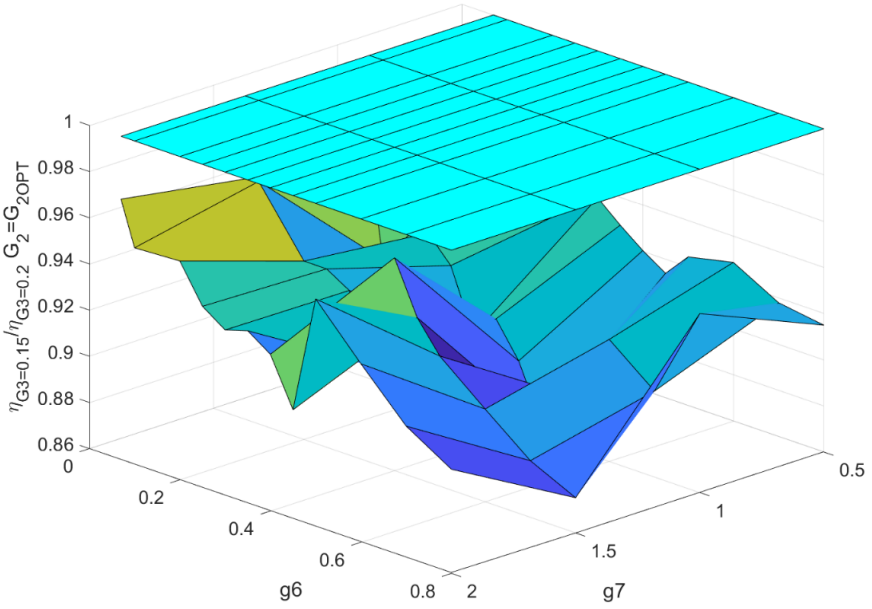


Figure 4.18 – Effectiveness ratio between models with different TMD damping ratio. 15% and 20% damping ratio in the G_6 and G_7 space. TMDs with 20% mass ratio

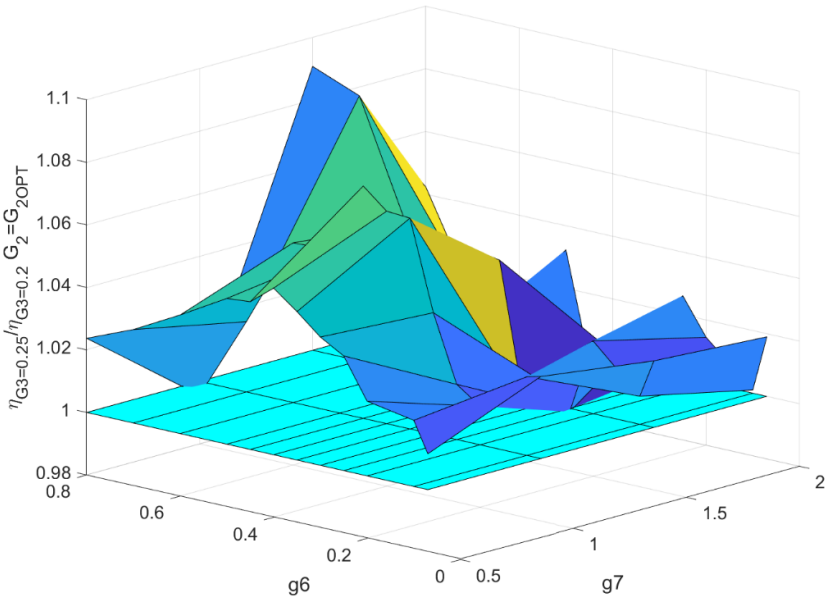


Figure 4.19 – Effectiveness ratio between models with different TMD damping ratio. 25% and 20% damping ratio in the G_6 and G_7 space. TMDs with 20% mass ratio

The same behavior was observed for even higher mass ratios. Therefore, it was deemed unnecessary to derive an analytic formulation predicting the optimal G_3, as it would be limited to only one of the mass ratios considered in the parametric analysis. Table 4.6 provides a complete overview of the occurrence percentages of the optimal G_3 values, differentiated by the various mass ratios.

Table 4.6 – Percentages of optimal G3 for each mass ratio G1

	% $G_{3,opt}$=0.15	% $G_{3,opt}$=0.20	% $G_{3,opt}$=0.25
G_1=0.1	28.24	47.45	24.31
G_1=0.2	0.23	7.41	92.36
G_1=0.3	0.00	1.16	98.84
G_1=0.4	0.00	0.00	100.00

To summarize the considerations for all cases belonging to the class G_1=0.1, i.e. for all soil-structure (SS) systems considered with a mass ratio of 10%, Figure 4.20 presents the ratios between the efficiency evaluated at the optimal G_2 alone and that evaluated at both $G_{2,opt}$ and $G_{3,opt}$. The figure displays the mean values and the standard deviations of these ratios.

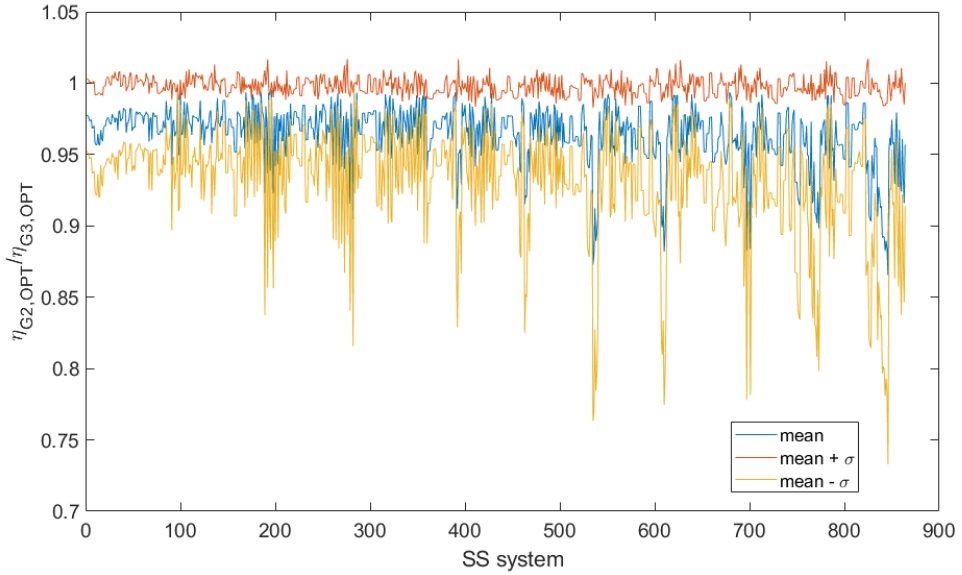


Figure 4.20 – Effectiveness ratio mean and standard deviation between Soil Strucure systems (SS) with 10% TMD mass ratio.

"SS" indicates a soil-structure system, identified by all groups except those related to the TMD (G_1, G_2 and G_3). The mean values refer, for each SS, to the average ratio between the maximum efficiency ($G_{2,opt}$ and $G_{3,opt}$) and that obtained with other values of G_3, while the standard deviation refers to the means for all SS systems.
If the effectiveness ratio mean values, shown on the y-axis in Figure 4.20, are plotted as a function of the groups G_6 and G_7, the region where the error in estimating a non-optimal damping ratio is most significant can be visualized. Figure 4.21 shows indeed a decrease of around 10% in efficiency for high values of structure-to-soil relative stiffness, associated with a specific structural slenderness value (1.5). Each point on this surface corresponds to

the mean of the vertical axis of Figure 4.20 of the ratio for all SS systems with the same G_6 and G_7 values. However, if the actual efficiency in this region is examined, as depicted in Figure 4.22, it is characterized by relatively low values, which are not particularly significant from an engineering application perspective. η_{opt} in the vertical axis in Figure 4.22 represents the max of the effectiveness of a given Soil-Structure system with fixed G_6 and G_7, and in correspondence of the optimum in the frequency and damping ratio of the TMD ($G_2=G_{2,opt}$ and $G_3=G_{3,opt}$).

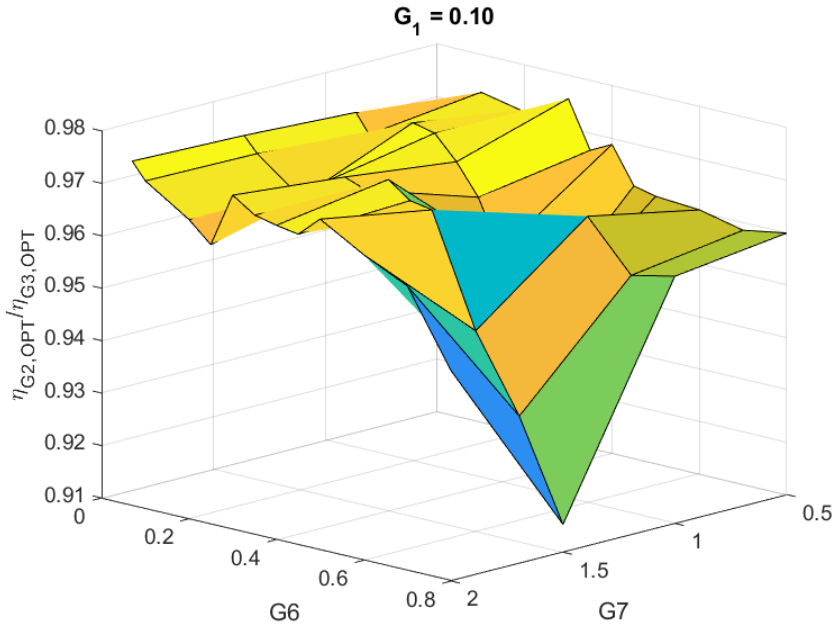


Figure 4.21 – Effectiveness ratios mean and its variability with G6 and G7, for 10% mass ratio TMDs.

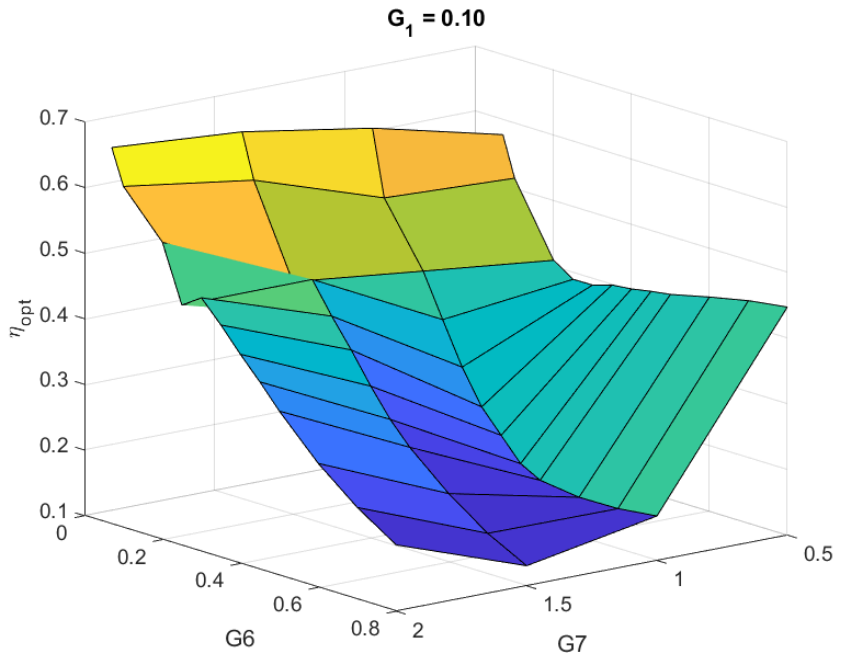


Figure 4.22 – Mean of the effectiveness in correspondence of the optimum and its variability with G6 and G7, for 10% mass ratio TMDs.

The design formulation obtained is therefore sufficiently accurate for designing TMDs with a high mass ratio. The reference building used in defining the interpretative model, which was the subject of analysis, consists of an existing reinforced concrete structure of the "moment-resisting frame" type, which has been extensively characterized and studied in previous sections. This raises the question of whether the formulation obtained can be considered valid when applied to buildings of different types, such as those with different construction materials.

Normalised foundation mass density G_{14}

Among the groups considered fixed in the parametric analysis, those deemed insignificant for efficiency in the work of Gorini and Chisari (2022) [29], is group G_{14}, the normalized foundation mass density, which was fixed as it had

been validated on a timber structure. As a final step in defining the design formulation, it was decided to introduce variability with this group as well.
Indeed, if we compare the value of G_{14} for the timber structure considered by the authors of the interpretative model (25.263) with that calculated for the reference building in this study (1.5362), a significant difference is observed, driven by the varying mass resulting from the construction type. The parametric analysis was then repeated, considering all the previously studied groups but with G_{14} fixed to the value for the timber structure.
A further comparison was then made on the $G_{2,opt}$ fitting, between the exact values (those obtained from the new analyses with G_{14}=25.263) and those predicted by the previously derived formulation, which had G_{14} fixed at 1.5362. The comparison was not very satisfactory, as it resulted in a low correlation coefficient and similarly poor performance in other statistical indicators.

Table 4.6 – Statistical indicators of the fitting with G14 set equal to 25.263 (timber structure)

R^2	0.4348
SSE	17.0587
SST	30.1819
MSE	0.0087
RMSE	0.0935
Average error	0.0526

Therefore, it was decided to introduce group G_{14} into the main equation of $G_{2,opt}$ through an additional coefficient, N. By appropriately selecting the coefficients of N, a direct dependency was established solely on groups G_9 and G_{13}.

$$G_{2,OPT}(G_1, G_6, G_7, G_9, G_{13}, G_{10}, G_{14}) = \\ = A + B \cdot G_6 + C \cdot G_7 + D \cdot e^{-\left[\frac{(G_7-1)^2}{0.1} + \frac{(G_6-0.8)^2}{0.05}\right]} + E \\ \cdot G_7 \cdot G_6 + F \cdot G_7 \cdot G_6^3 + H \cdot G_6 \cdot G_7^2 + L \cdot G_6 \cdot G_7^3 + M \\ \cdot G_{10} + N \cdot G_{14} \tag{4.12}$$

$$A, B, C, D, E, F, H, L, M, N = C_{i,1} + C_{i,2}G_1 + C_{i,3}G_9 + C_{i,4}G_1^2 + C_{i,5}G_1G_9 + C_{i,6}G_9^2 + C_{i,7}G_1^3 + C_{i,8}G_1^2G_9 + C_{i,9}G_1G_9^2 + C_{i,10}G_{13} + C_{i,11}G_{13}G_1 + C_{i,12}G_{13}G_9 + C_{i,13}G_{13}^2G_1 + C_{i,14}G_{13}^2G_9 \quad (4.13)$$

The table of coefficients in then provided

Table 4.7 – Coefficients of the fitting

	A	B	C	D	E	F	H	L	M	N
C1	1.125945	-0.66088	-0.10777	-0.0317	1.513666	-0.51898	-0.76409	0.163156	-1.61166	0.000785
C2	-2.3505	2.450657	0.888495	-0.50887	-3.17637	2.839898	-1.61058	0.797071	14.94456	0
C3	-0.0905	1.454318	0.169025	0.220781	-3.92571	1.260394	2.404972	-0.58172	0	-0.00162
C4	6.897391	-11.9612	-2.48738	1.365627	9.204886	-2.86624	6.481941	-3.36457	-64.0894	0
C5	-0.10484	-0.58261	-0.19943	0.262479	0.437745	-4.54184	2.294785	-0.68266	0	0
C6	0.06856	-0.49692	-0.11493	0.133977	1.620818	-0.63703	-1.06603	0.269717	0	0.000951
C7	-7.92963	24.04309	2.63734	0.167519	-37.8991	0.873954	15.51874	-1.6679	81.01575	0
C8	-0.00423	-8.99622	-0.02263	-2.05453	32.27268	2.022998	-28.7566	7.24487	0	0
C9	0.037006	2.90817	0.156332	0.24089	-9.91054	1.932422	7.217738	-1.70754	0	0
C10	0.034496	0.014284	-0.03241	0.047284	-0.11894	-0.00563	0.071716	0.001714	0	-0.00037
C11	0.135966	-0.46373	-0.33903	-0.06518	1.704859	-1.52291	-0.15153	0.026246	0	0
C12	-0.15811	0.757804	0.237881	0.018035	-2.1185	0.171278	1.620277	-0.45628	0	-0.00011
C13	-0.1769	0.288057	0.422634	0.003204	-1.24053	2.113919	-0.60269	0.145936	0	0
C14	0.238806	-1.06772	-0.38046	-0.10702	2.999872	-0.55625	-1.8667	0.511052	0	-0.0005

And the relative statistical data

Table 4.6 – Statistical indicators of the final fitting

R^2	0.7473
SSE	11.57
SST	45.81
Max_error	0.24
MSE	0.0066
RMSE	0.0814
Average error	0.0313

The correlation factor R^2 may seem significantly lower with the introduction of the additional group G_{14}, which is primarily due to a few data points where the discrepancy between the function and the exact values is notably high. Fortunately, this poor fitting is limited: the points causing an error greater than

0.1 in $G_{2,opt}$ make up only 1.8% of the total. Recalculating the determination coefficient while excluding these outliers yields an R^2 of 0.922, which is very close to the value obtained previously in the formulation without G_{14}.
The error resulting from the use of the formulation can be quantified and correlated to the different groups, allowing for a better understanding of the limits of the proposed formulation. In Figures 4.22-4.25, bar charts are presented, showing the percentage of cases that exceed a specified error threshold for certain groups. The error is evaluated as the difference between the exact values of G2,opt obtained from the analyses and those calculated through Eqs. 4.11-4.12.

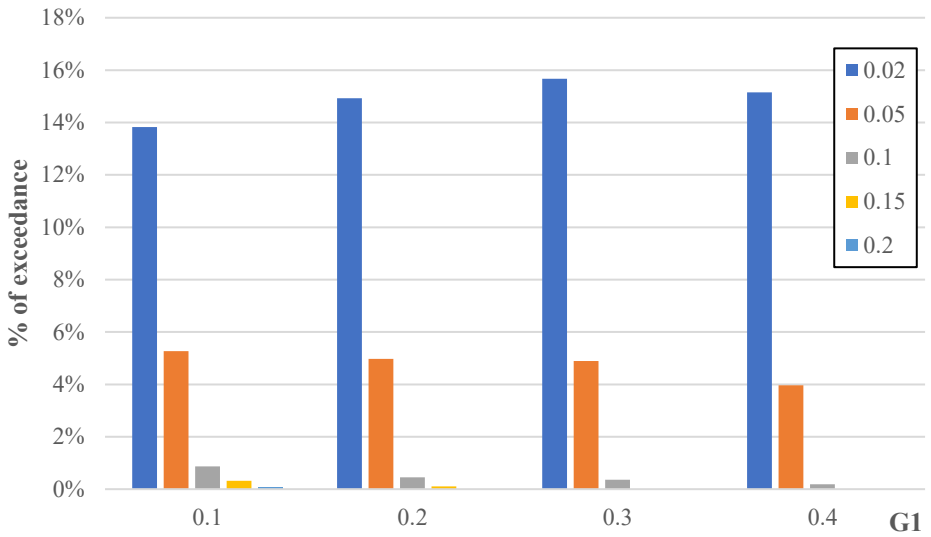


Figure 4.22 – Percentages of exceedance at threshold errors within the group G1

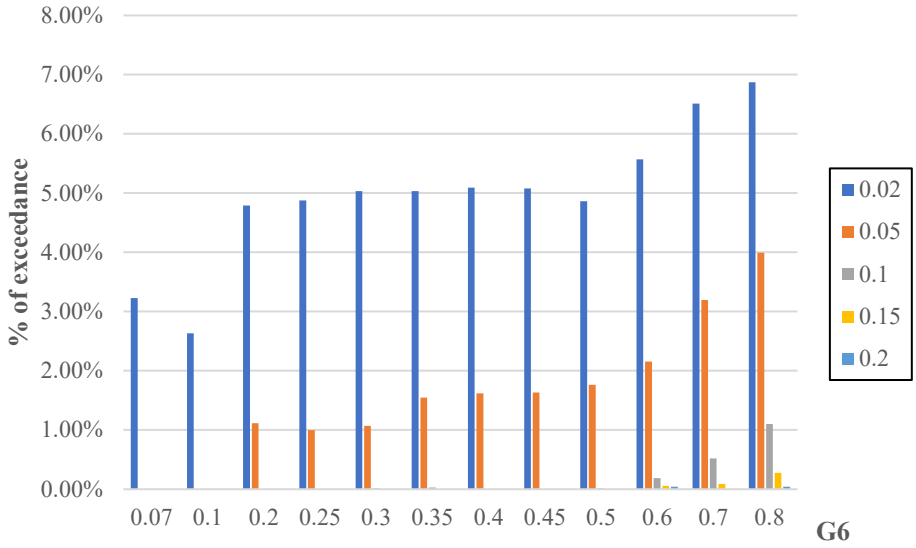


Figure 4.23 – Percentages of exceedance at threshold errors within the group G6

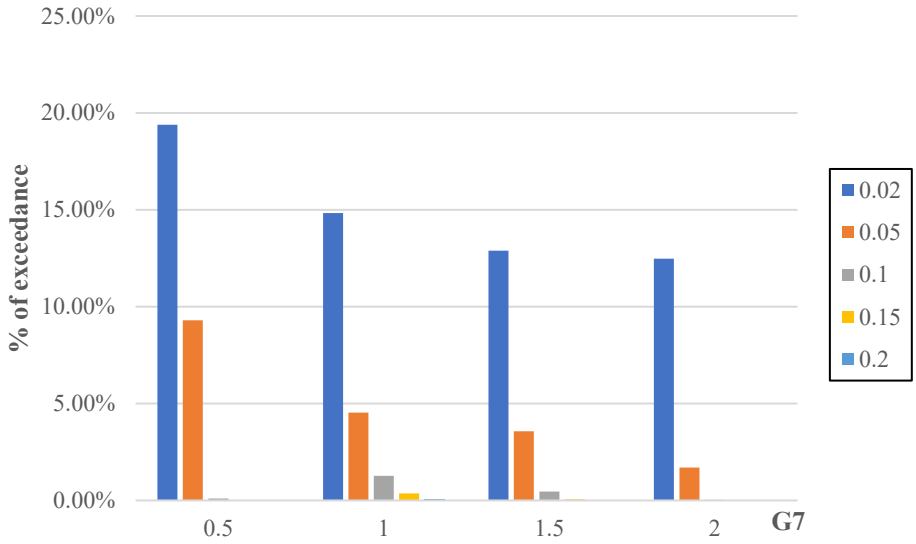


Figure 4.24 – Percentages of exceedance at threshold errors within the group G7

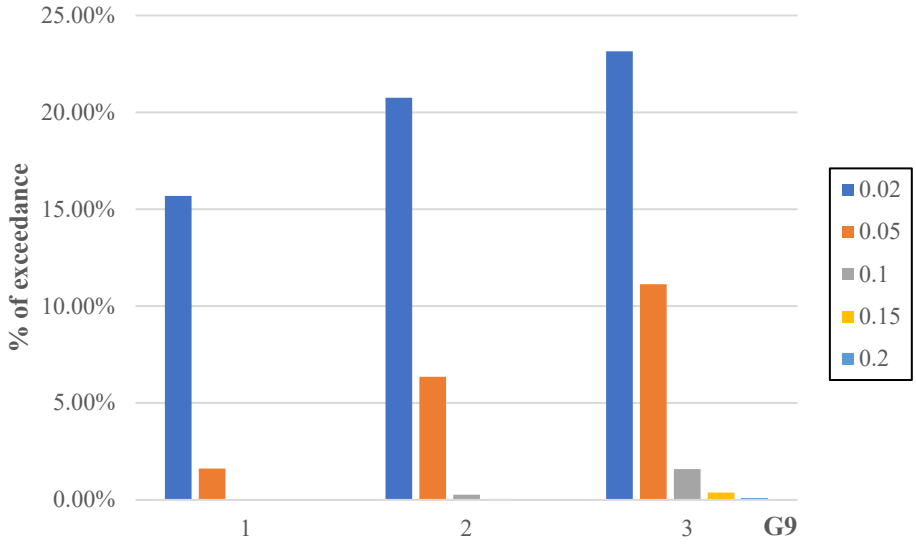


Figure 4.25 – Percentages of exceedance at threshold errors within the group G9

For the other groups, no significant error distribution was observed as the group values varied. However, for groups G_1 and G_7, a noticeable decrease in the number of points with high error is observed as their values increase. Conversely, for groups G_6 and G_9, the number of points with significant error increases as their values grow.

Finally, a representation of all cases is provided, in Figure 4.26 with efficiency on the x-axis and the corresponding error on the y-axis. The majority of points with high errors occur at very low efficiency values, which is a positive condition, as these scenarios may suggest that alternative approaches to TMD intervention could be more suitable for the existing structure.

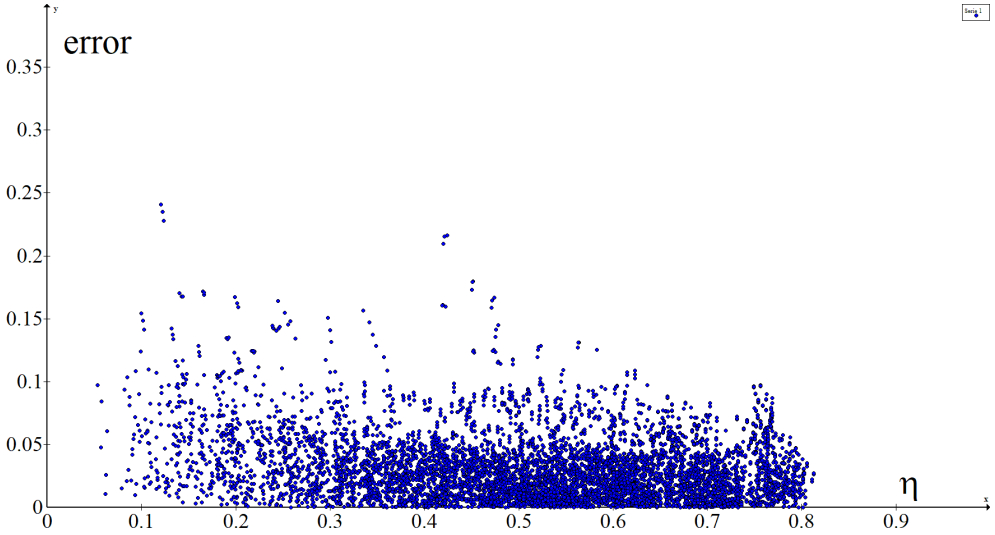


Figure 4.26 – Point cloud of the errors as function of the effectiveness

5 CHAPTER 5 VALIDATION

5.1 Validation on the similSDOF

Once the last group (G_{14}) has been introduced in the final formulation, a first validation can be made on the goodness of the fitting by recalculating the effectiveness on all the soil-structure systems considered previously. For each one has been evaluated the optimum of the frequency ratio ($G_{2,opt}$) obtained from the proposed formulation and then imposed for the group. By fixing a unique value for the groups G_2 and G_3 (reference value for the damping ratio of the TMD is 0.2) the total of the SSS to be analyzed is 6912. The effectiveness obtained are then compared with those of the parametric analysis and the comparison is shown in Figure 5.1 where the vertical axis represents the values obtained from the latter and the horizontal axis the former. The correlation factor is shown (0.974) and demonstrates a good accordance.

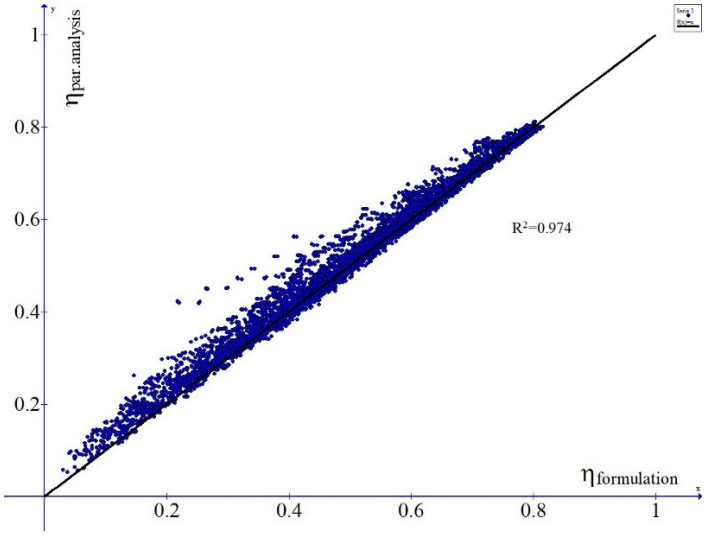


Figure 5.1 – Point cloud comparison of the effectiveness between analytical formulation and parametric analysis

To validate the proposed formulation, a comparison was made with a classical formulation (Den Hartog). The analyses were repeated on the previous cases, but with the difference that, for each soil-structure system, the optimal values of groups G_2 and G_3 were obtained using Den Hartog's formulation. Figure 5.2 presents the comparison with the efficiencies of the proposed formulation. The majority of the points, especially those with low efficiency, are positioned in favor of the proposed formulation.

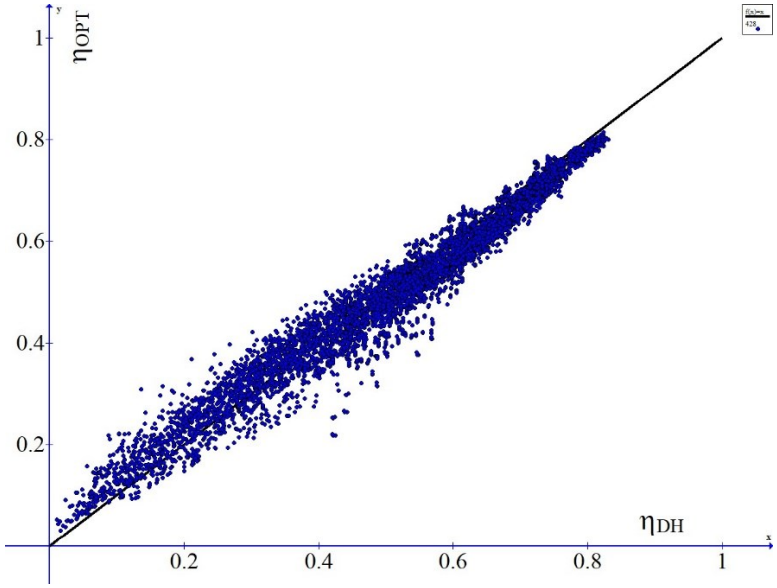


Figure 5.2 – Point cloud comparison of the effectiveness between a classical formulation and proposed one

Having observed a higher efficiency associated with high damping values (which, as seen in the previous section, always occurs for $G_1 > 0.1$), it was considered feasible to use Den Hartog's formulation to determine the optimal damping ratio of the TMD (Figure 5.3). This approach yields relatively high damping values for the examined cases, as it is dependent on the G_1 group.

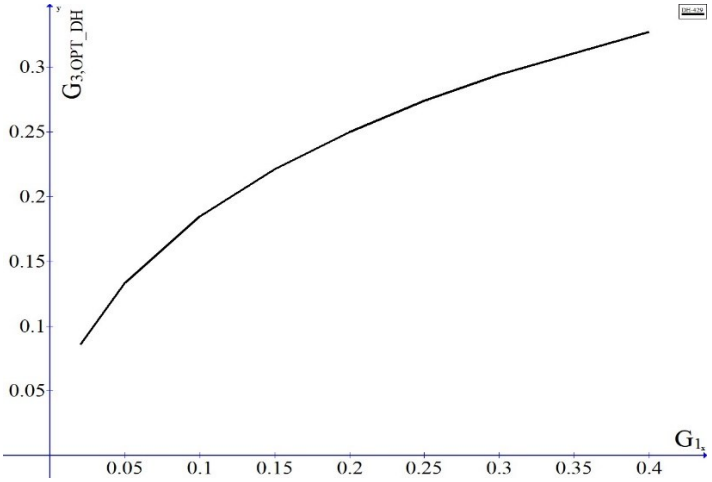


Figure 5.3 – Den Hartog's formulation for the Damping Ratio of TMD

The same cases were then reanalyzed once again, using the G_2 value obtained from the proposed formulation but the G_3 value derived from the classical formulation and results are shown in Figure 5.4, comparing them with the complete Den Hartog formulation (G_2 and G_3).

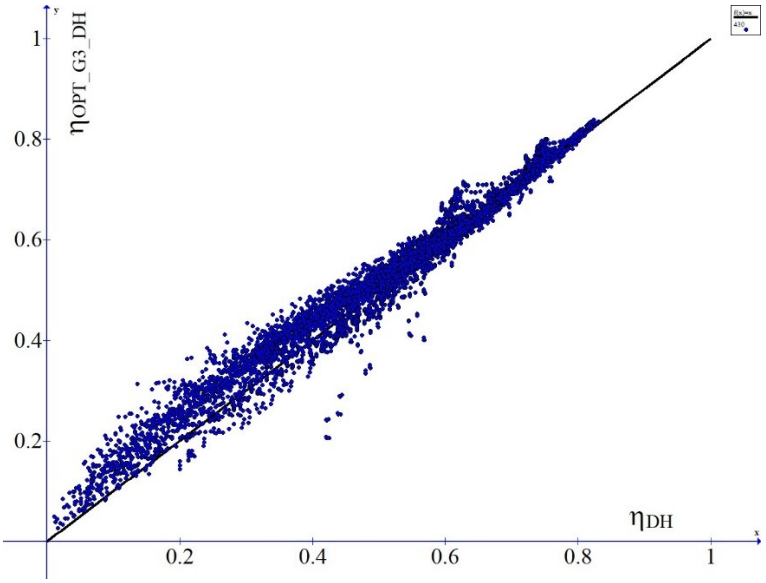


Figure 5.4 – Den Hartog's formulation compared with proposed formulation (assuming G_3 from DH)

If the ratio between the efficiency obtained in this way (G_2 according to the analytical formulation and G_3 according to the classic one) and that of the classical formulation is calculated and plotted as a scatter plot against the efficiency of the classical formulation, the representation shown in Figure 5.5 is obtained. In this form, a positive effect associated with the new formulation can be observed: when the efficiency obtained from the classical formulation is modest, a clear improvement is evident when adopting the new formulation.

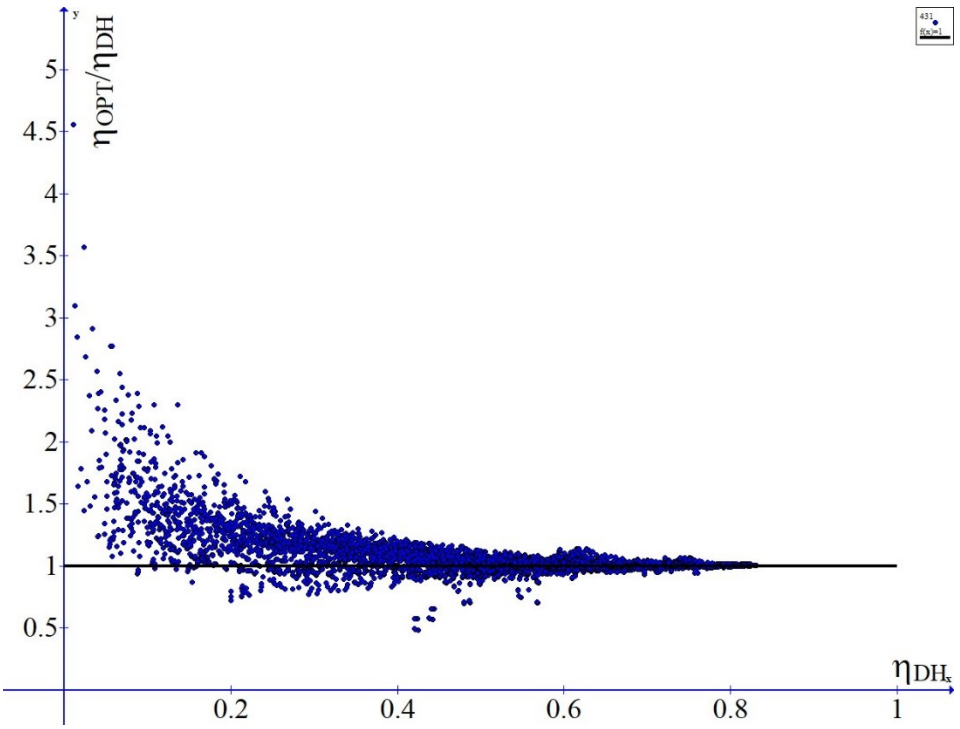


Figure 5.5 – Effectiveness ratio between proposed formulation and Den Hartog's, plotted as function of DH's

To better understand the variety of cases represented in the scatter plot, the variation of the efficiency ratio as a function of the groups considered in the analysis can be examined. The Figure 5.6 shows the trend as a function of group G_6 in statistical terms. As the value of G_6 increase, the ratio between

effectiveness increase. Also the standard deviation associated with high values of G_6 shows a greater dispersion.

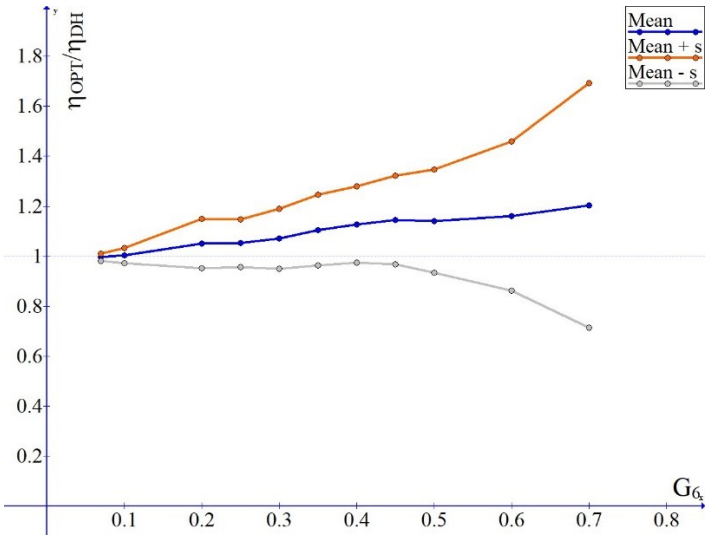


Figure 5.6 – Effectiveness ratio mean and standard deviation between proposed formulation and Den Hartog's, plotted as function of the group G_6

The comparison in terms of scatter plots can be performed for the main groups considered in this study.

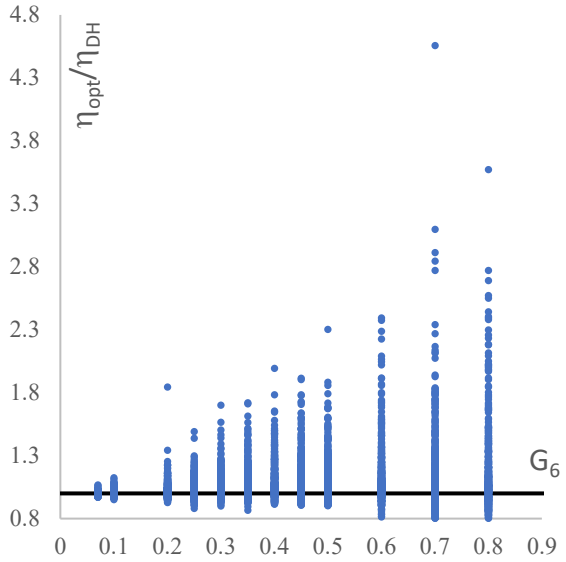


Figure 5.7 – Effectiveness ratio between proposed formulation and Den Hartog's, plotted as function of the group G_6

Figure 5.7 confirms the trend of Figure 5.6, with an arrangement of points closer to unity for low values of G_6, i.e. no soil-structure interaction, and a wider configuration of the considered effectiveness ratio that increase with the increase of the soil interaction effects. In Figures 5.8-5.13 the trends of the effectiveness ratio are shown for the main groups.

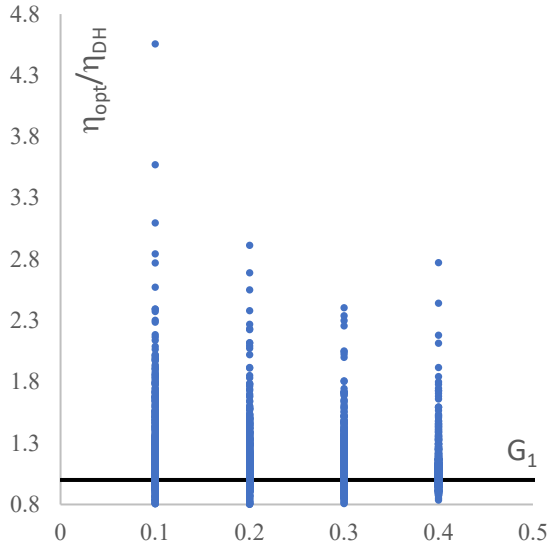


Figure 5.8 – Effectiveness ratio between proposed formulation and Den Hartog's, plotted as function of the group G_1

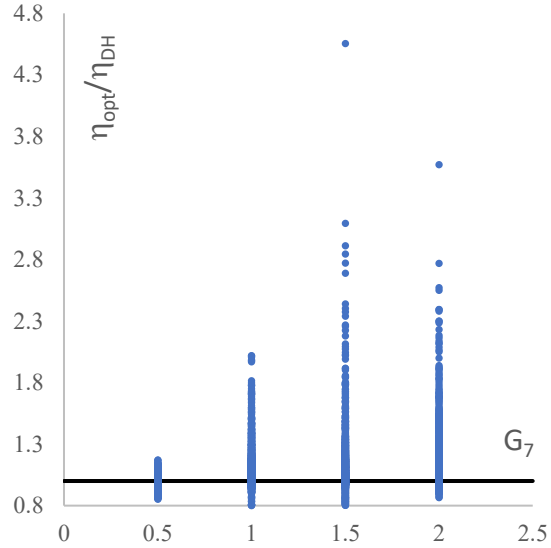


Figure 5.9 – Effectiveness ratio between proposed formulation and Den Hartog's, plotted as function of the group G_7

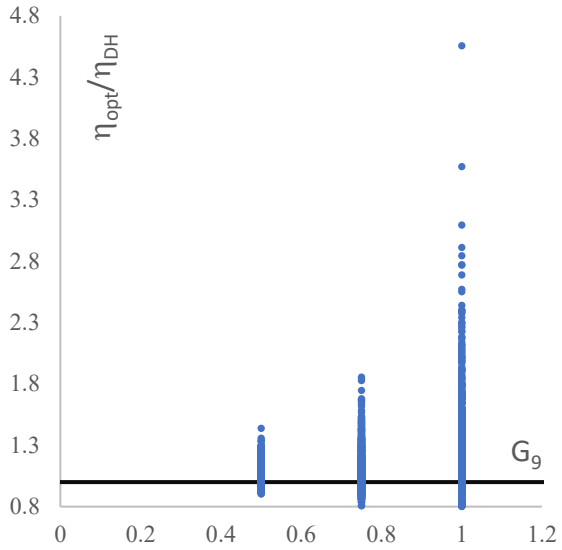


Figure 5.10 – Effectiveness ratio between proposed formulation and Den Hartog's, plotted as function of the group G_9

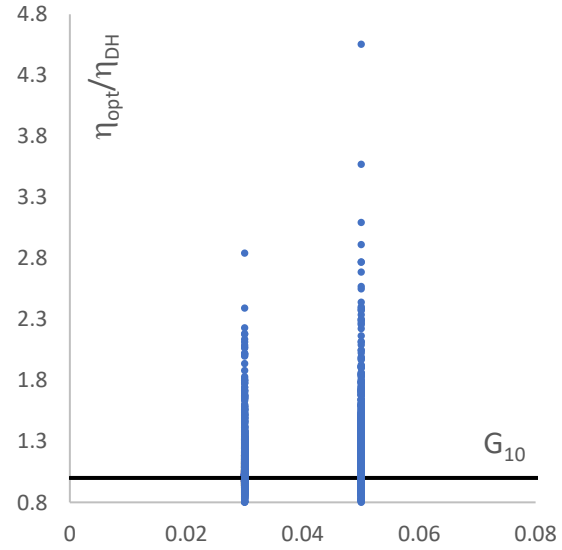


Figure 5.11 – Effectiveness ratio between proposed formulation and Den Hartog's, plotted as function of the group G_{10}

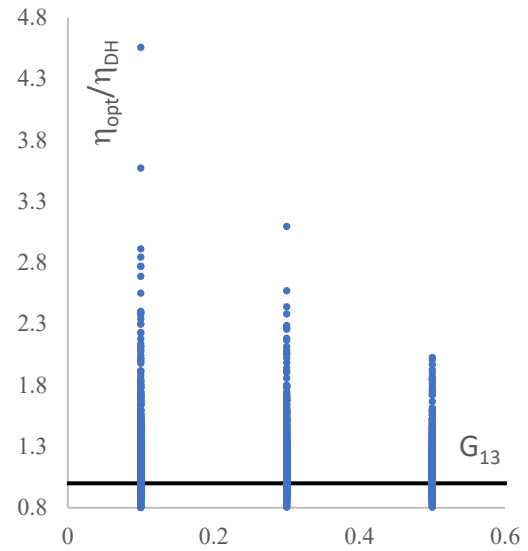


Figure 5.12 – Effectiveness ratio between proposed formulation and Den Hartog's, plotted as function of the group G_{13}

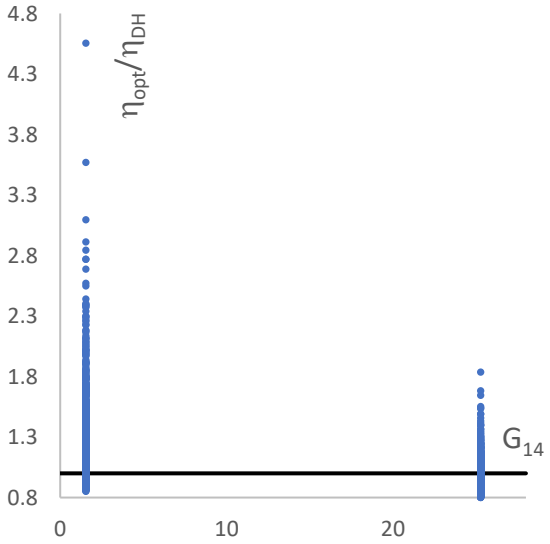


Figure 5.13 – Effectiveness ratio between proposed formulation and Den Hartog's, plotted as function of the group G_{14}

It is possible to represent, in the same manner and by groups, the ratio between the optimal frequency ratio (G_2) obtained from the proposed formulation and that of Den Hartog. In Figures 5.14-5.16 is shown the frequency ratio comparison where significant within groups (G_1, G_6, G_7).

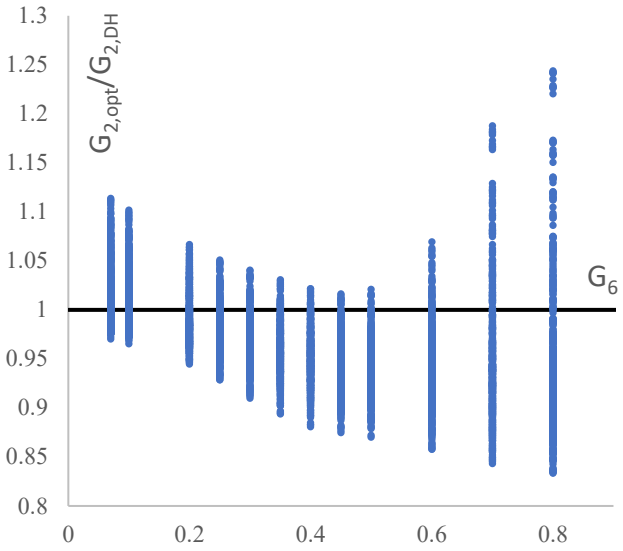


Figure 5.14 – Frequency ratio comparison between proposed formulation and Den Hartog's, plotted as function of the group G_6

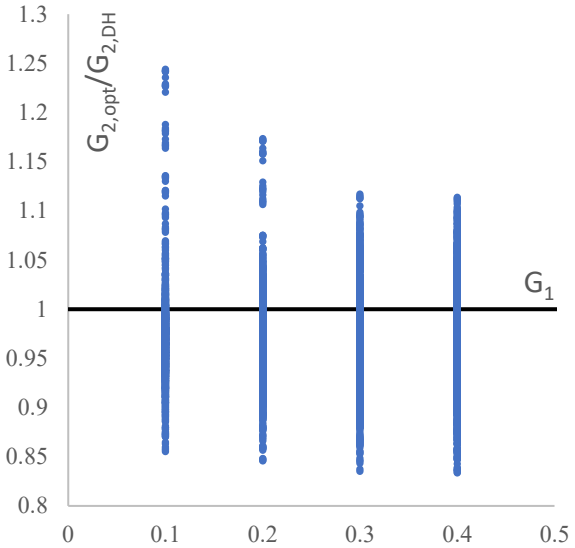


Figure 5.15 – Frequency ratio comparison between proposed formulation and Den Hartog's, plotted as function of the group G_1

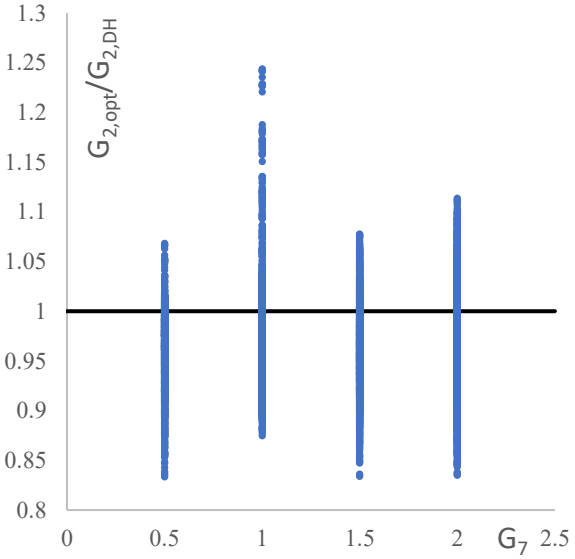


Figure 5.16 – Frequency ratio comparison between proposed formulation and Den Hartog's, plotted as function of the group G_7

With reference to the efficiency ratio (Figures 5.8-5.13), for the points below unity (which therefore represent cases where $\eta_{DH} > \eta_{opt}$), the probabilities of occurrence relative to the total cases have been quantified for each value of groups G_1, G_6, and G_7 in Figures 5.17-5.19.

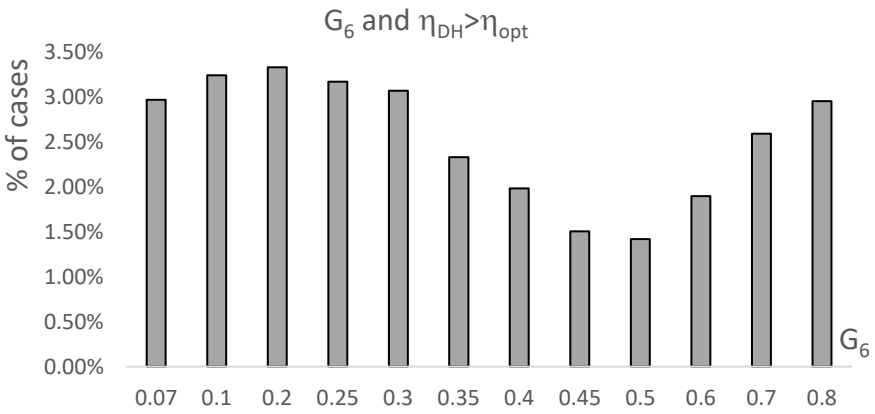


Figure 5.17 Percentages of cases with $\eta_{DH}>\eta_{opt}$ for each value of the group G_6

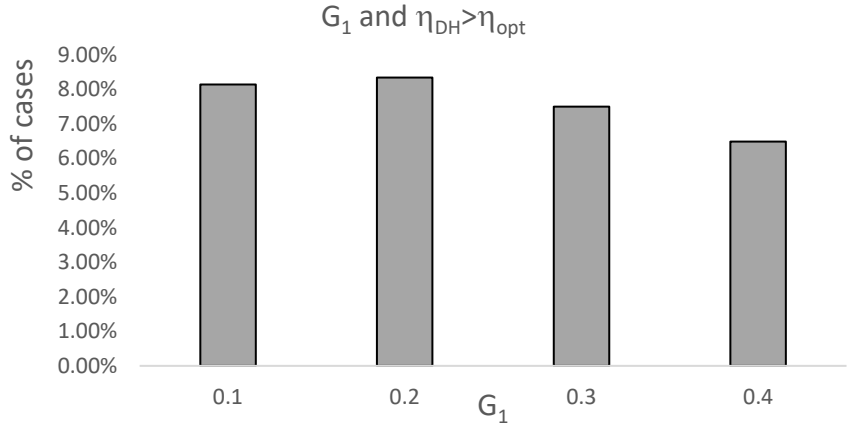


Figure 5.18 Percentages of cases with $\eta_{DH}>\eta_{opt}$ for each value of the group G_1

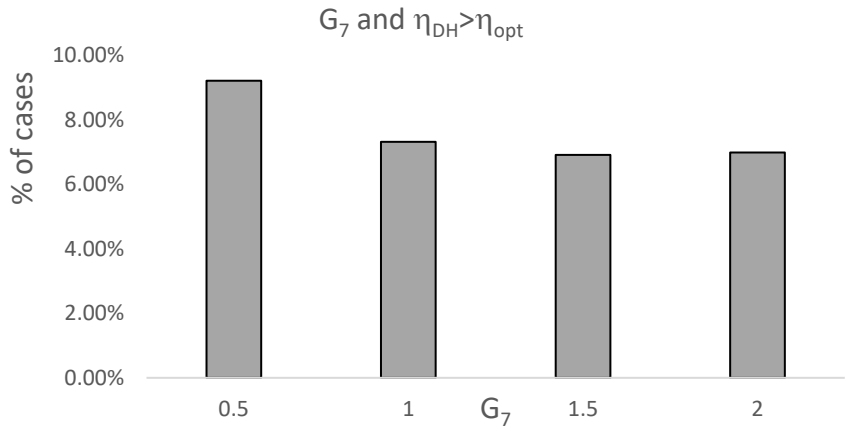


Figure 5.19 Percentages of cases with $\eta_{DH}>\eta_{opt}$ for each value of the group G_7

5.2 Validation on high-fidelity benchmark soil-structure-TMD models

The validation process of the proposed formulation concludes with its application to a real case study. Based on the structure analyzed in Chapters 2 and 3, the formulation can be concretized by designing a real TMD to be applied to the existing structure.

The reference structure described in the previous chapters exhibits a high vibration period (1.54s) associated with a high soil stiffness. Under these conditions of limited soil-structure interaction, the validation would be of little significance. Therefore, a modification was introduced to both the structural and soil stiffness parameters to ensure that soil-structure interaction phenomena become at least relevant. Following these adjustments, a value of 0.15 was obtained for the non-dimensional group (G_6) representing the relative stiffness between the soil and the structure. Based on this updated model, the superstructure was redesigned using an optimized TMD (Tuned Mass Damper). Similarly, the TMD was also redesigned according to the classical formulation presented in Chapter 2, in order to compare its effectiveness.

Considering the input parameters defined by the formulation and adapted to the structure under examination, with the fixed values $G_7 = 1.65$, $G_9 = 0.92$, $G_{10} = 0.05$, $G_{13} = 0.77$, and $G_{14} = 1.5362$, as well as $G_6 = 0.15$, and the variable

parameter G_1 = (0.05, 0.1, 0.2, 0.3), the corresponding optimal G_2 values ($G_{2,opt}$) are obtained, enabling the design of a seismically resistant superstructure, listed in Table 5.1. As in the previous chapters, the superstructure is implemented using a parallel layout of 22 elastomeric bearings placed along the perimeter and 20 flat sliders positioned at the internal nodes.

Table 5.1 – Application of the proposed methodology to the case study

System [-]	$G_{2,opt}$ [-]	T_{TMD} [s]	TMD MASS [Mg]	total TMD stiffness [kN/m]	device stiffness [kN/m]
T=0.8 s, Opt. TMD 5%	0.88	0.90	194.66	9405.47	427.52
T=0.8 s, Opt. TMD 10%	0.85	0.93	389.33	17668.83	803.12
T=0.8 s, Opt. TMD 20%	0.80	0.99	778.66	31182.26	1417.3
T=0.8 s, Opt. TMD 30%	0.75	1.05	1167.99	41260.56	1875.48

In the same way, the properties of the TMDs were recalculated according to the classical formulation, with reference to a structure with a fundamental period of 0.8 seconds. Table 5.2 lists the main parameters.

Table 5.2 – Application of a classic methodology to the case study

System [-]	$G_{2,opt}$ [-]	T_{TMD} [s]	TMD MASS [Mg]	total TMD stiffness [kN/m]	device stiffness [kN/m]
T=0.8 s, Classic TMD 5%	1.00	0.8	194.66	12007.98	545.81
T=0.8 s, Classic TMD 10%	0.88	0.9	389.33	18975.57	862.52
T=0.8 s, Classic TMD 20%	0.72	1.1	778.66	25405.31	1154.78
T=0.8 s, Classic TMD 30%	0.64	1.25	1167.99	29510.81	1341.4

Referring to record no. 2 (Northridge, Wonderland Ave) and an Intensity Measure (IM) of 0.5, the maximum interstory drifts recorded on the structures equipped with optimized TMDs and classical TMDs are reported. Figure 5.20 shows the comparison between the results obtained from the two different design methodologies.

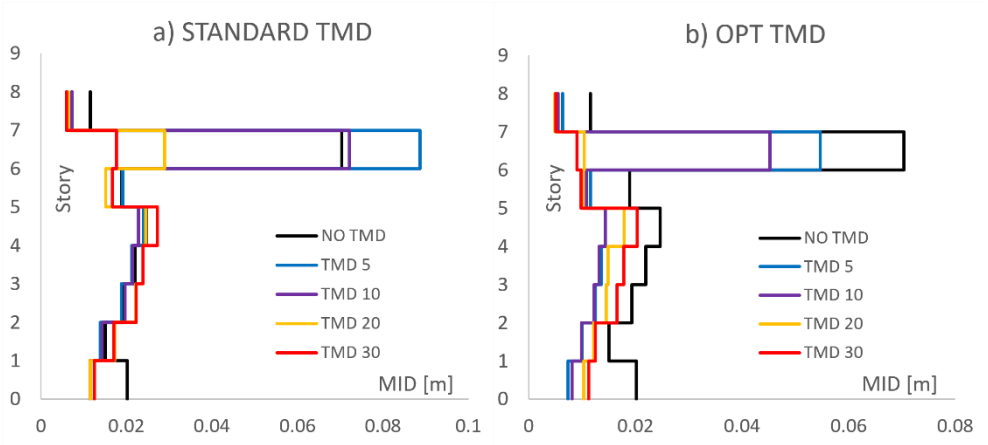


Figure 5.20 Comparison of the Max Interstory Drifts (MID) obtained with a) Standard TMD formulation and b) Optimized TMD formulation

It is important to highlight that, in the case of the standard configuration (Figure 5.20, a), the use of a TMD with a low mass ratio (G1=5-10%) can actually worsen the structural response, causing a significant increase in the maximum interstory drift (MID) at the sixth floor. This negative effect is mainly due to two factors.

The first concerns the local behavior at the sixth floor, where the column cross-sections are smaller compared to the lower stories. Under seismic loading, this configuration may activate a soft-story mechanism, leading to a peak in interstory displacement. This vulnerability stems from non-seismic design criteria adopted in the original construction of the building. As a result, the structure exhibits nonlinear behavior that the TMD, tuned to a simplified linear response, fails to capture, causing a mismatch between expected and actual dynamic performance.

The second factor lies in the tuning procedure itself: the TMD is calibrated based solely on the fundamental frequency in the x-direction, disregarding the bidirectional nature of seismic input. This leads to additional detuning, as the earthquake motion excites multiple vibration modes in both horizontal directions.

A TMD with a 30% mass ratio successfully prevents the activation of the soft-story mechanism (Figure 5.20, b), although this comes at the cost of increased drift demands on the lower floors.

The results described above can be represented in terms of efficiency in the (η–G_1) space to highlight the effect of different mass ratios. As shown in Figure 5.21, in the case of standard formulations, there are scenarios where the use of TMDs with low mass ratios actually worsens the structural response.
In contrast, when an integrated design approach is adopted, a positive efficiency is maintained even at low mass ratios, and this efficiency increases as G1 grows. This proves a higher robustness of the integrated formulation as compared with the classic one. It is also evident that at higher mass ratios (20–30%), a sort of saturation is reached—this applies both to classically designed TMDs and to those designed according to the proposed formulation.

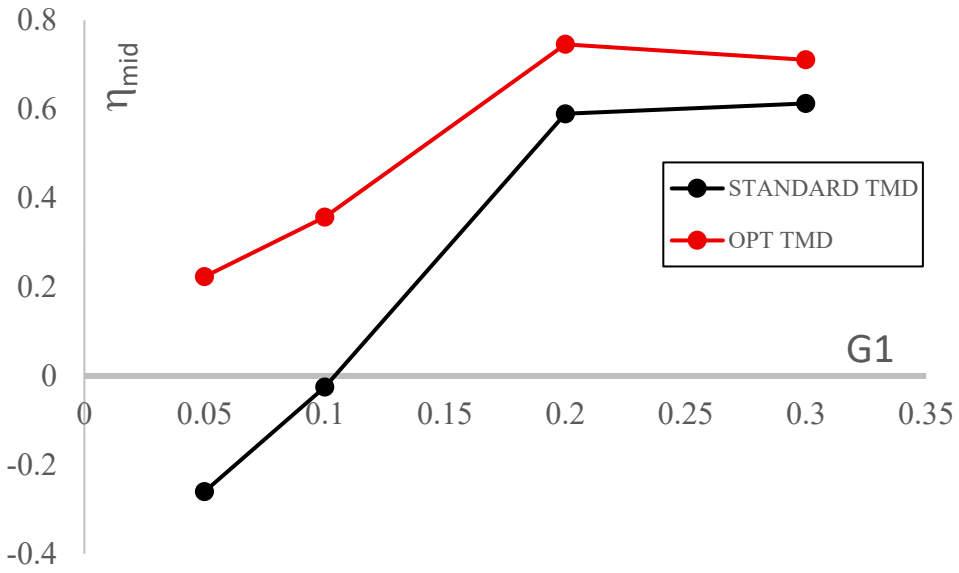


Figure 5.21 Comparison of the effectiveness in MID reduction obtained with Standard TMD formulation (black line) and Optimized TMD formulation (red line)

The robustness of the proposed integrated design was further evaluated by accounting for two additional sources of variability, namely record-to-record variability in the seismic input and changes in the structure-to-soil relative stiffness. To investigate the first aspect, the benchmark soil-structure-TMD system was subjected to both horizontal components of two additional

spectrum-compatible ground motions, the Loma Prieta and Northridge VRP records (rec 1 and rec 3 of the previous section, table 3.1), at the Life-Safety limit state. These records were chosen so as to represent different frequency contents and time-domain characteristics, while remaining consistent with the seismic demand considered. The comparison with conventional (fixed-base) design (Figure 5.22) showed that the integrated design criterion provides a systematic improvement in TMD effectiveness for both mass ratios examined, equal to 5% and 30%, whereas the standard design remains markedly sensitive to the specific input motion and may even become detrimental in the most adverse cases. This behaviour can be ascribed to the combined influence of nonlinear soil response, bidirectional seismic excitation, broad frequency content of the record, and activation of soft-story mechanisms in the superstructure.

The proposed design strategy was then tested under a modified soil-structure benchmark configuration characterised by a higher structure-to-soil relative stiffness. To this end, the original eight-story RC reference building was redefined as a six-story structure with unchanged plan dimensions, while the soil stiffness was reduced by assuming $V_{s,30}$=180 m/s. As a result, the structure-to-soil relative stiffness increases to 0.22, shifting the system further towards the range in which soil-structure dynamic coupling becomes dominant. Nonlinear dynamic analyses carried out under the same Life-Safety seismic scenarios, for the three selected records (Figure 5.23), confirmed that, under these more demanding SSI conditions, the conventional design undergoes an even more pronounced loss of effectiveness, especially for the lower TMD mass ratio. The integrated criterion maintained a clear beneficial contribution across the considered cases, showing its capability to perform tuning with the coupled translational-rotational response of the soil-foundation-structure system.

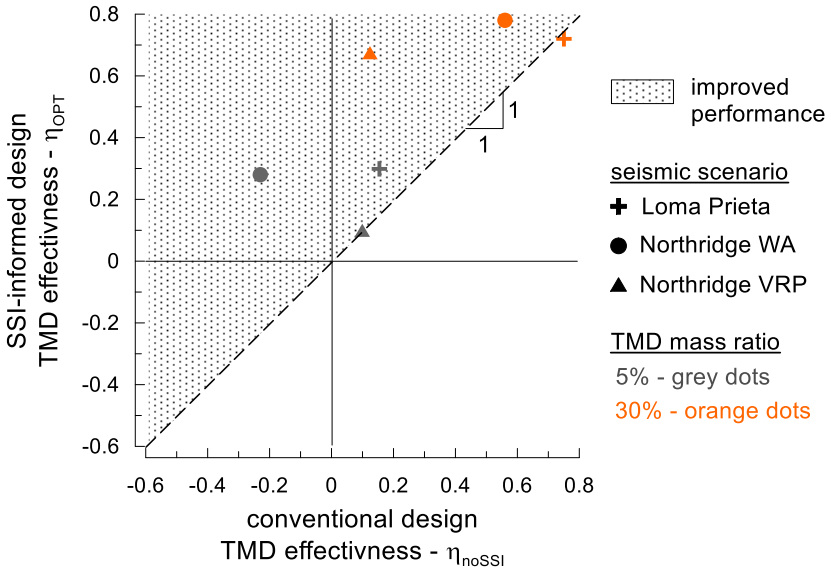


Figure 5.22 Results comparison, on the eight-story benchmark model, between the proposed integrated design and conventional design. [49]

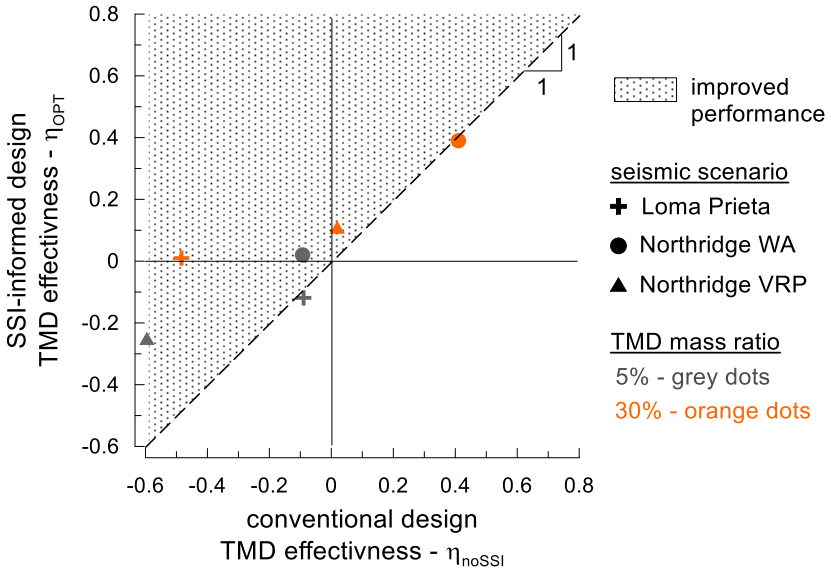


Figure 5.23 Results comparison, on the six-story benchmark model, between the proposed integrated design and conventional design. [49]

6 CONCLUSIONS

In this work, conventional and innovative configurations for TMDs have been examined in application to different soil-structure systems, employing a complementary level of accuracy. In the second chapter, case studies were presented concerning an existing reinforced concrete frame building, considered with a fixed base and designed according to an outdated design code. A first class of TMDs was introduced therein, differing from classical ones due to a higher mass ratio, designed based on generic and artificial seismic excitations. The results demonstrated that the proposed solution can be effectively used as a seismic improvement technique, providing greater control over the seismic response of the structure, particularly for high mass ratios and for seismic events of moderate intensity. In addition, a seismic-resistant superelevation is also favorable towards the protection of existing structures where strengthening techniques are not practicable.The outcomes of these analyses are summarized in designer-friendly charts, which are optimized to address both acceleration and displacement responses of the base structure. These charts offer an efficient and practical tool to achieve an optimal structural response by considering both acceleration and displacement factors.

Results from nonlinear incremental dynamic analyses indicated a considerable enhancement in seismic performance for systems equipped with unconventional TMDs. Particularly, in the inelastic range, the structure's behavior was positively impacted by the TMD under seismic intensities between 0.15 and 0.24 g. This improvement was further reflected by a reduction in Maximum Interstory Drift Ratio (MIDR) and a lower percentage of damaged elements at the end of the seismic events.

Integrating non-conventional TMDs into existing structures presents a promising strategy for improving their seismic resilience. The inclusion of designer-friendly charts in this study provides a thorough approach to seismic retrofitting, ensuring the safety and functionality of structures during earthquake events. The findings highlight the potential of high mass ratio TMDs in seismic retrofitting, particularly for buildings with outdated design standards, and offer a pathway toward more resilient urban environments.

In the third chapter, the same structure was incorporated into a system that included geotechnical modeling of the interacting soil, and TMDs were implemented based on the previously presented high mass ratio formulation. Again, the elevated mass proved effective in mitigating inter-story drifts, which are responsible for structural damage. The soil response was assessed in terms of displacements and response spectra, and its presence was explicitly considered in evaluating the efficiency of the TMDs. It was observed that soil nonlinearity could compromise both the structural and TMD seismic response if not accounted for in the design phase.
Results demonstrated that the LM-TMD effectively controls the maximum deformations in the structure, but it is less effective in reducing accelerations in the highest story due to the significant inertial effects produced by the LM-TMD. The high mass ratio (MR) of the LM-TMD proved to be still more efficient than traditional tuning devices.
Has been observed that soil-structure interaction can negatively impact the LM-TMD performance, particularly by influencing the multimodal response and tuning frequencies, but the dynamic response of the LM-TMD does not affect the foundation's response. LM-TMDs also demonstrated to be more effective than classical ones in the seismic mitigation against multi-directional motions.
Although these considerations are well known in the literature, the uniqueness of this study lies in the level of detail with which the entire soil-structure-TMD system was modeled as a fully coupled system rather than through sub-structure approaches.
Recognizing the importance of soil-structure interaction effects in the response of TMDs adopted for seismic risk mitigation, attention was then given to an interpretative model capable of capturing numerous structural and geotechnical aspects. Based on this model, in the last chapter a novel design formulation for TMDs was proposed, incorporating innovative elements compared to the state of the art, such as structural slenderness, mass distribution in the plan, foundation system shape ratio, and, most notably, the relative stiffness between the structure and the soil.
Through an extensive parametric analysis considering multiple soil-structure-TMD cases, optimal configurations that exhibited maximum efficiency were interpolated. The interpolation of results led to the formalization of a new

integrated design formulation, which, compared to existing approaches, is capable of explicitly accounting for the previously mentioned aspects.
Using the proposed formulation, various soil-structure systems were examined, and the efficiency of the TMD was compared with that obtained through designs based on classical formulations from the literature. It was highlighted that the proposed formulation demonstrated improved performance, especially in systems where soil-structure interaction effects are significant; effects that are not considered in traditionally designed systems.
The proposed formulation appears consistent in predicting the optimal configurations of TMDs for a wide range of structural types, thus making a significant contribution to the state of the art, which is currently lacking in this regard. From a future perspective, the natural evolution of this formulation will certainly need to account for structural and soil nonlinearities, an aspect that remains insufficiently addressed, especially in cases of high-intensity seismic events.

7 REFERENCES

1. J. P. Den Hartog, *mechanical vibrations* (New York: Mc-Graw Hill, 1956).
2. D. C. K. Poon, S. Shieh, L. M. Joseph, & C. Chang, Structural design of Taipei 101, the world's tallest building. *Proceedings of the CTBUH 2004 Seoul Conference, Seoul, Korea*, (2004) 271–278.
3. H. C. Tsai & G. C. Lin, Optimum tuned-mass dampers for minimizing steady-state response of support-excited and damped systems. *Earthquake Engineering and Structural Dynamics*, **22** (1993) 957–973. https://doi.org/10.1002/eqe.4290221104.
4. N. Hoang & P. Warnitchai, Design of multiple tuned mass dampers by using a numerical optimizer. *Earthquake Engineering and Structural Dynamics*, **34** (2005) 125–144. https://doi.org/10.1002/eqe.413.
5. R. Rana & T. T. Soong, Parametric study and simplified design of tuned mass dampers. *Engineering Structures*, **20** (1998) 193–204. https://doi.org/10.1016/S0141-0296(97)00078-3.
6. M. Gutierrez Soto & H. Adeli, Optimum tuning parameters of tuned mass dampers for vibration control of irregular highrise building structures. *Journal of Civil Engineering and Management*, **20** (2014) 609–620. https://doi.org/10.3846/13923730.2014.967287.
7. M. Babaei, Use of Tuned Mass Dampers in Controlling the Vibrations of Steel Structures with Vertical Irregularity of Mass. **2** (2018) 83–94.
8. R. S. Jangid & T. K. Datta, Performance of Multiple Tuned Mass dampers for torsionally coupled system. *Earthquake Engineering and Structural Dynamics*, **26** (1997) 307–317. https://doi.org/10.1002/(SICI)1096-9845(199703)26:3<307::AID-EQE639>3.0.CO;2-8.
9. R. Soto-Brito & S. E. Ruiz, Influence of ground motion intensity on the effectiveness of tuned mass dampers. *Earthquake Engineering and Structural Dynamics*, **28** (1999) 1255–1271. https://doi.org/10.1002/(SICI)1096-9845(199911)28:11<1255::AID-EQE865>3.0.CO;2-C.
10. H. Yamaguchi & N. Harnpornchai, Fundamental characteristics of Multiple Tuned Mass Dampers for suppressing harmonically forced oscillations. *Earthquake Engineering & Structural Dynamics*, **22** (1993) 51–62. https://doi.org/10.1002/eqe.4290220105.
11. M. Domizio, H. Garrido, & D. Ambrosini, Single and multiple TMD optimization to control seismic response of nonlinear structures. *Engineering Structures*, **252** (2022).
12. T. Igusa & K. Xu, Vibration control using multiple tuned mass dampers.

Journal of Sound and Vibration, **175** (1994) 491–503.
13. L. Zuo, Effective and robust vibration control using series multiple tuned-mass dampers. *Journal of Vibration and Acoustics, Transactions of the ASME*, **131** (2009).
14. M. Abé & Y. Fujino, Dynamic characterization of multiple tuned mass dampers and some design formulas. *Earthquake Engineering & Structural Dynamics*, **23** (1994) 813–835.
15. M. D. Symans & M. C. Constantinou, Semi-active control systems for seismic protection of structures: a state-of-the-art review. *Engineering Structures*, **21** (1999) 469–487.
16. M. Setareh, Application of semi-active tuned mass dampers to base-excited systems. *Earthquake Engineering & Structural Dynamics*, **30** (2001) 449–462.
17. M. Abé, Semi-active tuned mass dampers for seismic protection of civil structures. *Earthquake Engineering & Structural Dynamics*, **25** (1996) 743–749.
18. L. Wang, X. Zhao, & Y. M. Zheng, A combined tuned damper and an optimal design method for wind-induced vibration control for super tall buildings. *Structural Design of Tall and Special Buildings*, **25** (2016) 468–502. https://doi.org/10.1002/tal.1268.
19. C. Sun & S. Nagarajaiah, Study of semi-active tuned mass dampers with variable damping and stiffness under seismic excitations. *Structural Control and Health Monitoring*, **21** (2014) 890–906.
20. S. K. Rasouli & M. Yahyai, Control of response of structures with passive and active tuned mass dampers. *The Structural Design of Tall Buildings*, **11** (2002) 1–14.
21. M. De Angelis, S. Perno, & A. Reggio, Dynamic response and optimal design of structures with large mass ratio TMD. *Earthquake Engineering and Structural Dynamics*, **41** (2012) 41–60. https://doi.org/10.1002/eqe.1117.
22. P. R. Marrazzo, R. Montuori, E. Nastri, & G. Benzoni, Advanced seismic retrofitting with high-mass-ratio Tuned Mass Dampers. *Soil Dynamics and Earthquake Engineering*, **179** (2024) 108544. https://doi.org/10.1016/j.soildyn.2024.108544.
23. J. Wu, G. Chen, & M. Lou, Seismic effectiveness of tuned mass dampers considering soil-structure interaction. *Earthquake Engineering and Structural Dynamics*, **28** (1999) 1219–1233. https://doi.org/10.1002/(SICI)1096-9845(199911)28:11<1219::AID-EQE861>3.0.CO;2-G.

24. A. Ghosh & B. Basu, Effect of soil interaction on the performance of tuned mass dampers for seismic applications. *Journal of Sound and Vibration*, **274** (2004) 1079–1090.
25. J. Salvi, F. Pioldi, & E. Rizzi, Optimum Tuned Mass Dampers under seismic Soil-Structure Interaction. *Soil Dynamics and Earthquake Engineering*, **114** (2018) 576–597. https://doi.org/10.1016/j.soildyn.2018.07.014.
26. G. Bekdaş & S. M. Nigdeli, Metaheuristic based optimization of tuned mass dampers under earthquake excitation by considering soil-structure interaction. *Soil Dynamics and Earthquake Engineering*, **92** (2017) 443–461. https://doi.org/10.1016/j.soildyn.2016.10.019.
27. L. Shutong, L. Haochen, X. Jinlun, Y. Shutong, & L. Peizhen, Comparative study on seismic performance of structure with TMD and particle TMD considering SSI effects. *Journal of Building Engineering*, **77** (2023).
28. Z. Gao, M. Zhao, Y. Wu, M. Wang, & X. Du, Parameter design and performance evaluation of tuned mass damper (TMD) for seismic control of structure considering soil-structure interaction (SSI). *Structures*, **52** (2023) 1116–1129.
29. D. N. Gorini & C. Chisari, Impact of soil-structure interaction on the effectiveness of Tuned Mass Dampers. *Earthquake Engineering and Structural Dynamics*, **51** (2022) 1501–1521.
30. E. H. Vanmarcke, C. A. Cornell, D. A. Gasparini, & S.-N. Hou, *SIMQKE-I: simulation of earthquake ground motions*.
31. *Eurocodice 8, Progettazione di strutture in zona sismica* (2005).
32. Decreto Ministeriale 16 giugno 1976, Norme tecniche per la esecuzione delle opere in cemento armato normale e precompresso e per le strutture metalliche. (1976).
33. S. [2021], SeismoStruct 2021–A computer program for static and dynamic nonlinear analysis of framed structures. (n.d.).
34. F. McKenna, M. H. Scott, & G. L. Fenves, OpenSees. Nonlinear Finite-Element Analysis Software Architecture Using Object Composition. *Journal of Computing in Civil Engineering*, **24** (2010) 95–107.
35. D. N. Gorini, P. R. Marrazzo, E. Nastri, & R. Montuori, Effectiveness of an innovative seismic resilient superelevation in an archetype, existing soil-structure system. *Bulletin of Earthquake Engineering*, **23** (2025) 1677–1705. https://doi.org/https://doi.org/10.1007/s10518-024-02050-4.
36. D. N. Gorini, Soil-structure interaction for bridge abutments : two complementary macro-elements, Sapienza University of Rome, 2019.
37. D. N. Gorini & L. Callisto, A coupled study of soil-abutment-superstructure

interaction. *Springer Lect. Notes Civ. Eng. "Geotechnical Res. L. Prot. Dev.* (2019), pp. 565–574. https://doi.org/https://doi.org/10.1007/978-3-030-21359-6_60.

38. Ministero delle Infrastrutture e dei Trasporti, *Aggiornamento delle «Norme tecniche per le costruzioni».* (2018).
39. A. Arias, A measure of earthquake intensity. *Seismic Design for Nuclear Power Plants*, (1970) 438–483.
40. F. Taucer, E. Spacone, & C. Filippou, Filip, *A fiber Beam-Column Element for Seismic Response Analysis of Reinforced Concrete Structures. Report No. UCB/EERC-91/17* (Berkeley, 1991).
41. A. Neuenhofer & F. C. Filippou, Geometrically Nonlinear Flexibility-Based Frame Finite Element. *Journal of Structural Engineering*, **124** (1998) 704–711.
42. B. D. Scott, R. Park, & M. J. N. Priestley, Stress-strain behavior of concrete confined by overlapping hoops at low and high strain rates. *ACI Journal*, **79** (1982) 13–27.
43. O. C. Zienkiewicz & T. Shiomi, Dynamic behaviour of saturated porous media; The generalized Biot formulation and its numerical solution. *Numerical and Analytical Methods in Geomechanics*, **8** (1984) 71–96.
44. Z. Yang, A. Elgamal, & E. Parra, Computational Model for Cyclic Mobility and Associated Shear Deformation. *Journal of Geotechnical and Geoenvironmental Engineering*, **129** (2003) 1119–1127. https://doi.org/10.1061/(asce)1090-0241(2003)129:12(1119).
45. D. N. Gorini, L. Callisto, & A. J. Whittle, Dominant responses of bridge abutments. *Soil Dynamics and Earthquake Engineering*, **148** (2021). https://doi.org/DOI: 10.1016/j.soildyn.2021.106723.
46. D. N. Gorini, L. Callisto, & A. J. Whittle, An inertial macroelement for bridge abutments. *Géotechnique*, **72** (2022) 247–259.
47. FIP., Elastomeric Isolators (SI series) Manufacturing Catalogue. FIP INDUSTRIALE SpA. (2008).
48. D. N. Gorini & C. Chisari, Effect of soil-structure interaction on seismic performance of tuned mass dampers in buildings. *Earthquake Geotechnical Engineering for Protection and Development of Environment and Constructions- Proceedings of the 7th International Conference on Earthquake Geotechnical Engineering*, (2019) 2690–2697.
49. D. N. Gorini, P. R. Marrazzo, E. Nastri, & R. Montuori, An SSI-Informed Design for Tuned Mass Dampers with Small-to-Large Mass Ratios. *Earthquake Engineering & Structural Dynamics*, (2026).

https://doi.org/10.1002/eqe.70209